Summer 8-7-2012

Synthesis and Energetics of Gold Nanoclusters Tailored by Interfacial Bonding Structure

Tang Zhenghua
Georgia State University

SYNTHESIS AND ENERGETICS OF GOLD NANOCLUSTERS TAILORED BY INTERFACIAL BONDING STRUCTURE

by

ZHENGHUA TANG

Under the Direction of Gangli Wang

ABSTRACT

In addition to the well known quantum confinement effects resulted from size and shape, interfacial bond structure is another factor, affecting the properties of the nanomaterial that is rarely studied. Inspired by the "Au-S-Au" staple motif discovered from the crystal structure of monothiol protected Au102 nanocluster (*Science*, **2007**, *318*, 430), dithiol molecules (e. g. 1, 2-dithiol, 1, 4-dithiol, etc.) with molecular structural constraint have been employed to create dithiolate protected clusters or mixed monothiolate and dithiolate protected clusters. The structure and properties of the Au clusters are expected to change due to two effects: The entropy gain of dithiol over monothiol protection and the constraint to the formation of the thiol bridging motif. DMPS (1, 2-dithiol molecule) stabilized clusters with characteristic absorption bands have been obtained, and characterized by multiple techniques. Monolayer reaction on gold core surface between the monothiol tiopronin and dithiol DMPS has been performed, and the mechanism has been probed. Mixed phenylethanethiolate and durene-dithiolate (1, 4-

dithiol molecule) protected Au130 clusters with rich electrochemical features have been created, and the optical and electrochemical energetics have been successfully correlated based on core and core-ligand energy states. Furthermore, the impact of 1, 4-dithiolate-Au bonding on the near infrared luminescence has been studied.

INDEX WORDS: Au MPCs, Staple motif, DMPS, Au DTCs, Au4, Tiopronin, Monolayer reaction, Durene-DT, Au MTCs, Au130, Optical energetic, Electrochemistry, Near infrared luminescence, 1, 4-Dithiolate-Au bonding

SYNTHESIS AND ENERGETICS OF GOLD NANOCLUSTERS TAILORED BY INTERFACIAL BONDING STRUCTURE

by

ZHENGHUA TANG

A Dissertation Submitted in Partial Fulfillment of the Requirements for the Degree of

Doctor of Philosophy

in the College of Arts and Sciences

Georgia State University

2012

SYNTHESIS AND ENERGETICS OF GOLD NANOCLUSTERS TAILORED BY INTERFACIAL BONDING STRUCTURE

by

ZHENGHUA TANG

Committee Chair: Gangli Wang

Committee: Markus W. Germann

Shahab A. Shamsi

Electronic Version Approved:

Office of Graduate Studies

College of Arts and Sciences

Georgia State University

August 2012

DEDICATION

I want to dedicate this dissertation to my parents (Hongfa Tang and Genxiu Duan). Without you, I could not go so far. You always give the most valuable spiritual support as well as material support in all my way of studying and growing up as a man. Your love and care is the origin of my motivation to do research, to conquer difficulties I meet. I also want to dedicate this dissertation to my brother Dehua Tang, for all the efforts he has made to take care of my parents.

ACKNOWLEDGEMENTS

All the work has been done under the direction and support of Dr. Gangli Wang. I owe my deepest gratitude to him, and I am so thankful he is my Ph. D advisor. His inspiring suggestions on experiment design, rigorous thoughts to research results and self-motivated attitude to research itself will benefit my whole life, not only as a researcher, but also as a person.

The committee members of my dissertation Professor Markus W. Germann and Professor Shahab A. Shamsi are gratefully acknowledged.

Special thanks to Professors Jenny J. Yang and Binghe Wang for all the help.

I thank all the staff in Department of Chemistry at Georgia State University, especially mass spectrometry manager Dr. Siming Wang and her assistant Dr. Yanyi Chen.

I would like to thank all the current and past members (Dr. Bin Xu, Dr. Tarushee Ahuja, Dr. Baohua Wu, Donald A. Robinson, Nadia Bokossa, Juan Liu, Warren Brown, Dengchao Wang, Yan Li, Maksim Kvetny, Cecil Conroy) in Dr. Gangli Wang's group. Thank you for your help during those years of study, and I enjoyed working together with you.

My US brother Yuehua (Michael) Tang helped me with a lot of things, and I thank him for his great support!

I acknowledge the fellowship (2011-2012) from Center of Diagnostics and Therapeutics (CDT) at Department of Chemistry, Georgia State University.

The financial support for my research, including Gangli Wang startup at GSU, Research Initiation Grant at Georgia State University and National Science Foundation funding (CHE 1059022), are gratefully acknowledged.

TABLE OF CONTENTS

LIST OF SCHEMES

LIST OF TABLES

LIST OF FIGURES

LIST OF ABBREVIATIONS

Au NPs	Gold Nanoparticles
Au MPCs	Gold Monolayer-Protected Clusters
Au DTCs	Gold Dithiol-Protected Clusters
Au MTCs	Gold Mixed Thiolate Clusters
UV-Vis	Ultraviolet-Visible
XAFS	X-ray Absorption Fine structure Spectroscopy
SAXC	Small-Angle X-ray Scattering
XANES	X-ray Absorption Near-Edge Spectroscopy
XRD	X-Ray Diffraction
AFM	Atomic Force Microscopy
TEM	Transmission Electron Microscopy
STM	Scan Tunneling Microscopy
NMR	Nuclear Magnetic Resonance
COSY	Correlated Spectroscopy
DOSY	Diffusion Ordered Spectroscopy
TOCSY	Total Correlation Spectroscopy
HSQC	Heteronuclear Single-Quantum Coherence
HMBC	Heteronuclear Mutiple-Bond Correlation Spectroscopy
MS	Mass Spectrometry
ESI	Electrospray Ionization
MALDI-TOF	Matrix-Assisted Laser Desorption Ionization-Time of Flight
EA	Elemental Analysis
TGA	Thermogravimetric Analysis

XPS	X-ray Photoelectron Spectroscopy
ESCA	Electron Spectroscopy for Chemical Analysis
BE	Binding Energy
DMPS	Dimercaptopropanesulfonic Acid
MWCO	Molecular Weight Cutoff
CHCA	α-Cyano-4-hydroxycinnamic acid
FT-IR	Fourier-Transform Infrared Spectroscopy
PE	Place Exchange
Durene-DT	Durene-α1, α2-dithiol
DCTB	*trans*-2-[3-(4-tert-butylphenyl)-2-methyl-propenylidene]-malononitrile
HPLC	High Performance Liquid Chromatography
TBAP	Tetrabutylammonium Perchlorate
CV	Cyclic Voltammetry
DPV	Differential Pulse Voltammetry
SWV	Square Wave Voltammetry
PhC2S	Phenylethanethiol(ate)
OCPT	Open Circuit Potential Test
TOAB	Tetraoctylammonium Bromide
HOMO	Highest Occupied Molecular Orbital
LUMO	Lowest Unoccupied Molecular Orbital

1 INTRODUCTION

1.1 Au NPs: Synthesis, Characterizations and Fundamental Properties

Nanotechnology, an emerging technology, has penetrated into every aspect of daily life all over the world. It focuses on the study and dealing with ultra-small matters or devices, specifically, in the range of 1 to 100 nm even hundreds of nm. As we know, 1 nm = 10^{-9} m, and it is about 10^{5} times the width of a single human hair. In another word, in the regime of nanotechnology, the matter or device at ultrasmall range named "nanoscale" is investigated. Nanotechnology, ranging from the conventional physical devices to new approaches based on molecular assembly, stretches across physics, chemistry, material science, electronics, biology, medicine, environmental science, energy technology and so on. On the other hand, many problems, issues and concerns have been raised, such as the toxicity of nano-materials, the environmental and ecological impacts of nanomaterials and the potential conflicts of traditional ethics with applications of nanotechnology.

Nanoparticles, one of the most important materials in nanotechnology, are defined as bridges between bulk materials and single molecular or atomic structures. The well studied nanoparticles include quantum dots, metal nanoparticles, bio-constructed nanoparticles (DNA, protein based nanocomposite), colloid or gel, polymer nanoparticles and so on.

Gold nanoparticles (Au NPs), including gold nanocrystals or gold nanoclusters, are a classic type of metal nanoparticle of great importance. Generally speaking, nanocrystals are particles with dimensions over 100 nm, which can be considered "larger nanoparticles" or "microparticles", while nanoclusters refer to much smaller particles with diameter less than 2 nm, so-called "molecular level". My research mainly focuses on small gold nanoparticles, specifically, the synthesis, characterizations and property investigations of gold nanoclusters.

Gold is a subject of the most ancient theme of investigations in science, technology, medicine, engineering, decorating arts and so on.[1] In ancient China or Egypt, gold colloids had been used as therapeutic agents. These colloids, in fact, we now believe, were gold gel solutions. They were microparticles instead of nanoparticles. As the emergence of nanotechnology, gold nanoparticles gained a great deal of research interests, probably due to their extra-ordinary stability, tunable surface functionalities and size-dependent properties.

Ultra-small gold nanoparticles, also called gold monolayer-protected clusters (MPCs), are composed of gold core and self-assembled monolayers (SAMs), which are usually made of halide, phosphate and thiolate molecules. The gold core consists of ten to a few hundreds of gold atoms, and the gold atoms are packed with Au-Au bonding. The monolayers, can be not only organothiolate molecules, but also bio-molecules, for example, DNA, protein etc. **Figure 1.1** presents the cartoon of thiolate protected gold nanoclusters. The core and the surface are connected by the Au-S bond, or another way to say, the monolayer protects the gold core through Au-S interaction on the interface. The gold core enables the particle unique size-dependent capabilities; meanwhile the protection from the monolayer provides the particles robust stabilities. Moreover, the monolayer can be easily modified, which imparts the particle surface functionalities, such as chemical reactions. These gold nanoclusters, usually in a dimension less than 2 nm, are an intense research subject recently[1-5], thanks to their fundamental properties such as optical behaviors, surface reactivity and electrochemistry.

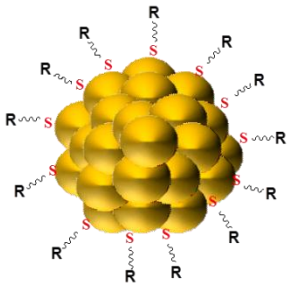

Figure 1.1 Cartoon of thiolate protected gold nanoclusters.

There are several ways to obtain Au NPs, mostly starting from the reduction of Au (III) derivatives. For the Au NPs normally employed in biological systems with ~20 nm diameter or even larger, the most widely used method has been developed by Turkevitch in 1951.[6] The stabilizer in his approach is trisodium citrate, and it is well recognized in colloid science that citrate molecules weakly coordinate with the gold core through multiple sites. Currently, this method is still being widely employed to prepare the precursor of more stable AuNP-biomolecule nanocomposite for further biomedical applications.

By using X-ray absorption fine structure spectroscopy (XAFS), the initial kinetic nucleation of such gold nanocrystals under the grain size of 1 nm has been reported,[7] which can be described as the formation of $Cl_3^-Au\text{-}AuCl_3^-$ dimer and the subsequent higher complexes "Au_nCl_{n+x}" in the early stage. The bulk gold nanocrystal formation mechanism has been deduced by four steps recently,[8] including nucleation (~2 nm), growth by aggregation (~3 nm), slow further growth (~5.5 nm) and fast final growth (~7.7 nm) through small-angle X-ray scattering (SAXS) and X-ray absorption near-edge spectroscopy (XANES) investigations.

In terms of preparing ultra-small gold nanoclusters, the Brust-Schiffrin method, first reported in 1994[9] and 1995[10], has a considerable impact on the overall field in less than 20 years. The synthetic scheme of nonpolar gold nanoclusters is shown in **Scheme 1.1**. Basically, chloroauric acid (Au(III)) was first transferred from aqueous solution to organic phase by tetraoctylammonium bromide (TOAB), and reduced by organic thiol molecules to form gold-thiolate (Au(I)) polymers. The organic soluble Au-S polymer can be further reduced by aqueous sodium borohydride solution. The produced materials are polydisperse gold nanoclusters with wide size distribution, ranging from ~ 5 nm to less than 1 nm. It is worth noting that, the metal can be gold, palladium, copper or other metals or alloy. Among all the metal nanoclusters, gold is the most widely prepared one by this method, probably due to their extraordinary stability and versatile applications. The as-prepared clusters are thermally stable and air stable, and they can be repeatedly isolated or redispersed in common organic solvents without aggregation or de-

composition of the structures. The facile method allows the reproducible synthesis of stable clusters with controllable quantities for the first time. Gold nanoclusters obtained by this method can be handled or modified as chemical reagents or molecular compounds, and one of the typical modifications is place exchange (PE) reaction, which is also shown in **scheme 1.1**. The ligand on the monolayer can be partially or totally exchanged by other thiol-containing molecules, depending on the reactivity of the incoming ligand, the chemical equivalents and other experimental conditions. This reaction can be performed to obtain new nanoparticles with modified surface, while the original ligand and the incoming ligand are not necessarily the same type, e. g. the original ligand is citrate and the incoming ligand is organic molecule or biomolecule with –SH group included.

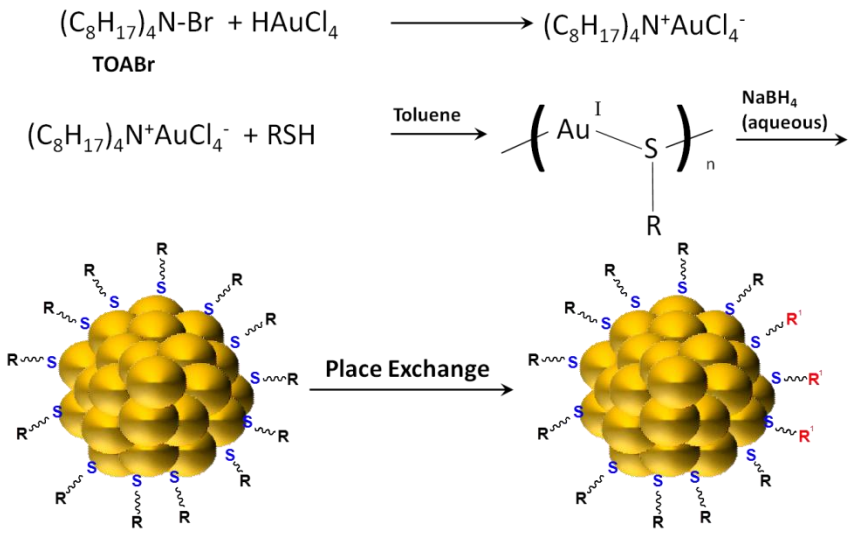

Scheme 1.1 The synthetic scheme of nonpolar gold nanoclusters with Brust-Schiffrin method and place exchange (PE) reaction.

There is ongoing debate on the mechanism of the nanocluster formation by this biphasic synthetic method. It has been reported recently by Lennox[11] and coworkers that the metal precursor before $NaBH_4$ reduction is not the generally believed a [Au(I)-SR] polymer but rather the [TOA][MX_2] complex. Based on this mechanism, Tong's group proposed an inverse-based synthetic procedure, which can offer

better control in forming different metal (Au, Ag, and Cu) NPs with different organo-chalcogen ligands as the stabilizers.[12] It is worth noting that, size evolution of thiol protected gold nanoclusters can be assisted by proton acids and halogen anions.[13] By employing mercaptobenzoic acid (MBA) as ligand, theoretical work of the AuNP growth mechanistic scheme including formation of a stable $Au_4(MBA)_4$ complex and Au_n NP growth and stabilization upon the interaction with the $Au_4(MBA)_4$ complexes has been recorded.[14]

The easy handling properties of the gold nanoclusters facilitate their structural and compositional analysis, which can be further divided into the core and the monolayer analysis.[1,2]

The formula of molecular gold nanoclusters can be described as $Au_n(SR)_m$, and the compositions of these clusters can be revealed by mass spectrometry. For clusters with multiple positive or negative charges, electrospray ionization (ESI)[15-20] is a good choice and has been extensively employed. For singly charged clusters or neutral clusters associated with singly charged counter ion, laser desorption ionization mass spectrometry (LDI-MS) especially matrix assisted laser desorption ionization mass spectrometry (MALDI-MS)[21-32] has proven to be a powerful tool to identify the molecular ion. Other mass spectrometric techniques, such as fast atom bombardment (FAB)[33] and ion-mobility mass spectrometry (IM-MS)[34,35] have been exploited to demystify the molecular structures of those clusters. Fragmentation information regarding the composition of exchanged nanoparticle can be obtained by tandem mass spectrometry (MS-MS),[36] while several successful cases can be found to detect the molecular ions with the combination of liquid chromatography or gas chromatography and mass spectrometry, which will be discussed later in separation section.

For the gold core, the most straightforward method to “see” it is high resolution transmission electron microscopy (HR-TEM). The gold core can be photographed by TEM technique. TEM has been widely used to characterize the gold metal clusters[37-44] since 1990s. The shape of the nanoparticle can be directly visualized and strip or ribbon formed from single particle or aggregated particles can be easi-

ly identified. Besides imaging the real particle, another advantage of TEM is that by counting the particles in a microscopic window, the particle size histogram can be obtained. The TEM image of tiopronin MPCs (3X, while X= Ligand-to-gold ratio during synthesis) is shown in **Figure 1.2.**

However, the gold core dimensions can also be characterized by other techniques, such as atomic force microscopy (AFM),[45-52] scanning tunnel microscopy (SEM),[53-59] small-angle X-ray scattering (SAXS),[8,60-63] X-ray diffraction (XRD)[64-68] and so on.

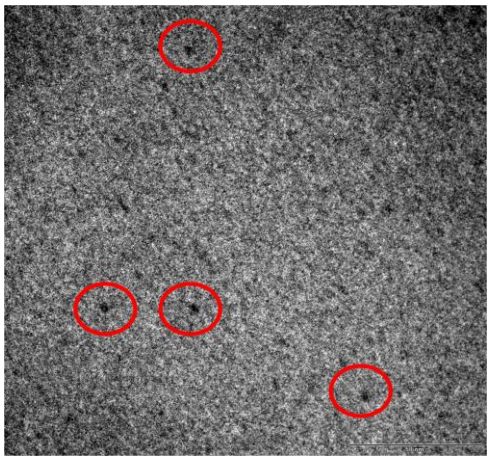

Figure 1.2 The TEM image of tiopronin MPCs (3X). The black dots circled by red line in the graph are the gold cores of the nanoparticles (unpublished results). The scale bar is 50 nm and the diameter of the gold core is ~2 nm.

For the monolayer, the ligand structure can be analyzed by nuclear magnetic resonance (NMR), and in most cases, polydisperse materials were examined, thus the data represents an average. Compared with sharp peaks of the ligand, the NMR peaks are significantly broadened, known as line-broadening effect.[69] Ongoing efforts in understanding the source of the line-broadening effects have been carrying on continuously.[70-74] The extent of such effects is strongly dependent on the nanoparticle size, shape, ligand type, monodispersity as well as the proximity to the gold core.[25,75-80] Moreover, NMR can also play an important role in structural elucidation of functionalized organic ligand modifications

with either place exchange reaction, chemical reactions, or dynamic study.[81-83] It is interesting to note that intramolecular ligand dynamics in organophosphate stabilized gold nanoparticles investigated by ^{2}H NMR has been reported recently.[84]

Two dimensional (2D) NMR techniques have also found versatile applications in structural analysis of the monolayer attached on the gold core. Nuclear overhauser enhancement spectroscopy (NOESY) and heteronuclear multiple quantum coherence (HMQC) spectra have been generated to assign all the NMR sensitive nuclei in the tiopronin ligand while diffusion-ordered spectroscopy (DOSY) provided information about the particle size distribution of water soluble Au MPCs in Murray's work.[77] In a recent report, DOSY has been described as a reliable alternative to TEM for determining the size of gold nanoparticles in organic solutions.[85] The identification of the uniquitin-gold nanoparticle interaction sites has been reported by [^{15}N-^{1}H]-heteronuclear single quantum coherence (HSQC) NMR technique in protein-nanoparticle interaction.[86]

The broad peaks in NMR resulted from line-broadening effects often lead to low resolution spectra, hence not much information can be obtained from the interpratation. To overcome this limitation, high resolution magic angle spinning (HRMAS) ^{1}H NMR technique has been introduced to characterize the organic molecules attached to the gold core recently.[87]

The mass fraction of the monolayer in the total nanoparticle can be analyzed by thermogravimetric analysis (TGA). In a TGA experiment, the monolayer of the gold clusters decomposes from the gold core as volatile disulfide, leaving elemental gold core. Hence, the organic/metal ratio can be calculated from TGA experiment, and this ratio has been widely applied to determine the average composition of the polydisperse gold clusters.[88-91] For monodisperse gold clusters with uniform size, the combination of elemental analysis (EA)[92,93] with this technique makes it more powerful for determining the molecular formula.

The nature of the gold core of these clusters can be examined by X-ray photoelectron spectroscopy (XPS). XPS is also known as electron spectroscopy for chemical analysis (ESCA), and is a quantitative technique that can measure the elemental composition, empirical formula, chemical state and electronic state of the elements present in the material.[94,95] The basic principle of this technique is that, the analyte is irradiated by an X-ray beam while the kinetic energy and the number of the electrons that escape from the top 1-10 nm of the surface are measured simultaneously. High vacuum experimental conditions are required, and this surface chemical analysis technique can be used to analyze all kinds of materials, such as inorganic compounds, alloys, polymers, semiconductors, ceramics, catalyst, glasses, and so on.

For gold nanoclusters, XPS can be performed to probe the charge state and the binding energy of the elements, in most cases gold, e. g. Au($4f_{5/2}$) and Au($4f_{7/2}$)[25,70,96-98], sometimes, sulfurs, e.g. S(2p)[99,100], or both.[101,102] It is interesting to point out that the survey scan in XPS experiment can always be treated as an elemental analysis experiment, which can be the proof of the existence of one element.

For metal nanocrystals, because all the molecular orbitals are filled with free electrons, the absorbance shows featureless exponential decay. Metal nanoclusters, specifically gold nanoclusters, often consist of tens to hundreds of atoms, and their size typically ranges from sub-nanometer to approximately 2 nm in core diameter. In such extremely small size regime, strong quantum confinement of electrons results in the occurrence of electron energy quantization, which strongly alter the fundamental characteristics of the gold clusters, such as UV-Visible absorbance, luminescence and electrochemistry. For example, instead of the appearance of plasmon excitation in nanocrystals, molecular gold nanoclusters normally show pronounced absorption bands, reflecting the discrete electron energy states.[1,3,5]

One of the best examples to demonstrate nanoparticle's unique fundamental properties including absorbance, luminescence, and electrochemistry, is the monodisperse $Au_{25}L_{18}$ nanoparticle.[103] The li-

gand here can be glutathione, phenylethanethiolate, hexanethiolate, or dodecanethiolate. $Au_{25}L_{18}$ has been a good target of studying nanoparticles because of their molecule-like properties, such as facile synthetic accessibility, easy isolation with great monodispersity and extraordinary stabilities.

Pioneering work to obtain this nanoparticle was done by Whetten and coworkers,[15,22] but unfortunately, it was labeled as $Au_{28}(SG)_{16}$ (SG= Glutathione) because of the analytical instrument limitations. Murray's group synthesized monodisperse $Au_{25}(SC_2H_4Ph)_{18}$ nanoparticle and studied the optical behaviors and electrochemistry on it thoroughly,[104,105] but they also mislabeled it as $Au_{38}(SC_2H_4Ph)_{24}$. By using ESI-MS technique, Tsukuda and coworkers[97] corrected the identity of glutathione protected gold nanoclusters as $Au_{25}(SG)_{18}$. The large scale synthesis of $Au_{25}(SG)_{18}$ through ligand exchange reaction of phosphine-stabilized Au11 clusters has also been documented by Tsukuda's group.[106] High resolution ESI-MS identification of $Au_{25}(SC_2H_4Ph)_{18}^-$ anion has been done by Murray's group,[17,18] and thus the molecular composition finally has been settled down as $Au_{25}L_{18}$.

The crystal structure of $Au_{25}(SC_2H_4Ph)_{18}^-$ anion with TOA^+ cation as counter-ion was reported by both Murray's group[107] and Jin's group[108] in 2008. X-ray crystal structure shows Au_{25} nanoparticle includes icosahedral Au_{13} core, which is surrounded by six $Au_2(SR)_3$ semi-rings. Note that, Au25 nanoparticle can possess three different charge states,-1, 0 and +1, which has been revealed by Tsukuda et al. in ESI-MS investigations[109]. The following work on the crystal structure of $Au_{25}(SC_2H_4Ph)_{18}^0$ neutral species showed that the neutral Au_{25} has almost identical structure with the anionic one except some small differences,[110] specifically, the slight structural distortion in the anionic Au_{25} were not observed in neutral one. Theoretical investigations[111-114] also play an important role in advancing the understanding of the electronic structure and the origin of the stability of this nanoparticle.

As shown in **Figure 1.3**, Au_{25} nanoparticles exhibit strong absorbance peaks at ~400 nm (3.11 eV), ~ 450 nm (2.76 eV) and ~670 nm (1.86 eV), with optical band gap of ~1.33 eV.[105] Notably, no matter what type of ligand was used, e. g. gluthathione, hexanethiolate, dodecanethiolate or phenylethanethi-

olate, as long as the nanoparticle adopts Au_{25} structure, the absorbance bears the similar features.[29] However, the absorbance of Au_{25} nanoparticle shows a slight difference at different charge states. For $Au_{25}(SC_2H_4Ph)_{18}$, it has been reported that the anionic species exhibit a distinct, broad shoulder at ~800 nm while the neutral one does not,[110] similar case of $Au_{25}(SG)_{18}$[29] and other Au_{25} nanoparticles stabilized by organothiolate ligands. From here, we can conclude that, both Au_{25} nanoparticles shown in **Figure 1.3** are anionic species, as ~800 nm shoulder can be clearly observed in both spectra. The ~670 nm absorption can be correlated with the electronic and geometric structure of the icosahedral Au_{13} core through density theory functional calculations.[108]

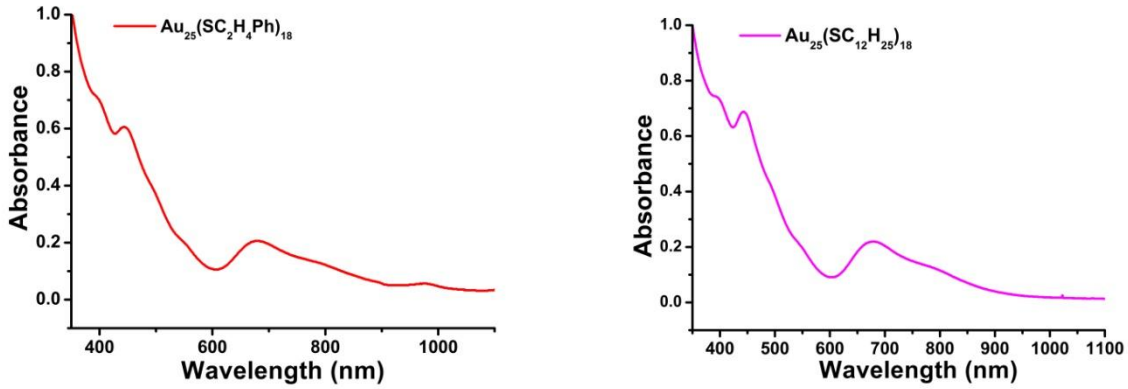

Figure 1.3 Absorbance spectra of Au25 nanoparticles, unpublished results. Left: $Au_{25}(SC_2H_4Ph)_{18}$, Right: $Au_{25}(SC_{12}H_{25})_{18}$.

The near infrared photoluminescence (PL) of $Au_{25}(SC_2H_4Ph)_{18}$ has also been reported[105]. However, this intensity is fairly weak, probably due to the polydispersity of the sample tested. **Figure 1.4** presents the emission spectrum of $Au_{25}(SC_2H_4Ph)_{18}$. Broad band from 600 nm to 850 nm even longer wavelength centered at ~720 nm can be observed from the emission spectrum. By using electron withdrawing ligands, the emission intensity can be improved significantly.[115] The origin of this PL is believed to arise from the surface states of the nanoparticle. The surface states can localize the free electrons hence causing a red-shift in luminescence.[116] High quantum yield up to 6% can be obtained from the bovine

serum albumin (BSA) protected Au25 nanoclusters.[117] Recent report found that charge state of the gold nanocluster and surface ligand can play an important role in enhancing the near-IR PL of Au25 nanoclusters.[118] Interestingly, the surface ligand can influence the luminescence either by charge transfer from the ligand to the metal core through Au-S bond or by direct donation of delocalized electrons of electronic-rich atoms or groups of the ligand to the metal core.[118]

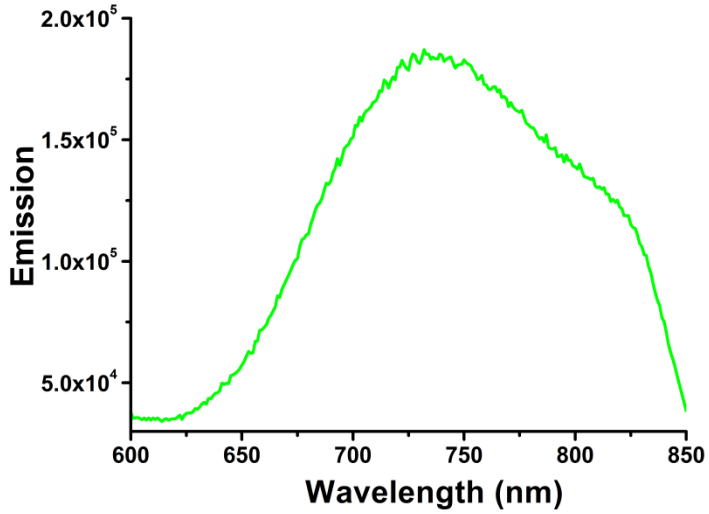

Figure 1.4 Emission spectrum of $Au_{25}(SC_2H_4Ph)_{18}$ nanoparticle, excited at 450 nm, unpublished results.

Functionalized gold nanoclusters exhibit unusual electrochemical reactivities, quantized double-layer charging voltammetry and molecule-like voltammetry.[4] The quantized double-layer charging behaviors can be observed in clusters with relative larger cores, e. g. Au144 nanoparticle, and this will be discussed later in Au144 part. The electrochemical properties of $Au_{25}(SC_2H_4Ph)_{18}$ and ligand exchange product have been probed by Murray and coworkers.[105] **Figure 1.5** shows the voltammetric measurement of $Au_{25}(SC_2H_4Ph)_{18}$ nanoparticles. Basically, for $Au_{25}(SC_2H_4Ph)_{18}$ nanoparticle, voltammetry in CH_2Cl_2 reveals a 1.62 eV energy gap between the first one-electron oxidation and the reduction gap, which corresponds with the sum of the corrected charging energy *ca.* 0.29 eV and the LUMO-HOMO energy gap 1.33 eV. Interestingly, the photoluminescence occurs at energies smaller than LUMO-HOMO gap, and a work

model regarding the correlation of the optical energy gap and electrochemical gap has also been proposed in this report.

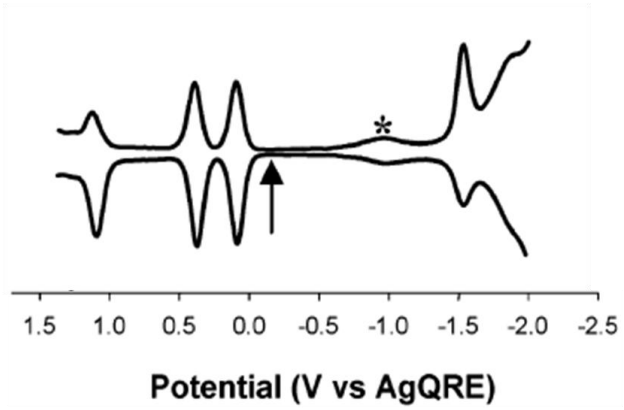

Figure 1.5 Differential pulse voltammogram (DPV) of $Au_{25}(SC_2H_4Ph)_{18}$ in CH_2Cl_2 at room temparature.[119] Adapted with permission from J. Am. Chem. Soc. 2004, 126, 6193-6199. Copyright 2004 American Chemical Society.

Another good example of molecular gold nanoclusters with interesting absorbance, luminescence and electrochemical properties is Au38 nanoparticle. The Au38 nanoparticle passivated by glutathione pertains to 8k Da of molecular mass was first reported by Schaaff et al.[120] However, at that time, the exact composition was not confirmed by MS, since LDI-MS often results in complicated fragments instead of molecular ions. Later on Au-SG cluster compounds from Au11 to Au39, including Au38, have been isolated by polyacrylamide gel electrophoresis (PAGE) by Tsukuda's group.[97] $Au_{38}(SC_6H_{13})_{22}$ has been successfully synthesized through an excess thiol etching method by Quinn's group,[121] and this 8k gold cluster of Au38 protected either by hexanethiolate or dodecanethiolate have also been obtained by Chaki et al. with the structural implication by MS.[122] The size focusing synthesis of $Au_{38}(SC_2H_4Ph)_{24}$ has been developed by Jin's group.[123] In their synthetic strategies, two steps are included: the formation of polydisperse Au-SG clusters and the excess thiol reaction with Au-SG clusters in water-organic phase at high

temperature. Similar work on the facile and large-scale synthesis of $Au_{38}(SC_{12}H_{25})_{24}$ has been documented by them.[124]

Au38 nanoparticles, stabilized by glutathione,[97] phenylethanethiolate,[123] hexanethiolate[121] or dodecanethiolate, exhibit discrete electronic energy states, mainly at ~1050 nm (1.18 eV), ~750 nm (1.66 eV), ~620 nm (2.00 eV), ~560 nm (2.21 eV) and ~520 nm (2.39 eV) with ~0.92 eV band gap. Among them, the most distinct peak is the one at 2.00 eV, which can be considered the distinct one of Au38 nanoparticle. Temperature-dependent emission spectra of $Au_{38}(SC_6H_{13})_{24}$ has been investigated. At room temperature only one emission band at near-IR region was observed, while at low temperature fine structural spectra can reveal at least four bands.[125]

Notably, the Au38 nanoparticle also exhibit different charge states, and electrochemistry provides elegant means to probe the electronic structure and chemical stabilities.[121] $Au_{38}(SC_6H_{13})_{22}$ with charge states of -1, 0, +1, +2 have been characterized by cyclic voltammetry (CV) and differential pulse voltammetry (DPV) by Toikkanen et al.[121] The HOMO-LUMO band gap was around ~1.2 eV, which agrees well with $Au_{38}(SC_2H_4Ph)_{24}$[123] reported by Jin's group.

A structural model of $Au_{38}(SR)_{24}$ has been established by Jiang et al,[126] and density-functional theory calculations have been performed by Aikens and coworkers[127] on the charity and electronic structure of $Au_{38}(SR)_{24}$ nanoparticle. Zeng's group proposed a face-fused bi-icosahedral Au23 core in the structure of $Au_{38}(SR)_{24}$ nanoparticle.[128] The theoretical work advanced the structure and property understanding of Au38 nanoparticle.

Besides Au25 and Au38 nanoparticles, other molecular nanoclusters have also been widely investigated. "Magic number" $[Au_{13}(dppe)_5Cl_2]Cl_3$ clusters have been obtained through a convergence of nuclearity strategy promoted by hydrochloric acid, and very strong near-IR emission was exhibited.[129] The synthesis of atomic precise $Au_{19}(SC_2H_4Ph)_{13}$ nanoparticle has been performed by Wu et al. recently through a combined approach of kinetic control and thermodynamic selection.[130] However, no pro-

nounced absorption can be observed in this cluster. Molecular pure $Au_{20}(SC_2H_4Ph)_{16}$ has been obtained by Zhu et al., and this cluster exhibit pronounced absorption peak at ~485 nm (2.56 eV) and a broad band at ~420 nm (2.95 eV) with a larger LUMO-HOMO band gap of ~2.15 eV.[93] As the crystal structure of the Au20 nanoparticle was not resolved, theoretical predictions done by Zeng's group showed that $Au_{20}(SC_2H_4Ph)_{16}$ nanoparticle may adopt a structure of a prolate Au8 core with new $Au_3(SR)_4$ motif.[131] Recently, the synthesis of Au36 nanoclusters completely protected by the aromatic thiol, $Au_{36}(SPh)_{23}$, has been documented by Dass's group. This nanomolecule shows a peak at ~566 nm (2.20 eV) and two shoulders at ~430 nm (2.89 eV) and ~370 nm (3.36 eV).[132]

$Au_{40}(SC_2H_4Ph)_{24}$, another molecular cluster, which possess ~8 kDa mass reported by Jin's group,[30] has been found to co-exist with $Au_{38}(SC_2H_4Ph)_{24}$. The Au40 nanoparticle was isolated from Au38 nanoparticle through size exclusion chromatography (SEC) and its composition was confirmed by ESI-MS and MALDI-MS. No pronounced absorption peak was observed and the optical band gap is ~1.0 eV, which is comparable with Au38 (0.9 eV). Recent work regarding semi-preparative scale separation of $Au_{38}(SC_2H_4Ph)_{24}$, $Au_{40}(SC_2H_4Ph)_{24}$ and larger clusters by SEC has been recorded by Knoppe et al.[133]

Au55 clusters protected by alkanethiolate with mass around 11 kDa can be obtained by chromatographic isolation in Tsukuda's report.[134] $Au_{55}(PPh_3)_{12}Cl_6$ nanoparticle, with a two core-shell close-packed cuboctahedron structure of Au13 surrounded by 42 gold atoms, was first reported in the early 1980s.[135,136] However, this phosphine-stabilized 1.4 nm gold nanoparticle has limited stability, because the phosphine ligand can dissociate easily. It is worth noting that the reaction of $Au_{55}(PPh_3)_{12}Cl_6$ with hexane thiol or other thiols can lead to the formation of Au75 nanoparticle, typically $Au_{75}(SR)_{40}$.[137]

$Au_{68}(SC_2H_4Ph)_{34}$ nanoparticle has been identified by mass spectrometry during the size-focusing transition process of $Au_{25}(SC_2H_4Ph)_{18}$ nanoparticle formation by Dass's group, however, they were not able to isolate and analyze this molecular nanocluster.[32]

Au102 nanoparticle protected by *para*-mercaptobenzoic acid (*p*-MBA), $Au_{102}(p\text{-MBA})_{44}$, is a water soluble polar cluster with molecular purity. Interestingly, the first report on this cluster is its crystal structure.[138] Note that, this is the first crystal structure of gold nanoparticle. X-ray diffraction is a powerful analytical approach that provides unambiguous information concerning the nanoparticle structure. The single crystal was obtained from a mixture by Kornberg's group in 2007. The 1.1 Å resolution crystal structure is very informative. The central 79 gold atoms in the Au102 core are packed with a markus decahedron and surrounded by the additional layers of gold and sulfur atoms of unexpected geometry "staple motif". Three gold atoms and two sulfur atoms form "staple motif" on the interfacial gold core and monolayer surface, and the Au102 core is an Au79 core protected staple motives. It is worth noting that although the ligand was non-chiral, the nanoparticle exhibited chirality, as two enantiomers alternating in the crystal lattice described in this paper.

The landmark achievement regarding the crystal structure of $Au_{102}(p\text{-MBA})_{44}$ and the revelation of the "staple motif" has greatly influenced the nanogold research community. First of all, the traditional simple Au-S bonding has been challenged by the "staple motif", and this "staple motif" may be the key of the extraordinary stability of these gold nanoclusters. Our research ideas and strategies are based on this "staple motif", which will be discussed later. Numerous reports, especially some theoretical calculation work, have been published to unravel the relationship of "staple motif" and the robust stability. Second, the success of the first crystal structure of gold nanoparticle strongly promoted and stimulated the great efforts of obtaining monodisperse material. A lot of research attention has been devoted to gain monodisperse nanoclusters, accompanying attempts at crystallization.

The synthesis and characterizations of $Au_{102}(p\text{-MBA})_{44}$ nanoparticle on a preparative scale in a high yield has been reported recently by the same group,[139] and this nanoparticle exhibits a featureless exponential decay in absorption spectrum with a small peak at ~260 nm.

The crystal structure of $Au_{102}(p\text{-MBA})_{44}$ immediately triggered a lot of research interest in theoretical calculations. Ab initio study of $Au_{102}(p\text{-MBA})_{44}$ on this cluster to model the electronic structure has been performed by Gao et al,[140] and Li et al. presented the first principles, density functional theory calculations of the structural and electronic properties of this cluster in 2008.[141] Based on this crystal structure, chemical analysis of the super-atom model of thiol-stabilized gold nanoparticle has been documented to gain the insight of the thermodynamic stability.[142] The electronic and vibrational signatures of $Au_{102}(p\text{-MBA})_{44}$ nanoparticle has been performed recently by Hakkinen and coworkers.[143]

The next molecular gold nanocluster will be discussed later is Au144 nanoparticle. $Au_{144}(SR)_{60}$ nanoparticle was previously assigned or reported as $Au_{(144\text{-}150)}(SR)_{(50\text{-}60)}$, which corresponds with 29 kDa mass. It was first revealed by MS by Schaaff et al.[144] and Chen et al.[145] Murray's group and Quinn's group described the quantized double-layer charging behaviors, which will be discussed separately in the next paragraph. Chaki et al. obtained dodecanethiolate protected Au_{144} nanoparticle and assigned the molecular composition as $Au_{144}(SC_{12}H_{25})_{59}$ by LDI-MS.[122] Qian et al. reported a facile, two step synthetic method to prepare monodisperse $Au_{144}(SC_2H_4Ph)_{60}$ nanoparticle,[92] which shows prominent absorption bands at ~510 nm (2.44 eV) and ~700 nm (1.78 eV). By following the method they reported, monodisperse $Au_{144}(SCH_2CH_2Ph)_{60}$ has been synthesized successfully, and the absorbance of Au144 is presented **Figure 1.6**. Step-like absorbance band at ~510 nm and ~695 nm can be observed, which is at least comparable, if not better defined as reported.[92]

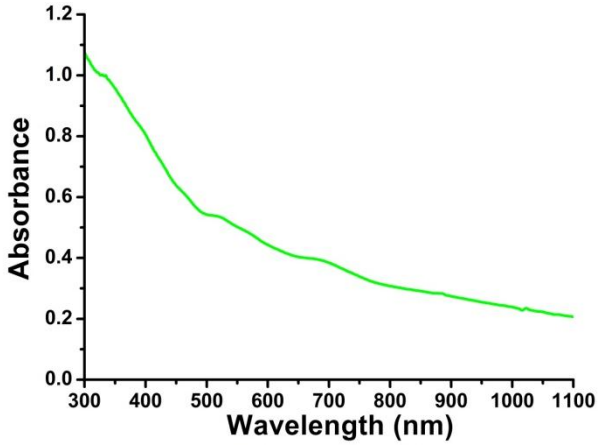

Figure 1.6 Absorbance spectrum of $Au_{144}(SCH_2CH_2Ph)_{60}$ nanoparticle, unpublished results.

Gold nanoclusters with core diameter less than 2 nm exhibit very small effective capacitance (C), which leads to single electron changes in the core occur at large voltage intervals (V=e/C), hence quantized double-layer charging happens.[146,147] The electronic charging behaviors of the high monodisperse Au144 nanoparticle protected by hexanethiolate, governed by electrical doubler layer properties, have been reported by Murray and coworkers,[148] as shown in **Figure 1.7**. The extraordinary electrochemical resolution of 15 oxidation states of this nanoparticle has been recorded by Quinn's group.[149]

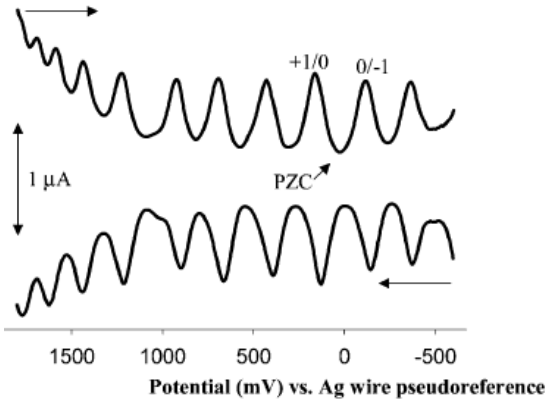

Figure 1.7 Quantized double-layer charging behaviors of Au_{144} nanoparticle protected by hexanethiolate.[148] Adapted with permission from J. Am. Chem. Soc. 2002, 124, 13322-13328. Copyright 2002 American Chemical Society.

For nonpolar gold clusters, the Brust-Schiffrin biphasic synthetic method offers a straightforward way to prepare nonpolar ligand stabilized Au NPs. For the polar gold clusters, Brust-like syntheses use water soluble functional thiols such as tiopronin,[88] glutathione (SG),[22] poly(ethylene glycol) (PEG)[150,151] and *para*-mercaptobenzoic acid (*p*-MBA)[138] etc. The best examples of molecular water soluble gold nanoclusters are the well studied $Au_{25}(SG)_{18}$[29,97,152] and $Au_{102}(p\text{-MBA})_{44,}$[138,139,143] which have been discussed above. Ackerson et al. summarized and screened 36 water-soluble organothiolates for their ability to form water-soluble MPCs in 2005.[153] Aggregation-resistant water soluble gold nanoparticles stabilized by zwitterionic ligands have been produced by Schlenoff's group.[154] The preparation and the properties of water-soluble gold nanoparticles protected by perfluorinated amphiphilic thiolates have been described by Pasquato and coworkers.[155]

One interesting water-soluble Au nanoparticle is tiopronin protected gold MPCs that are unfortunately polydisperse. The average composition of this gold clusters has been determined as $Au_{201}(Tiopronin)_{85}$ with core diameter of ~1.8 nm.[88] The size of the nanoparticle can be tuned by varying the ligand-to-gold ratio during the synthesis as demonstrated by the size-dependent absorbance. **Figure 1.8** shows the absorbance and emission spectra of 3X tiopronin MPCs, while X represents the ligand-to-gold ratio. The absorbance shows an exponential decay with two small bumps at ~260 nm and ~350 nm, while broad emission band rangies from 650 nm to 850 nm and even higher wavelength. The quantum yield is roughly ~0.1%.[116]

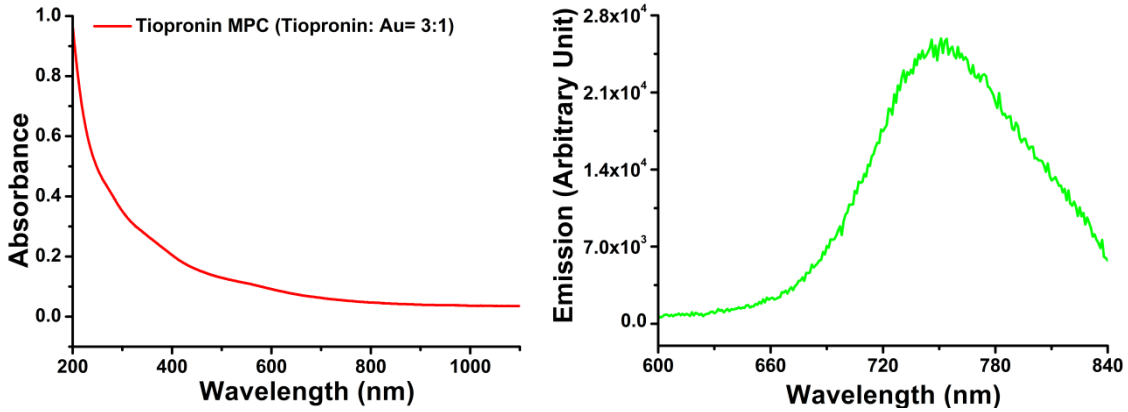

Figure 1.8 Absorbance and emission spectra of 3X tiopronin MPCs. Left: Absorbance spectra, Right: Emission spectra.

Interestingly, the nanoparticle size can be controlled by altering the ligand-to-gold ratio during the synthesis, and the optical behaviors such as absorbance are size-dependent due to the size confinement effects. As we know, with higher ligand-to-gold ratio employed in the synthesis, smaller sized particles are obtained. The nanoparticle formation is a core agglomeration process while more excess thiol can passivate the gold surface hence terminating the process at the initial stage to form smaller particles. **Figure 1.9** presents absorbance spectra of tiopronin MPCs with different ligand-to-gold ratios. The 1X sample display a band at around 522 nm, which is called surface plasmon band (SPB) and will be discussed in the next paragraph. The UV absorbance of the 3X and 100X sample decays in approximately an exponential fashion into visible, with no detectable SPB. Note that a much sharper decay occurs in the 100X sample than the 3X sample, indicating smaller core size in average. In fact, the core diameter of 1X sample is ~3.9 nm core diameter, 3X sample is ~1.8 nm while 100X is probably less than 1 nm.

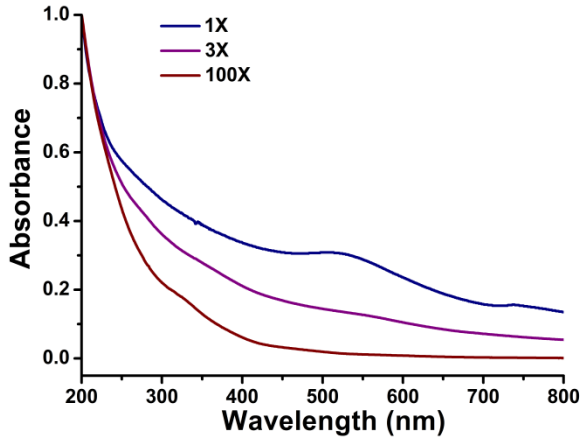

Figure 1.9 Absorbance comparison of tiopronin MPCs, 1X, 3X and 100X (X= ligand-to-gold ratio).

Surface plasmon band (SPB), reflected physically as a red deep color of gold nanoparticle solution, normally appears at about 520 nm. The mechanism of the band is believed to be due to the electron collective oscillation at the nanoparticle surface, which correlates the electromagnetic field of the incoming light.[1] The characterizations of the SPB are as follows: 1. it normally shows at around 520 nm, but the position is size dependent for nanoparticle larger than 2 nm, 2. the intensity decreases as the core size decreases for Au NPs with 1-5 nm core diameters because of the onset of the quantum confinements. The position and width of SPB are also influenced by the particle shape, solvent used, dielectric constant of the solvent, temperature and so on. The SPB is absent for bulky gold as well as Au NPs with core diameter less than 2 nm. Recent experimental results demonstrated that the critical size for the observation of quantum confinement of gold clusters is ~2.2 nm.[156]

1.2 Au NPs Used in Catalytic Regime

Bulk gold was thought to be catalytically inert for a long time.[157,158] However, the first breakthrough of nanogold catalysis was made in 1987 by using gold nanoparticles mixed with supported transition-metal oxides as the catalyst for the oxidation of carbon monoxide.[159] Since then, nanogold cataly-

sis has become a hot topic in chemistry and significant progress of heterogeneous gold nanocatalyst has been achieved. In 1998, the investigations made by Valden and coworkers regarding the onset on the catalytic activity of gold cluster on titania revealed that supported gold clusters might be valuable catalyst for CO oxidation or other reactions.[160] In the last decade, especially the last 5 years, the main focus of nanocatalysis has been on the study of the reactivity of small gold nanoparticles, hence called "Gold-Rush" Era.[161,162] The identification of active gold nanoclusters on iron supports on CO oxidation has been performed by Hutchings's group, and the high catalytic activity was correlated to the small clusters with diameter of ~0.5 nm with ~10 gold atoms contained.[163] The following study on iron-supported gold cluster catalysis demonstrated that, it was not mandatory for gold clusters with diameter of ~0.5 nm to gain high activity.[164] Very low temperature CO oxidation by heterogeneous colloidally deposited gold clusters on MgO or $Mg(OH)_2$ has been achieved as demonstrated by Jia et al,[165] and charge-mediated adsorption behaviors of CO on MgO-supported gold clusters have been found to play an important role in the catalytic process.[166]

Besides CO oxidation, gold clusters supported by transition metal oxides have also been found to be exceptionally active in various organic reactions, including hydrogenation, selective oxidation, nucleophilic additions, alkylation, carbon-carbon coupling reactions and so on.[167-169] Propene epoxidation with dioxygen catalyzed by Al_2O_3 or TiO_2 supported gold clusters has been documented.[170] TiO_2 supported gold clusters with 1.3 nm core diameter have been found to be markedly effective catalyst as hydrogen dissociation.[171] The demonstration of a new and green catalyst of gold nanoclusters supported by inorganic materials hydrotalcite for de-oxygenation of a diverse range of epoxides has been exploited,[172] meanwhile room-temperature de-oxygenation of epoxides with CO catalyzed by hydrotalcite supported gold nanoparticles in water was recorded.[173] Recent findings indicated that hydrotalcite supported gold clusters can selectively catalyze the de-oxygenation of the epoxides in the presence of molecular hydrogen as the reducing agent to form alkene through a concerted effect between gold nano-

particle and basic sites on a support.[174] The heterogeneous catalyst of TiO_2 or Al_2O_3 supported gold clusters has been reported dominating the process of sonogashira coupling reaction.[175] Gold nanoparticle supported on TiO_2 catalyzing the unprecedented oxidative cycloaddition of 1,1,3,3-tetramethyldiloxane to alkynes at R. T. and at very mild conditions has been published recently.[176]

In addition to heterogeneous catalyst, significant progress has also been made on the catalytic efficiency, selectivity, recovery and recyclability of homogeneous catalyst. To gain the mechanistic insight of the catalytic process, especially to unravel the relationship between the structure and property of the catalyst and the catalytic activity, homogeneous catalytic materials are prerequisite. Upon this goal, a great deal of research attention has been directed to obtain monodisperse gold nanoclusters as catalyst.[177] Gold nanoclusters stabilized by a hydrophilic polymer, poly(N-vinyl-2-pyrrolidone) (PVP: $(C_6H_9ON)_n$), with core diameter of 1.5 nm and 2.2 nm produced by conventional batch method have been employed as catalyst of aerobic oxidation of benzylic alcohol in water at ambient temperature by Tsukuda's group.[178] Size effects have been observed, indicating oxygen adsorption plays a key factor in catalytic process. Later on, the microfluidic synthesis and catalytic applications of PVP stabilized ~1 nm gold clusters has been reported.[179] The follow-up investigations on the catalyst made of gold nanoclusters stabilized by PVP, revealed that electronic structure of the gold clusters is directly related to the catalytic performance, as the enhanced catalytic activity corresponds with increasing negative charge on the core.[180] This aerobic oxidation reaction of benzylic alcohol catalyzed by reusable and durable gold nanoclusters with less than 4 nm dimension stabilized by well defined vinyl ether star polymer has been recorded.[181] Other effects on catalysis such as Ag doping on catalytic activity of this PVP-stabilized gold clusters has also been investigated.[182] Polymeric thiolate-ligand poly-(2-aminothiophenol) (PATP) stabilized gold nanoparticles have demonstrated unexpectedly high catalytic activity for Suzuki-Miyaura cross coupling reaction of aryl halides and arylboronic acid in water, and great recovery and reusability have

been described.[183] Other gold nanoparticle nanocatalyst employing polymer as the stabilizer has also documented.[184]

A recent research focus of the gold nanocatalysis community is the synthesis of monodisperse gold nanoclusters with precise number of atoms and their exploration on catalytic behaviors. Selective oxidation of styrene to benzaldehyde, styrene epoxide and acetophenone by $Au_{55}(PPh_3)_{12}Cl_6$ nanoparticle on inert support has been described.[185] In this report, a size threshold effect in catalytic activity has been found, that is, particles with diameters of ~2 nm and above were completely inactive. $Au_{25}(SC_2H_4Ph)_{18}$ nanoparticle demonstrated the remarkably strong capability of the chemoselective hydrogenation of α, β-unsaturated ketones and aldehydes to unsaturated alcohols with near 100% selectivity.[186] The speculative mechanism is that electron-rich Au_{13} core can facilitate the absorption and activation of the C=O bond. Efficient and selective epoxidation of styrene with *tert*-butyl hydroperoxide (TBHP) catalyzed by $Au_{25}(SG)_{18}$ on hydroxyapatite (HAP) has been exploited with 100% conversion and 92% selectivity.[187] The exploration of thiolate-protected $Au_n(SR)_m$ nanoparticles as catalysts for selective oxidation and hydrogenation processes of styrene have been performed and the molecular clusters included $Au_{25}(SC_2H_4Ph)_{18}$, $Au_{25}(SC_6H_{13})_{18}$, $Au_{38}(SC_2H_4Ph)_{24}$, $Au_{38}(SC_{12}H_{25})_{24}$, $Au_{144}(SC_2H_4Ph)_{60}$ and $Au_{144}(SC_{12}H_{25})_{60}$.[188] Similarly, Au_n clusters (n=10, 18, 25, 39) with atomically controlled size on hydroxyapatite (HAP) as catalysts for selective oxidation of cyclohexane to cyclohexanol and cyclohexanone has been investigated recently by Tsukuda and coworkers, and they found Au_{39} cluster demonstrated the best catalytic activity.[189]

Interestingly, the aggregation of gold nanoparticle also plays an important role in catalytic activity. In a recent published report of hydrosilylation reaction, when exposed to UV irradiation, the particles aggregate and catalysis is effectively switched off, and when exposed to visible light, the particles redisperse and regain the activity.[190]

1.3 Au NPs Used in Biomedical Applications

The use of nanomaterials merges with biology and medicine, hence a new cutting-edge science and technology burgeons as nanomedicine. In the past twenty years, the biomedical applications of nanoparticles have been a hot subject, reflected by the explosive growth of the related publications. The unique chemical and physical properties of the nanoparticles provide them with a fantastic platform to be engineered in the biological systems. The nanoparticles widely employed in biomedicine regime include: quantum dot, e. g. CdS, silica nanoparticles, e. g. SiO_2, metal oxide, e. g. Fe_3O_4, magnetic nanoparticles, e. g. FePt, novel metal nanoparticles, e. g. gold or silver nanoparticles, polymeric nanoparticles, e. g. nanogel and so on.[191]

Among all sorts of nanoparticles, gold nanoparticles command a great deal of attention in biomedical applications. Several review papers are summarized as references.[192-197] Au NPs have been considered a “gold standard” to evaluate the biological response by National Institute of Standard and Technology (NIST). First, gold nanoparticles, either nanocrystal or colloid, can be obtained by easy synthetic approaches, and their synthetic methods are reliable, reproducible, and often accompanied with high yields. The resulting nanoparticles are robust with high stabilities, easily isolated or separated, and can be handled like small organic molecules. The sizes and shapes of such nanoparticles can also be altered by controlling the synthetic thermodynamics or kinetics. Second, gold nanoparticles hold a lot of attributes that are suitable for biomedical applications. These attributes include unique size comparable to bio-molecules, e. g. DNA, protein, bio-polymers; rich optical properties such as absorbance, fluorescence, special electronic features, e. g. surface plasmon excitations; and high surface area to volume ratio for biomolecule loading or targeting. Third, Au NPs hold tunable enriched surface functionalities. The monolayer can be readily modified with ligands containing functional groups, such as thiols, phosphines, and amines. Additional moieties can be anchored to the ligands through these functional groups, and such moieties like oligonucleotides, proteins, peptides, antibodies and polymers can be used to fur-

ther impart the particles with even greater functionalities. The as-formed nanoconjugates or nanocomposites have engineered the nanoparticles with a wide range of investigations, which express great potential in biology and medicine. Fourth and the most important point for biomedical applications, Au NPs are biocompatible with low toxicities. In most reported experimental results, gold nanoparticles exhibit relativity low or even no acute cytotoxicities,[198] which will be discussed further separately. The toxicities of nanoparticles for biomedical applications have been attracting great attention in both basic research, pharmaceutical industry and the society.

The potential applications of engineered gold nanoparticles include: drug or gene delivery, imaging contrast agents, biosensors or biolabeling, surface enhanced raman scattering (SERS), cancer treatments and photothermal therapy, and so on.

1.3.1 Au NPs as Drug-Delivery Systems (DDS)

Drug-delivery systems (DDS) are drug carriers, which can carry or transport drugs to designated destinations. DDS can significantly enhance the efficacy of the pharmaceutical payloads, not only by improving the solubility, stability and the pharmacokinetics of drugs, but also by the interaction with specific tissues and cell types through the functionalized ligands.[199] To deliver the drug precisely and safely to its targeted sites, DDS must be designed to be capable of providing prolonged blood circulation, endosome and lysosome processes, and controllable drug release at designated sites.[200]

Gold nanoparticles can be used as DDS, mainly due to the ligand on the monolayer can hold covalent attachment to the drug to form bio-conjugates. Au NPs are great candidates for DDS because of the many desirable attributes. Au NPs are non-toxic, and can be easily and reproducibly obtained with a wide size range of 1.0 nm to 10 nm and even larger. Moreover, Au NPs are stable and have large surface area for efficient drug targeting and ligand conjugation.

The binding of the hormone insulin to gold nanoparticles and its application in transmucosal delivery for the therapeutic treatment of diabetes in Wistar rats have been documented.[201] A glutathione-mediated delivery and release system in vivo and in cell culture by mixed-monolayer protected gold nanoparticles has been established by Rotello and coworkers.[202] A highly efficient drug delivery vector system, which consists of PEGylated gold nanoparticle conjugates as a water-soluble and biocompatible cage, that allows delivery of a hydrophobic drug to its site of photodynamic therapy action has been developed.[203] The subsequent mechanistic and pharmacokinetic investigations demonstrated that the photodynamic therapeutic drug was able to penetrate into tumors, which further highlighted the attractiveness of the non-covalent drug-Au NPs as DDS.[204,205] A delivery vehicle based on polyvalent oligonucleotide and gold nanoparticle conjugates for cancer cell targeting platinum (IV) compounds has been devised by Mirkin's group.[206] Using gold nanoparticles as cage and carrier, anti-cancer drug can be delivered into the tumor tissues, with controlled release through UV irradiation.[207] Hydrophobic dyes or drugs can be entrapped in a hydrophobic pocket in the monolayer of Au NPs and released into tumor cell by membrane-mediated diffusion without the uptake of the nanoparticle carrier.[208] And the small sized nanocarriers with biocompatible surface functionalities can provide long circulation lifetime and preferential accumulation in tumor tissues by the enhanced permeability (EPR) effect.[209] The intracellular delivery of a membrane-impermeable enzyme has been promoted by functionalized gold nanoparticle coated with a short peptide, and it is worth noting that, the transported enzyme can escape from endosomes and retain its biological activity.[210] The payload of the delivery in tumor cylindroids can be tuned by the surface charge of the gold nanoparticle.[211] Positively charged particles improved delivery of payloads to most cells in tumor, whereas negative ones performed better when delivering drugs into tissues. A widely administered breast cancer treatment drug, Tamoxifen, conjugated with thiol-PEGylated gold nanoparticle has been created for enhanced potency and selective delivery for breast cancer treatment in vitro.[212] The active component of oxaliplatin, an anticancer drug, was able to pene-

trate the nucleus into the lung cancer cells by a complex formation between the platinum from the drug and the carboxylate group from the functionalized thiolated poly(ethylene glycol) (PEG) monolayer of gold nanoparticles.[213] The kinetics of short-distance drug release from nanocarriers to nanoacceptors based on a new gold nanoparticle model has been probed.[214]

1.3.2 Au NPs as Imaging Contrast Agents

Recent advances in nanotechnology and biomedicine have expanded our ability to design and construct functionalized nanomaterials that combine targeting, therapeutics, and diagnostic functions. The past decade has witnessed tremendous progress made in facilitated nanomaterials for molecular imaging.[215] Several types of nanomaterials have demonstrated their capabilities in biomedical purposes, including liposome, micelle, dendrimers, metal nanoparticles, carbon nanotubes, quantum dots, silica nanoshells, iron oxide nanocrystals and so on.[216]

Among these nanomaterials, gold nanoparticles have attracted a great deal of research interest in molecular imaging thanks to their easy synthetic accessibility, flexible surface functionalizations and most importantly their non-toxic nature. Magnetic resonance imaging (MRI), one of the most powerful non-invasive medical imaging techniques used in clinical diagnosis, currently suffers from the low sensitivity and invalid efficiencies. The contrast agent most widely employed is gadolinium chelates such as DTPA: Gd (DTPA: diethylenetriaminepentaacetic acid). Gold nanoparticles protected by a novel dithiolate ligand (DTDTPA), whose multilayer allows complexation of a significant amount of paramagnetic gadolinium have been devised as a type of very attractive contrast agent for MRI, since more pronounced enhancement effects were observed from each particle in contrast to single DTPA: Gd chelate.[217] Gold nanoparticle has also demonstrated great potential in X-ray imaging. Current iodine-based agents such as tri-iodobenzene impose several limitations on medical imaging: short imaging time, occasional renal toxicity, and poor contrast effect in large patients. Gold nanoparticles with 1.9 nm di-

ameter can be used as contrast agent with properties that overcome several of those limitations.[218] Functionalized gold nanoparticles applied as contrast agents for both in vivo X-ray tomography and MRI has been recorded.[219] The gold cores of those nanoparticles were encapsulated with a multilayered organic shell that is composed of gadolinium chelates. The gold core provided strong X-ray absorption, while the contrast enhancement in MRI stemmed from the gadolinium ions entrapped in the organic shell. Recently, tumor targeting gold particle nanoprobes for CT/optical imaging of cancer has been reported.[220] The gold nanoparticle was not only modified with glycol chitosan polymer for enhanced permeation retention effect, but also chemically conjugated to matrix metalloproteinase activatable peptide for specific tumor targeting.

1.3.3 Au NPs as Biosensors, Biolabeling Agents

The combination of nanotechnology with biology, medicine and pharmaceutical science to develop ultrasensitive detection of biomolecules such as DNA, protein, bacterial is of ever-increasing importance in the last decade. Gold nanoparticle based biosensors are extremely attractive in biological and pharmaceutical field, probably due to their unique optical properties (e. g. surface plasmon resonance absorption, resonance light scattering), tunable surface coatings and excellent biocompatibilities.[221]

The surface plasmon resonance (SPR) originates from the collective oscillation of electrons in resonance with incident electromagnetic radiations.[1] For gold, the oscillation resonance frequency is governed by its bulk dielectric constant. Since the gold nanosphere has a high surface-to-volume ratio, the frequency is exquisitely sensitive to the dielectric nature of its interface.[221] Any change to the environment of gold nanoparticle (particle aggregation, monolayer surface modification, local medium change, etc.) leads to colorimetric changes, which is accompanied with the distinct color change of the gold nanoparticle dispersion. Therefore, gold nanoparticle based colorimetric biosensors have been widely exploited and found a great deal of applications.

The design of colorimetric metal sensors based on DNAzyme-directed assembly of gold nanoparticles and their use for sensitive detection and quantification of metal ions, particularly lead, has been described by Lu's group.[222] Subsequently, they expanded this methodology, and a colorimetric adenosine biosensor based on aptazyme-directed assembly of gold nanoparticles has been reported.[223] A new approach to colorimetric kinase activity screening to detect kinase inhibitor has been developed based on kinase-catalyzed modification of gold nanoparticles.[224] Highly sensitive and selective colorimetric sensors for unalyl (UO_2^{2+}) have been created by labeled and label-free DNAzyme-Gold nanoparticle systems.[225] A gold nanoparticle-based colorimetric biosensor for sensitive and visual detection of sequence-specific DNA-binding protein has been documented.[226] Multifunctional gold nanoparticle dendrimer-based surface plasmon resonance sensor has been fabricated for improved insulin detection.[227] Fluorosurfactant-capped gold nanoparticles have been employed for colorimetric detection and inhibition of S-Adenosylhomocysteine hydrolase.[228] Assembled supramolecular gold nanoparticles can be used as optical probes for protein detection when the state of aggregation was modulated by the enzyme urease as a label for an immunoassay.[229] Colorimetric detection of HIV-1 ribonuclease H activity by gold nanoparticle has been performed with fast assay response.[230] Gold nanoparticle-antibody conjugates based localized surface plasmon resonance (LSPR) biosensor has been developed to obtain signal enhancement, which might pave a way for single molecule detection and clinically relevant diagnosis.[231] A colorimetric assay uses gold nanoparticle plasmon absorption to realize quick detection of β-agonists from liquid samples has been reported recently.[232]

Rotello and coworkers developed the concept of "chemical nose" or "chemical tongue"[233,234] based on gold nanoparticle. Gold nanoparticles, accompanied with rich physical and optical properties, bear commensurate sizes with bio-macromolecules. Thanks to the tunable surface modifications and other interactions, gold nanoparticles can easily be connected with other molecules covalently or non-covalently, thus forming an array, which could be designed to bind selective receptors, such as protein,

bacteria and mammalian cells. That array-based sensor with nanoparticles is “chemical nose” or “chemical tongue”. A chemical nose/tongue made of gold nanoparticle-polymer conjugates have been developed as a rapid and effective array based approach to differentiate normal and cancerous cell lines.[235] The method based on positively charged gold nanoparticles and negatively charged green fluorescent protein (GFP) formed array for identifying different types of mammalian cells have been described as a chemical nose/tongue.[236] Enzyme-gold nanoparticle array based sensor has been employed for the sensing of protein with very high sensitivity because of the enzymatic amplification.[237] A colorimetric enzyme-gold nanoparticle conjugate system has been developed as chemical nose/tongue for bacterial sensing recently, and the bacterial concentration can be quantified.[238]

Gold nanoparticle based probes or biosensors have also found other versatile applications in biomedical areas. A microarray based on gold nanoparticle-phosphorylated peptide conjugate with high sensitivity and selectivity for kinase functionality and inhibition has been developed.[239] An integrated sensing system comprised of self-assembled glucose oxidase and an osmium molecular wire on core-shell gold nanoparticles has been devised to respond to millimolar glucose concentration in solution.[240] A novel high-throughput gold nanoparticle probe has been created as a microarray to study carbohydrate-protein interactions.[241] Gold nanoparticle combined with aptamers bearing highly specific molecular recognition properties has been developed as a dry-reagent strip biosensor that enabled qualitative and quantitative detection of protein within minutes.[242] Strong signal enhancement has been acquired in electrical detection of oligonucleotide by using aggregates of gold nanoparticle instead of single gold nanoparticle as conductive tag.[243] A single gold nanoparticle tracking-based method on a supported lipid bilayer platform has been developed for detecting and quantifying molecular binding to membrane receptor-binding targets.[244] A multispot gold-capped nanoparticle array chip has been fabricated to detect the most corneal dystrophies successfully.[245] Diagnostic detection of human lung cancer-associated antigen by a gold nanoparticle-based immunosensor has been performed.[246] A simple, fast and sensitive

approach for visual detection of single nucleotide polymorphism based hairpin oligonucleotide-functionalized gold nanoparticle has been reported.[247] A novel high-throughput toll to screen lectin-binding specificity of bacterium by gold-nanoparticle-labeled lectin-microarray based assay has been developed.[248] Mixed stimuli-responsive magnetic and gold nanoparticle system has been utilized for rapid purification, enrichment and detection of protein biomarkers from human plasmon.[249] Single gold nanoparticles have been successfully employed as real-time optical probes for detection of intracellular metabolic enzymatic pathways recently.[250]

Gold nanoclusters with strong fluorescence, such as near infrared photoluminescence, make them potential labels for biologically motivated experiments.[194] Gold clusters have less significant cytotoxic effects than commonly used CdS/CdSe quantum dots, which make them as potential alternatives as biological labeling agents. The gold clusters capped with dihydrolipoic acid (DHLA) conjugated with biologically relevant molecules such as PEG, BSA, avidin, and streptavidin has been applied to label fixed cells specifically.[251] The use of camera cell phone to detect the gold nanoparticle-labled immunoassay results on microfluidic chip has been described.[252] With the combination of gold nanoparticle labeling, monoclonal antibody recognition and inductively coupled plasma mass spectrometry detection, a rapid assay has been demonstrated for *E. Coli* with high sensitivity and specificity.[253]

1.3.4 Au NPs for Surface-Enhanced Raman Scattering (SERS)

Surface-enhanced raman scattering is probably one of the most widely pursued spectroscopic techniques, mainly because it can identify the “fingerprint” region through the characteristic vibration frequency of a specific molecule.[193] The current generally accepted mechanisms include surface electromagnetic field enhancement and chemical contribution.[193] Nanomaterials have been employed as surface enhancers for raman scattering, and gold nanoparticles are ideal candidates because of their plasmonic properties. Specifically, gold nanoparticles contain free electrons that can be collectively and

resonantly excited at optical frequencies, which leads a larger electromagnetic enhancement near the nanoparticle surface.[254]

A unique gold nanoparticle aggregate has been shown as excellent substrate for SERS applications for detection of rhodamine 6G in 2004.[255] An effective architecture of DNA-bridged gold nanoparticle assemblies for detection of sequence-specific protein-DNA interactions via SERS has been created in 2007.[256] Colloidal gold nanocrystals coated by thiolated block polymers have been engineered as stimuli-responsive SERS nanoparticles, and the plasmonic coupling and surface raman enhancement can be controlled by conformational change.[254] A label-free, highly selective and ultra sensitive SERS probe for TNT recognition has been demonstrated based on citrate capped gold nanoparticle.[257] The physical origins of chemical enhancement of SERS have been investigated using a gold nanoparticle coated polymer substrate.[258] The detailed structure-activity relationships in gold nanoparticle dimers and trimers for SERS has been investigated.[259] Aptamer-conjugated popcorn-shaped gold nanoparticles have been employed for targeted diagnosis, therapy treatment and in-situ monitoring of photothermal therapy response of prostate cancer cell by using SERS.[260] SERS has also been extended to non-traditional substrates, and the most notable is tip-enhanced raman scattering (TERS) where a gold tip acts as the raman signal amplifier. Instead of a gold tip, gold nanoparticle with monolayer coated an ultrathin shell of silicon or aluminia has been reported. Such a shell mode possesses many virtues, for example, ultrahigh detection sensitivity, no direct contact with probed substrate and vast practical applications to various materials with diverse morphologies.[261] A method for ratiometric surface enhanced raman quantification of ligand adsorption onto a gold nanoparticle has been developed.[262] The synthesis, self-assembly and applications to SERS of chiral ionic liquid monolayer-stabilized gold nanoparticle has been reported.[263] Magnetic capture of raman-active gold nanoparticle for SERS detection of DNA derived from the west nile virus genome has been recorded.[264] A label-free ascorbic acid coated gold nanoparticle based SERS assay for direct cyanide detection at 110 ppt level has been established recently.[265]

1.3.5 Au NPs for Cancer Treatments and Photothermal Therapy

In the past decades, significant progress has been made on enabling nanomaterials to target cancer treatment. Nanomaterials, especially nanoparticles, have somehow revolutionized nanomedicine at three levels,[266] drug delivery systems, which has been discussed above, tumor contrast imaging agents, which has also been discussed previously and early detection of cancer cells, which will be discussed in this part. Among all the nanomaterials employed in biomedical applications, gold nanoparticle has demonstrated great potential for cancer treatment, and great efforts on animal study and early clinical testing are currently underway.[267]

Early investigations on the intracellular uptake of different sized and shaped colloidal gold nanoparticles showed that kinetics and saturation concentration are highly dependent on the physical dimensions of the nanoparticles.[268] Nanoparticle tumor targeting efficiency has been examined systematically, while the physical and chemical properties of the nanoparticles influence their pharmacokinetic behavior, which ultimately determine their accumulation capacity.[269] The application of small organic molecule coated gold nanoparticles as effective inhibitors of human immunodeficiency (HIV) fusion has been reported.[270] Glycan encapsulated gold nanoparticles have been designed and synthesized to selectively inhibit Shiga Toxin 1 and 2.[271] A new apoptosis imaging probe in live cells based on a near-infrared dye-gold nanoparticle composite has been fabricated.[272] A method of local laser hyperthermia with gold nanoparticles under noninvasive optical monitoring of nanoparticle accumulation in tumor tissue in vivo has been developed.[273] The dynamics of cellular uptake and nanoscale localization of gold nanoparticles in cancer can be measured by using label-free confocal raman microscopy.[274] High fidelity amplification of telomerase products form concentrated cell lysates can be directly measured by using 12 nm gold nanoparticles, which are attached to the telomere strand primer.[275] The ability of near-infrared absorbing gold/gold-sulfide nanoparticles to ablate tumor cells for photothermal cancer therapy has been demonstrated.[276] Gold nanoparticles capped with mercaptoethanesulfonate has been employed as ef-

fective inhibitors for HSV-1 attachment, entry and cell-to-cell spread.[277] Quantitative evaluation of cellular uptake and trafficking of plain and polyethylene glycol-coated gold nanoparticles has been conducted.[278] Sub-nanometer gold quantum dots have been engineered with functionalized peptide to function as molecular probe for the real-time monitoring of cellular apoptosis.[279] Supramolecularly assembled gold nanoparticle has been synthesized to enhance photothermal effects and been employed to demonstrate the targeted photothermal treatment of a subpopulation of cancer cell through target-specific ligands.[280] Light-triggered release of DNA from gold nanoparticle-based plasmon resonant nanoshell could be visualized in live cells, which could be of great promise for gene or drug delivery.[281] Fluorescent gold nanoclusters stabilized by lipoic acid derivatives as a biocompatible marker for in vitro and in vivo tracking of endothelial cells has been investigated.[282] The study of the therapeutic efficacy of multifunctional gold nanoparticles, which can carry heat and drugs specifically to tumors through active targeting has been performed.[283] Recent research efforts demonstrated that gold nanoparticle uptake in live cells can be visualized through liquid scanning transmission electron microscopy.[284] DNA-gold nanoparticle hybrid conjugate has been employed for the ultra-selective detection of a single-base mutation in the breast cancer gene type 1 susceptibility protein.[285] A multi-functionalized nano-construct based on gold nanoparticle has been employed to lead neuroblastoma cells to die by multiple pre-mediated attacks recently.[286]

1.3.6 Nanotoxicity of Au NPs in Biomedical Applications

As an emerging and cross-disciplinary technology, nanotechnology has undergone an explosive growth in the past decade. As this technology continues to mature and thrive in the future, the consumption of more and more products containing nanomaterials can be envisioned. On the other hand, concerns from either individuals or organization regarding the risk to health still exist and such “fear” can’t be completely removed unless the “nanotoxicity” issue is justified. In fact, nanotoxicology, has be-

come an interdisciplinary challenge, which demands further sustainable developments.[287] It is worth noting that, because of the so-called "knowledge gap" in nano-toxicity area, some misconceptions regarding the use of nanomaterials has been perceived in public and individuals to some extent.[288] For example, due to the lack of reliable data on nanoparticle types, a perception that many nanoparticles are inherently hazardous has been fostered.[288] In fact, the type of nanoparticle, shape, concentration, dosage, different cell lines nanoparticle exposed to, the time span of exposure, different experimental conditions, all of these factors, play an important role in nanotoxicities of those nanomaterials.[289]

Specifically, as gold nanoparticles hold an expansion of potential biomedical applications as discussed above, the understanding of their human safety concern becomes quite necessary. In an earlier report, the spherical gold nanoparticles with a variety of modifiers can be taken up by human cells but did not cause acute cytotoxicity, although the precursors of nanoparticles may be toxic.[198] Although a significant number of papers regarding the in-vitro and in-vivo bio-distribution and toxicity of gold nanoparticles are available in literature, the correlation between nanoparticle itself and biological effects have not been established, mainly due to the significant discrepancy on experimental conditions under which the biological effects and toxicity were evaluated.[290] A recent review paper summarized the in-vitro and in-vivo studies of toxicity of gold nanoparticles.[290] In this review, colloidal gold with different sizes, different shaped nanoparticles (sphere, rod, etc.), different surface coating, different cell lines or animals employed, the dosage and exposure duration as well as the different methods used have been examined. Interestingly, some data on gold nanoparticle toxicity have been found to be contradicting so far.[290] For gold nanoclusters, it is worth noting that the unexpected toxicity of monolayer protected nanoclusters can be eliminated by PEG-thiol place exchange reactions, which highlights the importance of monolayer in the biological effects of nanocluster.[291]

1.4 Au NPs Used in Other Areas

Besides the catalytic regime and biomedical application area, gold nanoparticles or nanoclusters have also found great potential applications in other areas. In matrix-assisted laser desorption ionization –mass spectrometry-time of flight (MALDI-MS-TOF) studies, gold nanoparticles have been employed as assisted matrix to resolve the molecular structure of peptides, small carbohydrates and bio-molecules.[292-294] Single gold nanoparticles have been reported to act as antennas for enhancing the fluorescence of emitters for high-resolution near-field fluorescence microscopy, as well as the light absorption of protein.[295,296] As the development of more advanced techniques as well as the better physiological property understanding and control of gold nanoclusters, more and more applications in chemistry, physics, biology, medicine, energy storage and conversion, catalysis, environmental science and other areas are envisioned in the future.

2 SYNTHESIS AND STRUCTURAL DETERMINATION OF MULTIDENTATE 2, 3-DITHIOL STABILIZED GOLD CLUSTERS

2.1 Background and Research Strategy

Au nanoparticles and small clusters have attracted continuous research interest over decades due to their rich optical features, electrochemical properties, and surface functionalities, which render them extensive potentials in nanoelectronics, biomedicine and catalysis applications.[1,3,199] It is well known that the size and shape affect nanomaterials properties due to quantum confinement effects. In the context

of sub-2nm Au clusters, recent breakthroughs have revealed a novel thiol bridging surface Au-S bonding motif, experimentally discovered by X-ray single crystallography[108,138,297] and theoretically predicted by density function theory calculations.[111,112,298] The immediate questions to address next would be: what properties are affected by the novel surface bond structure; to what extent are the properties affected; and ultimately can the bond formation be manipulated to create new clusters with novel properties? The approach of this paper is illustrated in **Figure 2.1**. Inspired by the thiol bridging structure illustrated on the left panel, a dithiol molecule with two adjacent thiol groups, 2,3-dimercaptopropanesulfonate (DMPS) shown on the right, has been employed to synthesize Au dithiol clusters (DTCs). While entropy gain is expected if both thiol groups bind to Au (one dithiol molecule taking the places of two monothiol molecules), the constraint by linking two thiol groups on the same molecule would have an impact on the thiol bridging bonding motif, which could result in novel properties compared to the well established monothiol Au MPCs.

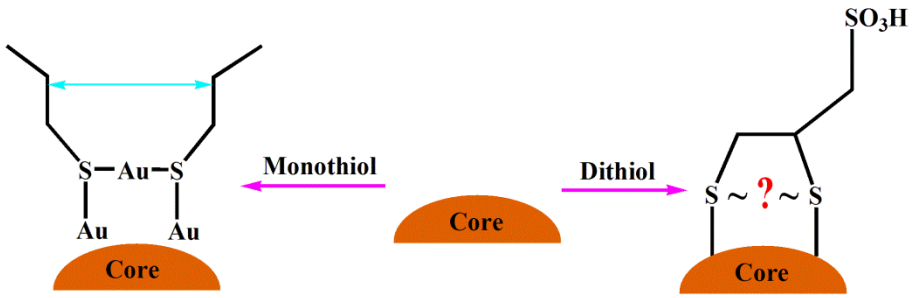

Figure 2.1. Structural illustration of two monothiol molecules versus one dithiol molecule on Au core surface. Left: thiol-bridging motif discovered on monothiol MPC, Right: DMPS dithiol on core surface.

Au clusters with core size a few nanometers or less are of extensive interests not only in fundamental studies but in practical applications. In the biological and medical regime, to be efficiently excreted by body clearance to avoid prolonged stay in various tissues, a criteria has recently been reported

of less than 5.5 nm hydrodynamic diameter and non-adsorptive coating for nanomaterials.[299] In catalysis, recent experiments indicate that sub-2 nanometer gold clusters might be the most active species for CO oxidation.[300] To tailor the size of Au nanoclusters, extensive efforts have been devoted to control the thermodynamics and kinetics of the core agglomeration and surface passivation. The factors such as solvent polarity, reaction temperature and mixing condition in the synthesis have been systematically studied.[3,124,301,302] In the context of ligand molecules, most successes to synthesize small stable clusters have been achieved by using bulky and polymeric ligands and by adopting a high ligand-to-metal ratio in the synthesis.[106,303-306,296-299]

Multidentate ligands have been widely used in inorganic and analytical chemistry in the context of chelates or metal-ligand complexes. Oligonuclear Au complexes with thiol, ylide, phosphine or other complexing agents have been developed as therapeutic agents and as fluorophores for decades and continue to be extensively explored.[307-311] While polydisperse Au(I)-thiolate complexes are known to be the intermediates to the formation of Au MPCs or nanoparticles before the reduction by $NaBH_4$, recent experimental and theoretical results suggest that $(AuSR)_4$ complexes are key units in the formation of monothiol Au MPCs and ligand exchange reactions.[16,113,312]

Multidentate approach has recently been employed to enhance surface layer stability of nanomaterials with the consideration of the entropy effects. Semiconductor quantum dots with tuned and miniaturized hydrodynamic sizes have been synthesized.[313,314] Aggregation of metal nanoparticles of larger sizes was effectively inhibited by designed multi-thiols by Lee and coworkers.[315-317] Dihydrolipoic acid (1,3-dithiol) has been used to directly synthesize Au nanoparticles.[318,319] Without the reduction by $NaBH_4$, various Au(I) complexes have been synthesized by employing meso-2,3 dithiol dimercaptosuccinic acid by the Tsukuda group.[320] Multi-thiol anchored oligonucleotide-Au nanoparticles have also been reported with improved stabilities.[321,322] With the novel S-Au-S bonding motif discovered, we believe that employ-

ing the multidentate approach would significantly enhance our ability to control the nanomaterials formation process, therefore to achieve better size control. More importantly, it could result in novel bonding structures due to the constraint imposed by the linker between the multidentate sites within the individual ligand. In this paper, Au DTCs stabilized by DMPS ligands have been synthesized and characterized. Size transition from small Au_4 complexes up to ~3 nm Au DTCs is achieved. The structure and properties of the Au DTCs tailored by controlling the dithiol Au ratio in the synthesis are reported.

2.2 Results and Discussion

2.2.1 UV-Visible Absorbance of DMPS clusters

UV-Visible absorbance spectroscopy was used to monitor the synthesis and to characterize the products, as the extinction coefficient changes with respect to Au oxidation states and cluster size. **Figure 2.2** shows the absorbance spectra of DTCs and the 3X intermediate (before NaBH4 reduction). A characteristic absorbance band at 282 nm is present in each sample. As the DMPS:Au ratio decreases in the synthesis, the 282 nm band becomes less dominant while the lower energy absorbance in visible range intensified. Further increase of dithiol:Au ratio does not lead to further enhancement of the intensity of 282 nm peak (the spectra of 6X DTC and 6X intermediate completely overlaps with 3X samples thus omitted). Surface Plasmon (SP) band at ca. 520 nm can only be distinguished in the spectrum of 0.5X sample, indicating the Au core sizes of other Au DTCs are less than 2 nm.[15,97,323] In comparison, the synthesis with 1X monothiol (0.5X dithiol) always produces larger Au MPCs that display a more obvious SP band. The gain of entropy by employing dithiol over monothiol in the synthesis obviously altered the cluster formation. Based on previous studies of monothiol MPCs, in which lower thiol:Au ratio synthesis produces larger particles that display higher absorbance at lower energies (visible range), the absorbance features suggest that the Au core size of DTCs decrease from 0.5X to 3X. However, the spectra of

6X (not shown) and 3X DTCs overlap, indicating that further increase of dithiol ratio (more than 3X) does not affect the size distribution of Au DTCs. The finding suggests that the synthesis with 3X dithiol has already produced the smallest stable clusters under the experimental condition, and is supported by the results presented next.

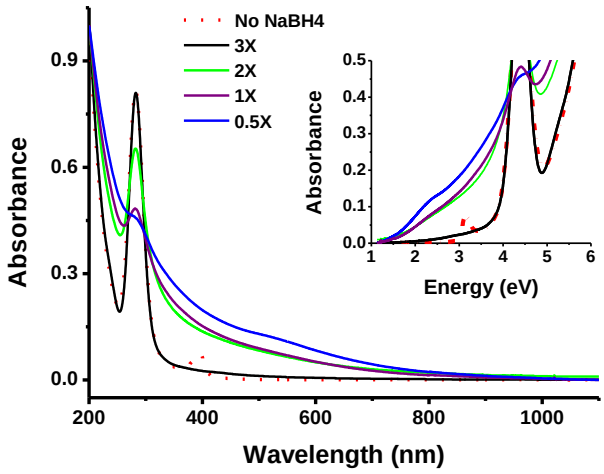

Figure 2.2. UV-Visible absorbance spectra of DMPS Au DTCs. Solid lines from bottom to top at 400 nm represent the spectrum from 3X, 2X, 1X and 0.5X samples. Spectrum of dashed line is the intermediate of 3X sample before the addition of $NaBH_4$. Inserted are the same data plotted in energy instead of wavelength.

The absorbance spectra of all intermediates (3X – 0.5X), generally believed to be polymeric complexes and confirmed by mass spectrum discussed next, are included in **Figure 2.3**. At dithiol:Au ratio larger than 1X, the intermediates feature similar absorbance bands at ca. 282 nm and 395 nm, similar to those observed by Tsukuda and coworkers.[324] This could result from the unique one or a few species present in the intermediates, which have been theoretically predicted in the case of monothiol-Au interactions.[325] The energy states that correspond to the lower energy absorption band disappear upon the reduction by $NaBH_4$, which indicates that the energy state of the corresponding species was filled during

the reduction, or the species in the mixture changed its chemical composition. This is confirmed by the change of mass spectrum and will be further probed by the ongoing separation attempts.

In the inserted plot, the optical band gap from the 3X sample after the addition of $NaBH_4$ can be identified as ca. 4.0 eV while other samples at about 1.5 eV. The band gap of each intermediate is larger than 2.5 eV. The characteristic 282 nm absorption band, or 4.0 eV gap, is in excellent agreements with the predicted Au4 cluster/intermediate that has been identified as a common stable species in several monothiol MPCs.[16,325]

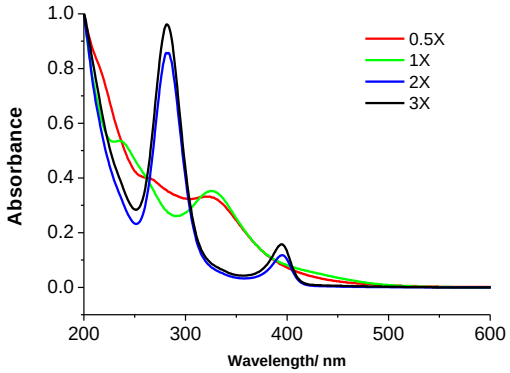

Figure 2.3. Absorbance spectra of pre-DTC intermediates.

2.2.2 Hydrodynamic Size Distribution of DMPS DTCs by NMR Studies

Upon Au-S bond formation, the NMR signals of ligand protons will shift as the chemical environment changes. Line broadening is observed due to the slower diffusion, a consequence of the formation of bulky MPCs.[77,104,326] The effect has been used to confirm the removal of non-bonded thiols and other organic molecules in purification.[70,77,326] 1D Proton NMR spectra of free DMPS ligand and purified DTCs (0.5X, 1X, 2X and 3X) are presented in **Figure 2.4**A. Each spectrum is aligned as illustrated by the dashed line; the sharp peak at 4.70 ppm originating from the residual HOD in D_2O solvent. Compared to the free DMPS ligand, significant shifts of ligand C2 and C3 proton signals (at ca. 3.14 and 2.92 ppm) and line

broadening effect is observed from DMPS DTCs, indicating complex formation. The thiol proton (-SH) signals are missing due to their fast exchange with D_2O. Significant line broadening effect can be observed in the spectrum of the 0.5X DTCs that display a small SP band in absorbance spectrum. As the ratio of DMPS: Au increases, there is less line broadening, indicating the DTC size becomes smaller. The trend agrees well with the absorbance features. For 3X and 6X DTCs (overlapping with 3X, not shown), five magnetically different proton peaks are identified and further discussed in the 2D NMR results.

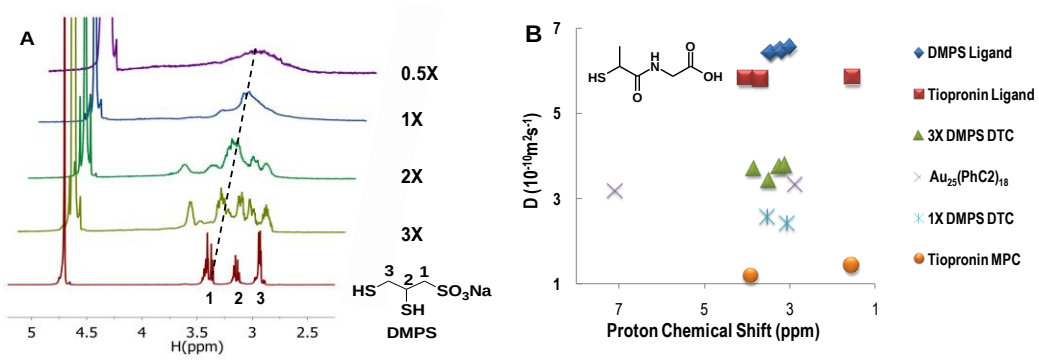

Figure 2.4. A: NMR spectra of DMPS ligand and Au DTCs. The sharp peak at 4.70 ppm is from residual protons in D2O. Dashed line illustrates the same chemical shift in each spectrum. The spectrum of the 6X sample is the same as the 3X sample (not shown). B: Comparison of diffusion coefficient calculated from diffusion NMR studies. For convenience, the molecular structure of tiopronin ligand is inserted.

In contrast to imaging on solid surface or invasive MS studies, the hydrodynamic size of the Au DTCs, revealing the natural states of the DTCs in solution, can be estimated based on Stokes-Einstein equation.[327]

$$D = \frac{kT}{6\pi\eta r}$$

In this equation, k is Boltzmann constant at 1.38 x 10^{-23} $m^2 \bullet kg \bullet s^{-2} \bullet K^{-1}$; T is temperature; η is viscosity of the solvent and r is the radius of the analyte. At 25°C the viscosity of D_2O is 1.10 x 10^{-3} $Pa \bullet s^{-1}$.[77] From any known or measured diffusion coefficient (D), the hydrodynamic radius (r) can be determined accordingly.

Therefore the size differences of DTCs reflected in the broadening of proton peaks can now be quantified indirectly by DOSY technique, as larger sized DTCs would display slower diffusion. The underlying assumption is that DTCs are in spherical shapes. From a DOSY spectrum, representative proton peaks from a chemical are selected to extract the diffusion coefficient (D) of corresponding species, by Stejskal–Tanner exponential fitting of peak intensity versus the z-axis gradient strength with the error +/- 5%.[328] Diffusion coefficients can be obtained by this method for species with well resolved NMR signals and significant differences in diffusion coefficient. If the components in the sample mixture have overlapped NMR signals, similar diffusion coefficients, or high molecular weight dispersity such as polymers, Stejskal–Tanner exponential fitting outputs an estimated average diffusion coefficient.[329,330] The results obtained by Stejskal – Tanner exponential fitting are presented in **Figure 2.4**, panel B. Tiopronin MPC (with ligand-to-gold mole ratio being 3 in the synthesis, average composition of $Au_{201}Tio_{85}$), Au25PhC218 MPC, and tiopronin and DMPS ligands, with known average size or molecular weight, were used as references to characterize the newly synthesized DTCs. DOSY experiment of $Au_{25}(PhC2S)_{18}$ MPCs was performed in $CDCl_3$. The presented data has been corrected for solvent viscosity with the assumption that no significant hydrodynamic size differences exist for the MPCs between solvent D_2O and $CDCl_3$. The two ligands (ca. 200D MW) display faster diffusion compared to the Au clusters. The diffusion coefficient decreases in the sequence of 3X DMPS DTCs, the corrected Au25 sample, 1X DMPS DTC, and tiopronin MPC. As the average core size of tiopronin MPC was reported to be *ca.* 1.8 nm (without ligand) and has no SP band in the absorbance spectrum, the 1X sample is estimated to be smaller than Au201 (Tiopronin MPC) but larger than Au25, which is also supported by the featureless absorbance spectrum (the 282 nm peak will be addressed separately). It is interesting to find that the 3X sample is smaller than Au25, consistent with the less obvious peak broadening observed in 1D proton NMR spectrum. Known to be polydispersed, only 1X DTC was tested to demonstrate the size differences. Isolated monodisperse samples would provide more definitive results.

The hydrodynamic radius of the DTCs is calculated using Stokes-Einstein equation and reported in **Table 2.1**. The results of home-synthesized tiopronin MPCs and those in the literature are included, through which excellent agreement can be found as a reference.

Table 2.1 Hydrodynamic sizes of monothiol and dithiol clusters.

	3X DMPS DTC	1X DMPS DTC	3X Tiopronin MPCs	3X Tiopronin MPCs (reference[77])
D (10-10m^2/s)	3.92	2.51	1.43	1.4-1.7
Radius (nm)	0.51	0.79	1.39	1.4-1.2

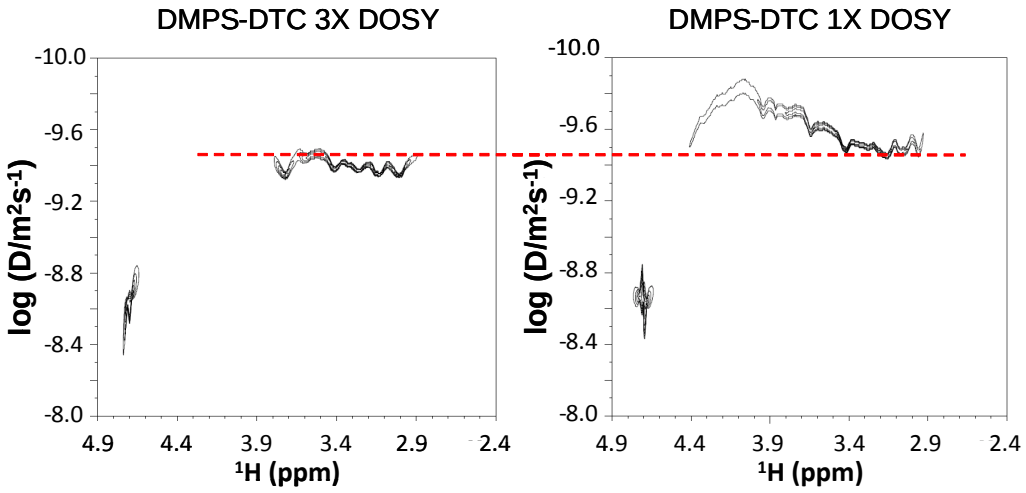

Figure 2.5. NMR DOSY spectra of 3X and 1X DMPS Au DTCs. The signal at 4.7 ppm is from residue water in D_2O. The dashed line is added to aid the comparison.

Complete DOSY spectra of 3X and 1X DMPS DTC samples are presented in **Figure 2.5**. The logarithm of diffusion coefficient ($m^2 \bullet s^{-1}$) is plotted against proton chemical shifts (ppm). A very narrow distribution of the logD, ranging from -9.32 to -9.49 for all ligand proton signals, is detected from 3X sample. The signal can be assigned to individual species of same or similar sizes, as logD has an error range of +/-

0.1 due to the mathematic processing. However, the 1X sample has a much wider range of logD, from -9.42 to -9.76, suggesting a mixture of polydisperse species. The up-field species has faster diffusion with logD from -9.42 to - 9.55 while the low-field species moves much slower with logD of -9.76. Although the majority of 1X sample moves slower, the logD range of up-field species in 1X sample partly overlaps with that of the 3X sample, indicating components of same or comparable hydrodynamic sizes present in both samples. Considering the common 282 nm absorbance band, the results suggest a common species in each sample but with a different abundance.

2.2.3 Composition of 3X DMPS DTCs by MALDI-MS Studies

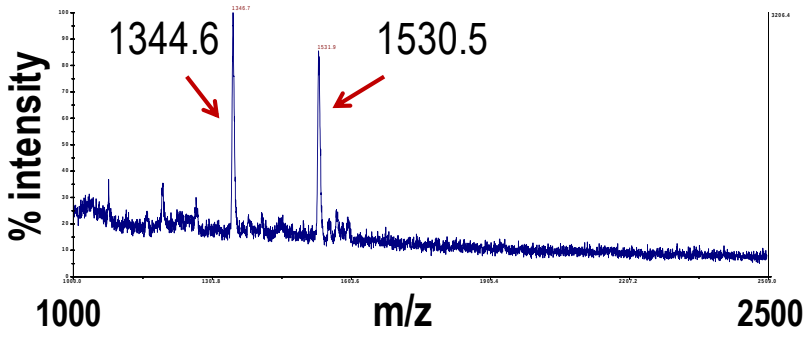

Figure 2.6. MALDI MS results of the 3X DMPS Au DTCs. The results were collected under linear negative mode using widely used protein matrix CHCA (α-cyano-4-hydroxycinnamic acid). No signal was detected in higher m/z region. The two labeled peaks at 1344.6 and 1530.5 m/z were attributed to Au_4L_3 and Au_4L_4 respectively.

The Au DTCs were analyzed by matrix assisted laser desorption ionization (MALDI) MS in an attempt to identify the molecular ion/s.[24,27] The MALDI results of the 3X sample detected in linear negative mode are presented in **Figure 2.6**. Mass features below 1000 are not included due to the overlapping with the matrix backgrounds. No detectable peak is observed above 2000 m/z. Two abundant species

can be identified. The accurate values of m/z 1344.6 and m/z 1530.5 are calibrated with the results under reflectron mode included in **Figure 2.7**, collected using a separately synthesized 3X sample that has different polydispersity (thus cannot be directly compared to NMR and other related results discussed in the main text). If the cluster has one ligand with deprotonated sulfonate group, the composition of Au_4L_3 and Au_4L_4 would have m/z 1344.7 and m/z 1530.7 respectively. The well matched numbers confirm that both thiol groups have been converted into thiolates. It is worth pointing out that the relative abundance of the two peaks varies from sample to sample, as could be observed in **Figure 2.8**. This suggests that Au_4L_3 exists in the original sample instead of being a fragment of Au_4L_4. The argument is supported by the TGA results presented at the end. It is also interesting to find that stand-alone Au dithiol clusters share the same Au composition with the Au4 unit, a key component in monothiol MPCs and as inorganic complexes with crystal structure resolved.[331-333] Known to be polydisperse, other Au DTCs were not thoroughly studied with MS but multiple peaks have been observed over wide m/z ranges.

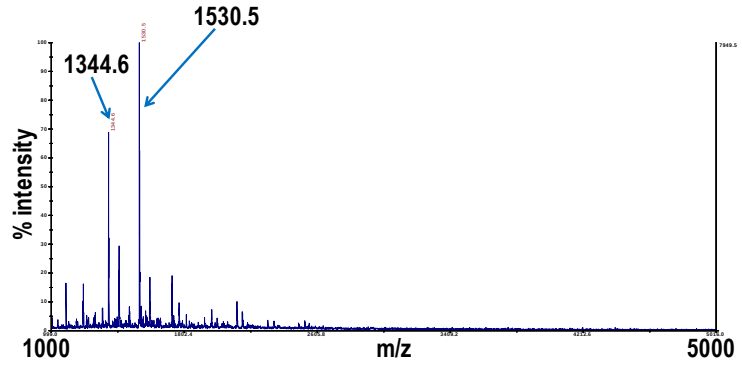

Figure 2.7. 3X DTC MALDI MS spectrum collected under reflectron negative mode of another synthetic batch.

An interesting pattern reflecting polydisperse species has been detected from the 3X intermediate shown in **Figure 2.8**. The species could be generally described as $Au_xL_y(Au\text{-}S)_z$. In the specific spectra, those species with reasonable intensity have the composition of x ranging from 5 to 25, y ranging from 2

to 3 and z ranging from 2 to 8. Signals corresponding to Au4 clusters can also be found. Combined with NMR results, the 282 nm absorbance band is assigned to Au4 clusters, dominant species in the samples synthesized with dithiol:Au ratio larger than 3X. The abundance of Au4 clusters decreases as the ratio decreases and the total absorbance is determined by clusters of larger sizes.

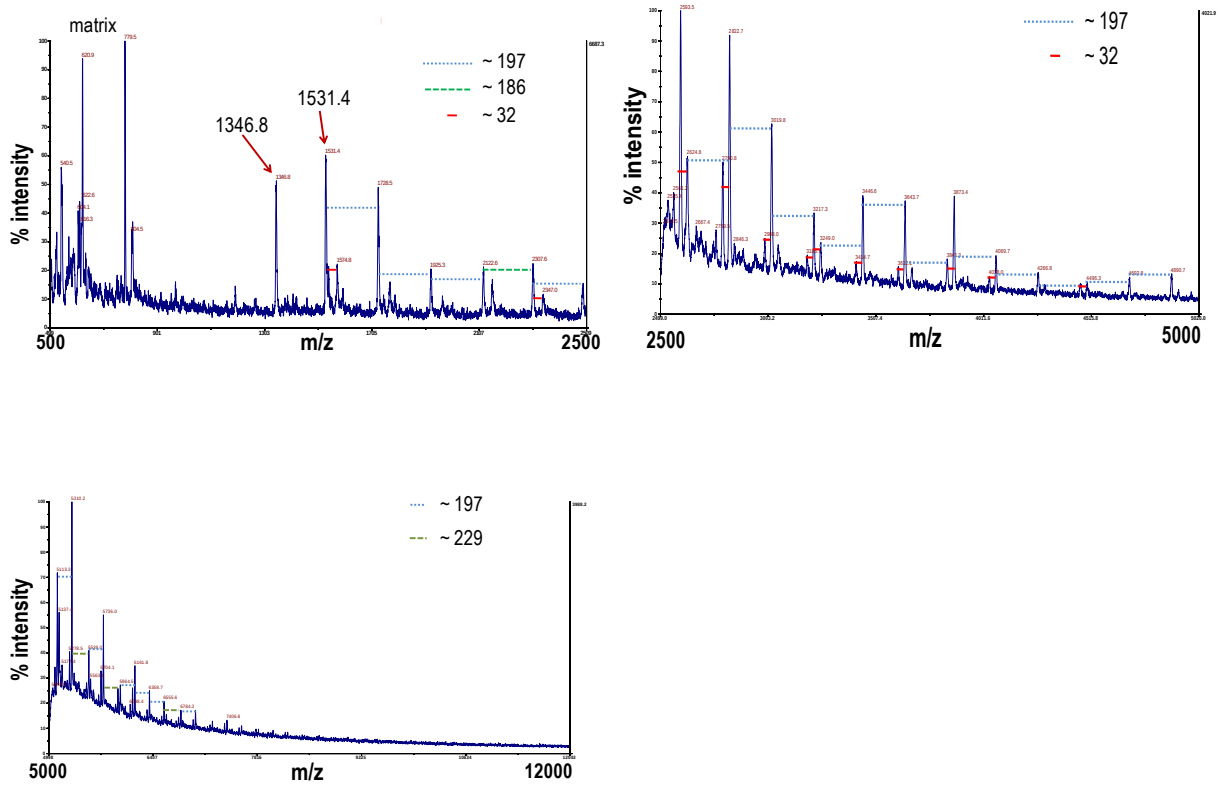

Figure 2.8. 3X Pre-DTC MALDI MS spectra collected under linear negative mode.

2.2.4 Size on a Solid Support Imaged by AFM

Size transition of DMPS DTCs is confirmed by AFM. Sample solution was drop-cast onto freshly cleaved mica before imaging under ambient conditions. Images from 1X and 3X DTCs are presented in Figure 6. The tip radius is ca. 10 nm, which limits the lateral resolution. From the height profiles shown in the section panel, the size of the particles can be analyzed. Unlike TEM in which ligands are not observed, the ligand monolayer is part of the height measured by AFM. Averaged by 80-120 particles on

surface, the overall size of 1X sample is found to be 1.5±0.6 nm while that of 3X 1.0±0.3 nm. Much larger size distribution was observed from 0.5X sample, ranging from ca. 2 to 5 nm. The trends agree well with optical and NMR results. The heights of 3X and 1X DTCs find excellent agreements with those calculated by diffusion NMR (twice of the hydrodynamic radius).

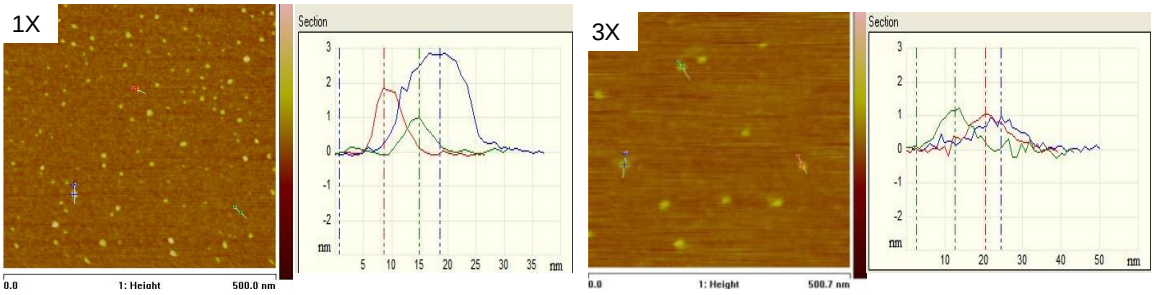

Figure 2.9. Representative AFM images of 1X and 3X DTCs. The scale of the color bar is 5 nm for 1X sample and 4 nm for 3X sample. The right panel is the section plot presenting the height profiles of three randomly selected particles on mica surface.

2.2.5 Chemical Environments of 3X DMPS DTCs Revealed by NMR 2D ^{13}C-^{1}H HSQC

The experimental design of employing dithiol over monothiol is to tailor the bond structure thus the property of Au clusters and nanoparticles. Whether dithiol would alter the 'staple' bonding motif depends on whether only one or both thiol groups on one dithiol molecule form Au-S bonds. Such information could be provided by X-ray studies. However, single crystals are difficult to obtain. Consequently, we resort to NMR chemical shift changes to address this issue.

The chemical shift of the C2 and C3 protons is expected to exhibit significant changes upon Au-S bond formation, therefore full assignment of individual peaks in 3X Au DTC NMR spectrum is required. The assignment of proton and carbon resonances was accomplished using COSY, TOCSY and ^{13}C -^{1}H HSQC 2D NMR experiments. In the ^{13}C -^{1}H HSQC spectrum of 3X DTCs presented in **Figure 2.10.**, each pair of cross peaks (two projections on proton axes symmetric to the 1D peak, and one projection on carbon) represents a unique C-H bond characterized by corresponding ^{1}H and ^{13}C chemical shifts pro-

jected on each axis, as indicated in the figure. We also noticed that similar approach has been attempted to resolve a well-established Au25PhC2S MPC system.[29] In this edited HSQC, the signals from CH (C2, middle peak at ca. 49.1 ppm) can be readily differentiated from CH_2 groups (C1 and C3) by the phase differences of the signals and the fact that C2 is only coupled to a single proton. The peak at ca. 57.1 ppm is assigned to C1 (attached directly to the sulfonate) according to the chemical shift of DMPS ligand. The assumption is that its chemical shift of C1 is not changed significantly since it is not the carbon immediately next to the S-Au bond. This assignment is created for the purpose of relative comparison of chemical shift changes of C2 and C3 with respect to C1 before and after bond formation. The high field signal at ca. 43.1 ppm is thus attributed to C3. Compared to free DMPS (C1 57.1 ppm, C2 38.6 ppm and C3 32.5 ppm), both C2 and C3 signals are shifted by 10.5 and 10.6 ppm respectively, indicating both C2 and C3 carbon atoms experience similar changes in the chemical environment upon Au-S bond formation. This suggests both –SH sites participate in the formation of Au-S bonds for each DMPS ligand.

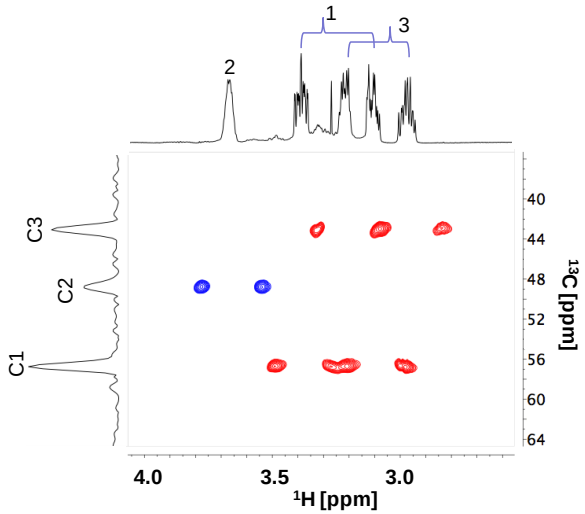

Figure 2.10. ^{13}C- ^{1}H multiplicity edited F2 coupled HSQC spectrum of 3X DMPS Au DTCs. The vertical and horizontal axes represent ^{13}C and ^{1}H chemical shifts. Positive contours (blue) correspond to CH and negative contours (red) are from CH_2 groups. The cross peaks originating from the same C-H are separated by the ^{1}JCH coupling. Assignments are indicated on the 1D projections.

These observations are further supported by the proton spectra where significant chemical shift differences are also noted. The C2 proton, shifts from 3.14 ppm in the free ligand to 3.65 ppm, indicating S-Au bond formation. In the free ligand the protons of the methylene group C1 are degenerate as are those of C3. Upon complex formation the C1 methylene group protons (3.38 ppm) become non equivalent and resonate at 3.42 and 3.10 ppm. Similarly, the two protons of C3 which resonate at 2.92 ppm in the free ligand appear at 3.20 and 2.95 ppm. For both C2 and C3 one proton experiences significant chemical shift changes signaling significant chemical environment changes due to the formation of S-Au bond. This is further supported by the results of ^{1}H-^{1}H COSY and TOCSY listed in **Figure 2.11.** Additionally, the non-equivalence of the C2 and C3 methylene protons suggests that the ligand is constrained after complex formation. The ligands with limited flexibility are in line with our proposed structure presented at the end. The Au_4L_4 and Au_4L_3 complexes, detected by MALDI-MS, are not differentiated by NMR. In addition to the similarity of the two complexes, making it challenging to resolve, there is a possibility that the Au_4L_3 originates from the fragmentation of Au_4L_4.

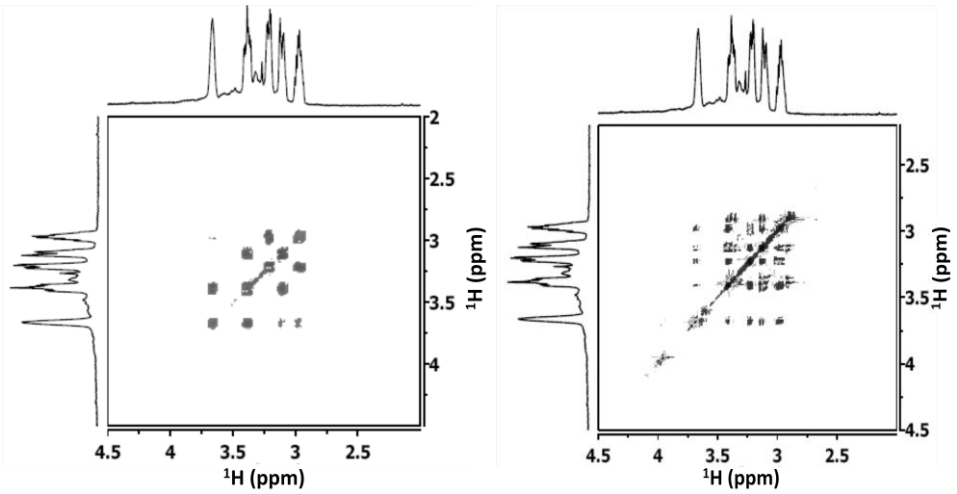

Figure 2.11. ^{1}H -^{1}H COSY spectrum (Left) and TOCSY spectrum (Right) of 3X DMPS Au DTCs.

2.2.6 X-ray Photoelectron Spectroscopy Studies of Au-S Bonding

The nature of Au dithol interaction is further probed with XPS. **Figure 2.12** shows the Au(4f) and S(2p) photoemission spectra of DMPS DTCs. The presence of -Cl and -Br were ruled out by the survey scan in **Figure 2.13**. In the case of monothiol MPCs, the binding energy (BE) of Au($4f_{7/2}$) increases as the MPC size decreases, ranging from Au(0) film of ca. 83.8 eV up to Au(I) compounds of ca. 86.0 eV.[9,70,97,327,334] From 0.5X to 2X DMPS DTCs, the BE of Au($4f_{7/2}$) increases, within the range of Au(0) and Au(I). The broadening effect could result from the polydispersity of the sample but has not been ascertained. It is surprising to find that BE of Au($4f_{7/2}$) of 3X sample is larger than that of Au(I) and approaches that of Au(III) ($AuCl_4^-$ at about 86.9 eV).[335] The results suggest that additional charge transfer or bond exists, which is also reported in other metal clusters.[336] The S(2p) spectra display similar trends. The BE of S($2p_{3/2}$) also increases from 0.5X to 3X samples, or from larger to smaller clusters. For reference, the BE of S(2p) from thiol 2D SAM on Au(111) and MPCs ranges from 162.0-162.3 eV.[70,99] The peak at higher BE is assigned to the SO_3^- group, which is known to be at ca. 168 eV, reflecting oxidized S. For 3X sample, the BE of S($2p_{3/2}$) is even larger than the S element at 164.2 eV. Considering the sample is synthesized under reduction by $NaBH_4$, the stability of this electron deficient sample compared to the Au(I) thiolates is impressive. Though XPS data were collected after the sample has been synthesized and purified over days with the exposure to air (O_2), the absorbance features of samples immediately after reduction remain unchanged over days/weeks in solution under comparable condition. Some samples do decompose over time (months) presumable due to the presence of oxygen and light.

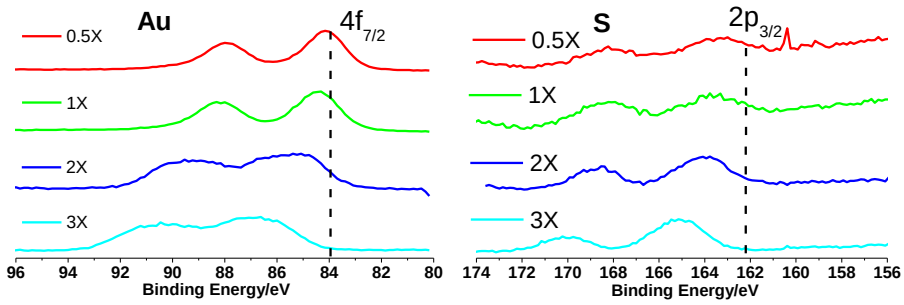

Figure 2.12. XPS spectra of DMPS DTCs. The binding energy of Au(4f) and S(2p) electrons is presented.

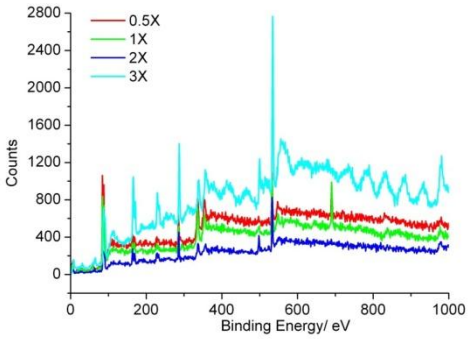

Figure 2.13. XPS Survey Scan of DMPS DTCs. N, Cl, and Br were not found.

In the reported monothiol Au4 ring-like structure, each Au directly interacts with two S atoms. In-complete charge donation between Au and S observed in these small clusters will generate non-integral charge states of corresponding atoms. As a matter of fact, charge transfer in Au4 system has been calculated to be +0.4 eV for Au. S atom,[325] on the other hand, interacts with one carbon atom and two Au atoms. The high BE values of Au(4f) and S(2p) suggest additional bond or interaction in the 3X DMPS DTCs, which would further change the charge states of Au and S.[336] An extended ring of $(Au\text{-}S\text{-}C\text{-}C\text{-}S\text{-})_4$ is basically a Au(I) compound, which is unlikely since both Au and S XPS signals are significantly shifted away from the reported Au(I) thiolate compounds. In conjunction with different chemical environments revealed in proton chemical shifts by NMR, a tentative structure is proposed as shown in **Figure 2.14**. A 3D structure (ball-stick) that is relaxed by preliminary molecular mechanics approach can be found in **Figure 2.15**. The Au4 ring holds off-plane boat-form structure as Au is at ca. positive III states instead of I. An extended Au(I) ring structure, Au16 stabilized by phosphine complexes, has been reported.[337] The sulfonate groups are positioned to take trans- configuration, on the opposite sides of the Au plane to minimize the potential charge repulsion. It is not clear how the two thiolate groups on one DMPS ligand replace two individual DMPS ligands to form a stable Au_4L_3 complex. One tentative structure is included in **Figure 2.16**. In the proposed Au4 structures, Au-Au distances are measured to be ca. 4 angstroms,

longer than the Au(I)-Au(I) bond at ca. 2.7-2.9 angstroms previously reported.[338] Based on the proposed structures, the size of the proposed structure is estimated to be ca. 1.0 ± 0.1 nm for Au_4L_4 and 0.85 ± 0.1 Au_4L_3 respectively, pending the direction of measurement. The dimension matches reasonably well with experimental results from AFM and diffusion NMR. Further theoretical calculation of energy favored Au4 structures is underway. The less symmetric Au_4L_3 complex would incur broader features in XPS and other spectra as both Au and S atoms encounter several different chemical environments. It is important to point out that the Au4 units found in monothiol Au MPCs is located on core surface, which means multiple interactions exist between the inner atoms and the Au4 units. In the proposed structure, the off-plane interactions of Au-S bonds and Au-sulfonate 'ion pairing' stabilize the stand-alone Au4 clusters.

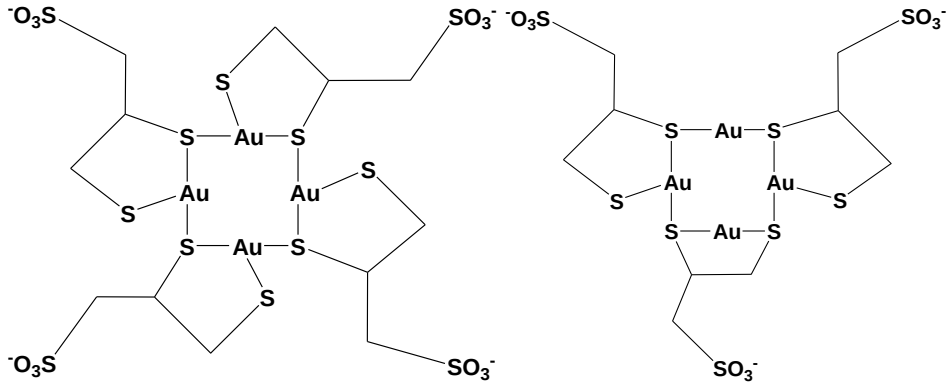

Figure 2.14 The proposed Au_4L_4 and Au_4L_3 cluster structure.

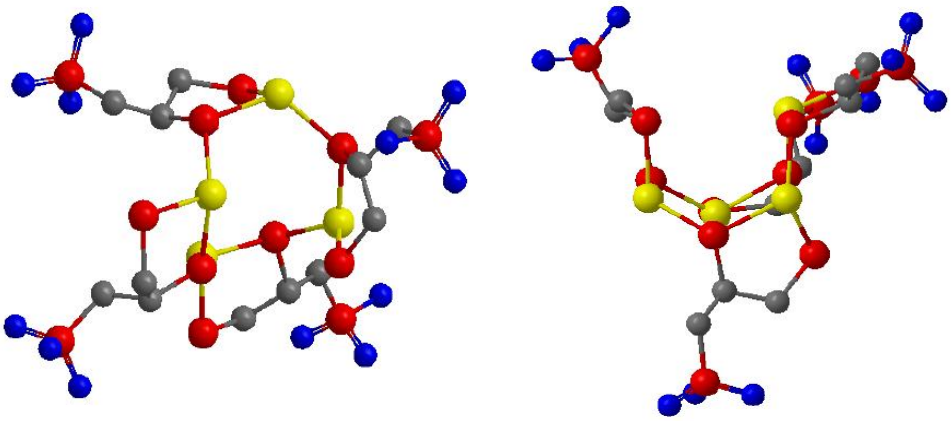

Figure 2.15 The relaxed 3D structure of Au_4L_4 by molecular mechanics (Yellow: gold, Red: sulfur, Gray: carbon, Blue: oxygen, hydrogen is omitted for better view, chemdraw software courtesy by Dr. Binghe Wang).

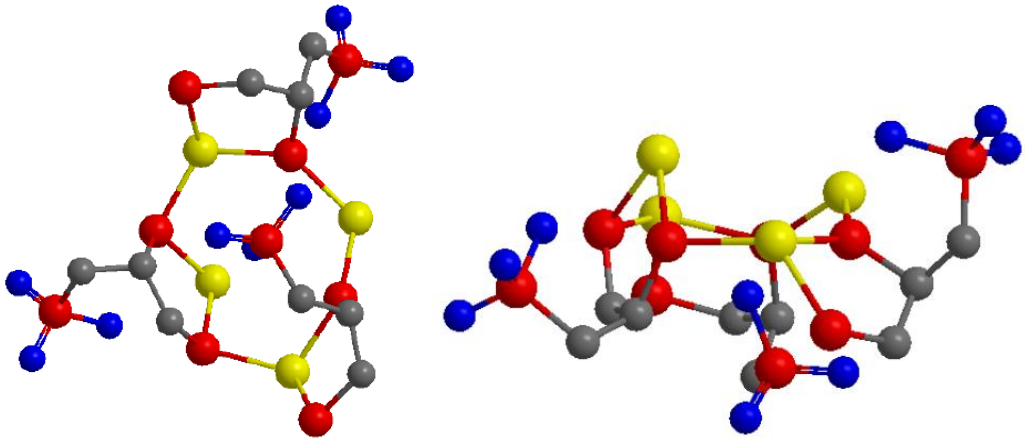

Figure 2.16 The relaxed 3D structure of Au_4L_3 by molecular mechanics (Yellow: gold, Red: sulfur, Gray: carbon, Blue: oxygen, hydrogen is omitted for better view, chemdraw software courtesy by Dr. Binghe Wang).

2.2.7 Further Structural Confirmation and Properties

Au-S bond formation is further confirmed by the disappearance of -SH stretching of the free ligand at 2543 cm^{-1} in the infrared spectrum (**Figure 2.17**). The ligand-to-gold ratio was probed by TGA measurements in **Figure 2.18**. Mass loss corresponding to organic components starting at ca. 260 ^{o}C over the

residue is calculated to be 0.85 for 3X sample. Compared to the MS results of Au_4L_3 and Au_4L_4 at almost equivalent abundance, which have L:Au mass ratio of 0.70 and 0.94 respectively, excellent agreements is found from TGA results. The enhanced thermostability of DTCs compared to monothiol MPCs affirms the multi-interaction by dithiol ligands with Au and support the structure proposed.

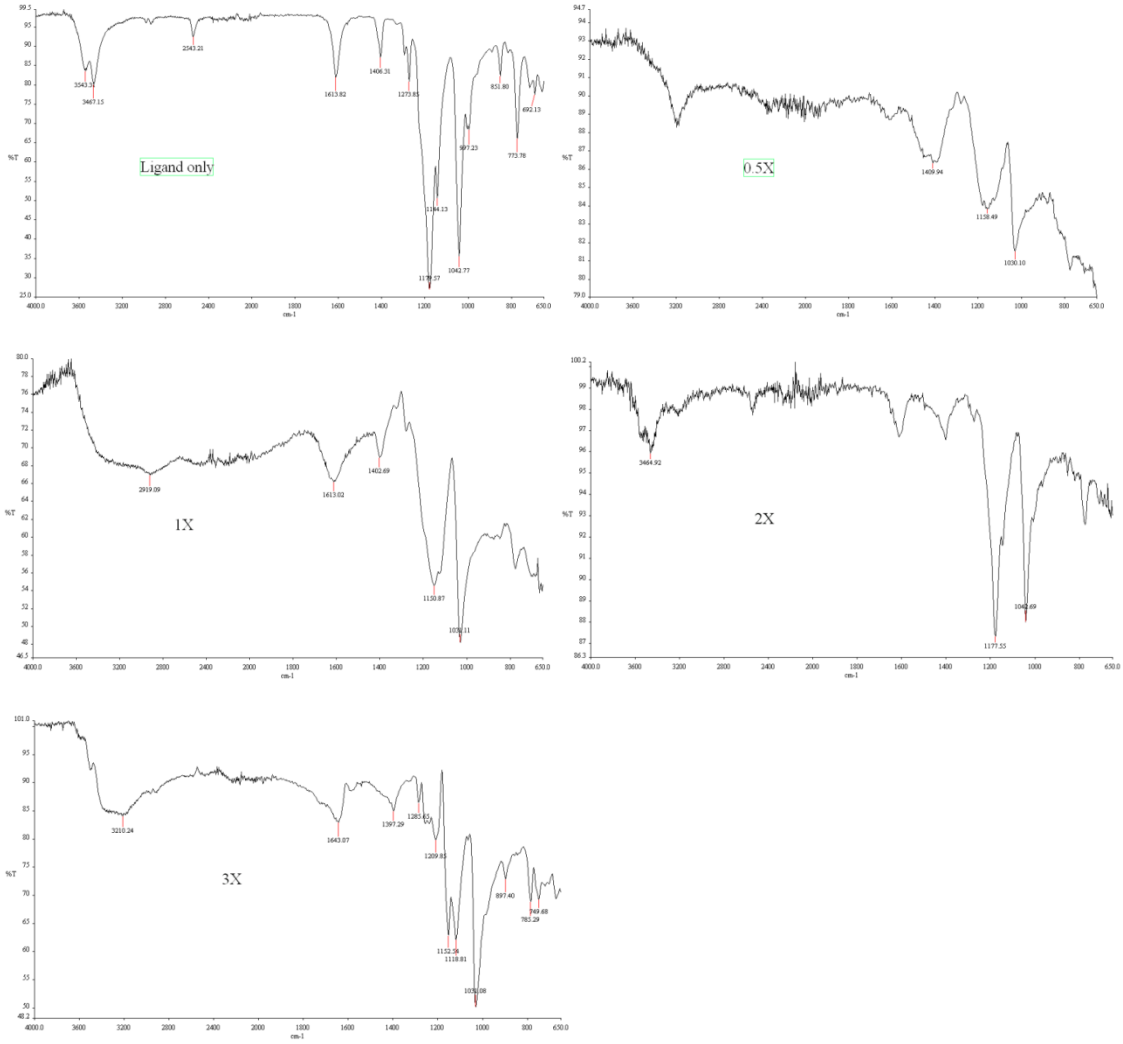

Figure 2.17 Infrared spectra, from top to bottom: DMPS only, DMPS DTCs of 0.5X, 1X, 2X, 3X.

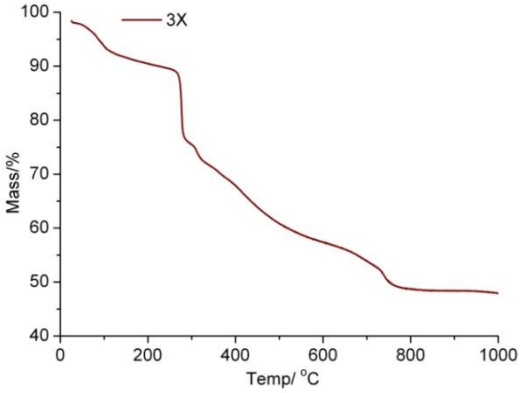

Figure 2.18 Thermogravimetric analysis of 3X DMPS Au DTCs.

Near IR luminescence, ranging from *ca.* 700 nm to 1000 nm when excited at higher energy (e.g. 450 nm), observed from Au MPCs with core diameter smaller than 2 nm and mostly with polar ligands,[98,116,339-343] is not detected from these DTCs with a full spectrum scan. Not precisely correlated with the MPC energetics, the origin of the luminescence has been postulated to surface localized states.[116,341] It is interesting to notice that one Au atom is positioned away from the core in the thiol bridging surface bond structure. The disappearance of near-IR luminescence from all synthesized DTCs strongly suggests fundamental differences between MPCs and DTCs. Surface bond structures of DTCs of large sizes are currently being studied; they are believed to differ from monothiol MPCs, as different properties in luminescence and place exchange reactions have been observed.[343]

2.3 Experimental Section

2.3.1 Chemicals

Tetrachloroauric acid ($HAuCl_4 \cdot 3H_2O$, >99.99% metals basis, Aldrich), sodium 2,3-dimercaptopropanesulfonate monohydrate ($C_3H_7O_3S_3Na \cdot H_2O$, ~95%, Aldrich), sodium borohydride

($NaBH_4$, 99%, Aldrich) were used as received. Water (18.2 MΩ·cm) was purified by Barnstead Nanopure system. Other chemicals were used without further purification.

2.3.2 Measurements

UV-Visible absorbance spectra were recorded with a Shimadzu UV-1700 spectrophotometer. Mass spectrometry spectra were acquired on ABI 4800 MALDI TOF-TOF analyzer. Widely used for small protein analysis, α-Cyano-4-hydroxycinnamic acid (CHCA) was used as matrix. XPS analysis was conducted with a SSX-100 X-ray photoelectron spectrometer (Surface Science laboratories Inc., Georgia Institute of Technology Nanotechnology Research Center) using an Al K-alpha X-ray source (1486.6 eV) with the analysis chamber pressure lower than 1×10^{-8} Torr. Atomic Force Microscope images were collected with a MultiMode instrument (Veeco) under tapping mode. The tips used in all measurements were LTESP (Veeco, USA) with a radius of ca. 10 nm. A PerkinElmer Spectrum 100 FT-IR spectrometer was employed in the infrared studies. Thermogravimetric analysis (TGA) was performed with a Seiko RTG 220 robotic TGA system, on 3-5 mg purified materials, and recorded from 25 to 1000 °C at a heating rate of ~3 °C/min. Luminescence was tested with a Horiba Jobin-Yvon Fluorolog 311 spectrometer with T channel, through which a PMT detector in visible range and an InGaAs near IR detector (800-1500 nm) can be used. Optical spectrum of the Au DTCs is collected in aqueous solution.

For NMR analysis, the samples were dissolved in D_2O. Proton NMR (1D) spectra were acquired on a Bruker Avance 400 MHz spectrometer. Diffusion ordered spectroscopy (DOSY) measurements were performed on a 600 MHz Bruker Avance equipped with a 10A gradient amplifier using a 5mm QXI probehead ^{1}H (^{31}P, ^{13}C, ^{15}N) with a shielded Z-gradient coil. To reduce the effects of convection during the diffusion experiment, the data was acquired at 25 °C with nitrogen with flow rate of 535 $L \cdot h^{-1}$. Furthermore, the pulse sequence consisting a double stimulated echo with bipolar gradient pulses was utilized to reduce the constant velocity effects of convection.[344] The gradient pulse duration was set to 1.5

ms with a diffusion time of 200 ms. The gradient strength was increased linearly over 16 experiments from 2 to 95% of the maximum at 53 $G \cdot cm^{-1}$ for the probe. Typically, 32 scans were accumulated to increase signal-to-noise ratio for each experiment. DOSY spectra were processed using the DOSY package of XwinNMR 3.5. Two dimensional ^{1}H -^{1}H correlated spectroscopy (COSY), total correlation spectroscopy (TOCSY) and ^{13}C -^{1}H heteronuclear single-quantum coherence (HSQC) spectra were collected on Varian Inova 500 and 600 MHz spectrometers.

2.3.3 Synthesis of DMPS Clusters

The DMPS clusters were synthesized and purified with a modified procedure of water soluble monothiol Au MPC synthesis.[345,346] Based on the strategy used to synthesize smaller core sizes by using higher monothiol:Au ratios,[3] dithiol:Au ratios were varied in the synthesis at 1: 2, 1: 1, 2:1, 3: 1 and 6:1, denoted as *n*X respectively. In a typical 3X (DMPS:Au) synthesis, 70.0 mg of DMPS sodium salt (0.32 mmol) and 39.4 mg of gold chloride trihydrate (0.1 mmol) were co-dissolved in 10 mL nanopure water. As Au(III) is reduced in dithiol solution,[320] referred to as intermediate[70,347], the solution color became lighter within minutes. After 30 minutes, the absorbance spectrum stabilized but the color is still light yellow. Reductant $NaBH_4$ (38 mg, 1 mmol) in 5 mL nanopure water was added into the Au-dithiol mixture under vigorous stirring at 0 ^{o}C ice bath. The solution turned brown within a few minutes. Final solid of 3X and 6X are brown. The DTCs at lower thiol:Au ratio (0.5X, 1X) appear to be black. The solvent was removed by rotary evaporation at room temperature after three hour reaction.

The crude product was easily soluble in water and purified by dialysis with cellulose ester or regenerated cellulose dialysis tube (MWCO 500 or 3500). The pH of the crude product solution was adjusted to ca. 1 with concentrated HCl prior to dialysis under slow stirring in a 2L beaker filled with nanopure water. Fresh nanopure water was recharged every 12 hours over 72-hour period.[16,348] In the last step, solvent was removed under vacuum at room temperature. Effective removal of free ligands from the

final materials was confirmed by 1D proton NMR spectroscopy. The final products of 0.5X, 1X and 2X appeared to be black while the 3X and 6X appear to be dark brown. The final clusters remained stable after repeated drying-dissolving procedures.

2.4 Summary

In summary, multidentate ligand DMPS stabilized Au DTCs have been synthesized at different dithiol:Au ratio. The DTCs have been found to differ significantly in composition, structure and physical properties with their counterpart monothiol Au MPCs, which reflect the impacts by the designated dithiol molecular structures. The composition and sizes are analyzed by mass spectrometry and AFM imaging. Believed the smallest building units in monothiol MPC system, stand-alone Au_4 clusters with three or four DMPS ligands have been directly synthesized at high purity. A characteristic 282 nm absorbance band, or a 4.0 eV optical gap in absorbance spectra, has been attributed to the Au_4 DTCs. Diffusion coefficients, reflecting the hydrodynamic size of the DTCs, is reported from diffusion NMR studies. Based on proton and carbon NMR chemical shift information, and with the binding energy of Au(4f) and S(2p) XPS data, thiol bridging surface structure discovered in monothiol MPCs is obviously changed in the Au_4 DTCs, as presented in the proposed structure.

3 MONOLAYER REACTIONS OF PROTECTED GOLD NANOCLUSTERS WITH MONOTHIOL TIOPRONIN AND 2, 3-DITHIOL DIMERCAPTOPROPONIC SULFONATE

3.1 Background and Research Strategy

Chemically bonded or physically adsorbed molecules, termed ligands, prevent nanomaterials from aggregation and reserve the novel properties resulted from quantum confinement. In small nanoparticles and nanoclusters, a significant amount of core atoms participates in ligand bonding, which affects if not dominates the physical properties of those materials. The unique thiol-bridging motif (RS-Au-SR) has recently been discovered in the case of Au monolayer protected clusters (Au MPCs), which obviously challenges previous understanding based on simple Au-S bonding.[107,108,138] The concept of superatom has been proposed in which the overall energetics of the Au MPCs is determined by the valence electrons involved in core-ligand Au-S bonding.[112] Interestingly, it has been experimentally observed and predicted that the number of RS-Au-SR units vary with respect to the surface curvature, with extended dimer or trimer units observed from smaller Au MPCs and single units from larger Au MPCs.[92,107,108,111,113,131,298,325,349]

The novel surface bond structures stimulated our report of the direct synthesis of dithiol stabilized Au clusters (Au DTCs) with 2, 3-dimercaptopropanesulfonate (DMPS) as ligands.[350] The rationale is that the two thiol groups of one dithiol molecule impose structural constraints on the surface bond formation with entropy gain upon binding to Au compared to monothiols. In this paper, the composition, interfacial bonding, and optical properties of Au clusters are tailored by the competition between monothiol tiopronin and dithiol DMPS ligands in the monolayer. Two types of monolayer reactions are investigated: tiopronin MPCs with DMPS molecules and DMPS DTCs with tiopronin molecules. The intriguing near infrared (IR) luminescence of the Au clusters is efficiently turned ‘off’ and ‘on’ by DMPS-tiopronin exchange and tiopronin attachment respectively. A two step reaction mechanism, facile dithiol exchange

followed by the sluggish core etching, is elucidated by the analysis of reaction kinetics of tiopronin MPC with DMPS molecules.

Au nanoparticles and nanoclusters have attracted tremendous research interests due to their optical and electrochemical properties, chemical and catalytic reactivity and bio-compatible composition.[1,3,186,300] The fundamental properties and structural flexibility render the thiolate Au MPCs broad applications in material science, energy technology, chemistry, medicine and biology.[2,3,9,199,351] A common challenge in Au MPCs and other nanomaterials research is the polydispersity in size/composition, which complicates the property interpretation and application design. Extensive research efforts have been devoted to create uniform materials, to establish property-composition correlation, and to tailor the property for targeted applications. The approaches include the design and development of new synthetic procedures, post synthesis separation and isolation, and further derivatization of the synthesized materials.[22,70,97,121,124,148,149,301,348,352-354] General synthetic variables include the type of thiol molecules, thiol-Au mole ratio, the solvent, and the duration of each reaction step.[70,124,301] Chromatography and electrophoresis techniques are effectively employed to reveal the respective properties (mostly optical) of separated Au MPCs.[22,97,348,352-354] Annealing or etching processes have been found effective to enrich the thermodynamically favored species.[22,121,148,149]

The applications of Au MPCs in labeling and sensing in biology and bottom-up assembly demand binding in a controlled manner.[351,355] The structural flexibility and monolayer reactivity of the Au MPCs have been achieved via coupling reaction,[356,357] mixed thiol synthesis[358-360] and ligand exchange process.[98,106,361-363] As thiols are known to be mobile on Au surface,[364,365] ligand exchange reactions have been widely employed to conveniently introduce novel functional groups into the MPC monolayer.[2,199,351,366] Controlled DNA binding and assembly of Au MPCs with designed ligands have been reported.[367-370] Rotello and coworkers have recently demonstrated assisted transport of membrane-impermeable enzymes by peptide activated Au MPCs and the inhibition by Au MPCs of enzymatic ampli-

fication.[210,237] The transport through cell membrane of Au MPCs with randomized mixed ligands and those striated in the monolayer has also been analyzed.[371] Other biological applications of functionalized Au nanoclusters include optical labeling,[251] X-ray contrast enhancement,[218] and magnetic resonance imaging contrast enhancement.[217]

With the discovery of the thiol bridging interfacial bond structure, the energetics of Au25MPCs in correlation with the absorbance features has been convincingly addressed. However, the impacts of the novel bond structure on other physiochemical properties remain to be explored.[18,19,326] Specifically, luminescence spanning over UV visible near IR range has been reported from dendrimer protected Au clusters,[372,373] Au(I) species,[337,374] and Au MPCs. [116,115,339,341] The physical origin of the Au cluster luminescence is poorly understood, as each type of material displays a correlation to the electronic structures revealed by absorbance and/or electrochemistry. Furthermore, the reaction mechanisms of the ligand exchange process, known to generally follow a first order kinetics, were previously interpreted based on simple Au-S bonding and need to be further addressed.[78,98,361-363,375]

Accordingly, multidentate dithiol ligands DMPS have been employed to tailor the composition and physical property of Au DTCs in our group.[350] Other multi-thiols have also been employed to enhance the stability of Au nanoparticles and designated biointeractions.[376-379] With comparable core sizes and ligand polarity to those luminescent Au MPCs, including mercaptopropanesulfonate (monothiol) Au MPCs,[341] the DMPS (dithiol) Au DTCs display no near IR photoluminescence. In this report, the impacts of the structural constraint imposed by the dithiols on the physical properties and ligand exchange process are further investigated. Optical properties (absorbance and luminescence) and structural transition are non-invasively characterized by UV visible absorbance, luminescence and NMR spectroscopy. Two types of monolayer reactions of 1: monothiol tiopronin Au MPCs with DMPS dithiol molecules and 2: DMPS Au DTCs with tiopronin monothiol molecules, are studied. In the reaction of tiopronin Au MPCs with DMPS molecules, the analysis of the reaction kinetics reveals a two step mechanism, with a facile ligand re-

placement followed by a sluggish core etching process. The reverse approach, tiopronin molecules with DMPS Au DTCs, results in the addition of tiopronin into DMPS monolayer instead of ligand exchange. Near IR luminescence is efficiently quenched upon tiopronin release in the first type of reaction, and generated upon tiopronin attachments in the reverse approach. The finding proves that near IR luminescence is uniquely related to Au-tiopronin bonding unavailable in Au-DMPS interactions. The study also suggests that interfacial bond structures, in addition to the quantum confinement, could affect or even dominate the physical properties of nanomaterials that have a significant percentage of atoms participating in surface bonding.

3.2 Results and Discussion

3.2.1 Optical Properties Monitored by Absorbance and Luminescence of Tiopronin MPCs with DMPS Molecules

Monothiol tiopronin MPCs, with an average composition of $Au_{201}(Tiopronin)_{85}$ as previously reported, display broad near infrared luminescence in 600-850 nm range when excited at *ca.* 500 nm or shorter wavelength.[345,380] At this size range, a featureless decay from ultraviolet to visible range is generally observed in the absorbance spectrum, as the core size is too small for an obvious surface plasmon (SP) band but too big for discrete energy states, or absorbance band/s to form. Upon the addition of DMPS dithiol molecules, the transition of absorbance and emission features is presented in **Figure 3.1**, with the arrows indicating the trend over time. In the absorbance panel, an absorption band centered at 282 nm intensifies while the absorbance in visible range around 400 nm decreases gradually. The emission intensity at 600-850 nm decreases, shown in the inserted panel, but at a much faster rate. The final absorbance spectrum with the strongest 282 nm absorbance band was collected after *ca.* 3 weeks while the 600-850 nm emission diminished within ~2 days. A characteristic absorbance band at 282 nm has

been reported from the directly synthesized DMPS Au_4 clusters.[381] The change of absorbance reflects the core transition of tiopronin MPCs into DMPS Au_4 DTCs, as confirmed by the mass spectrometry results discussed next. The transition is also strongly supported by the isosbestic point at *ca.* 310 nm, which indicates the change of species with different extinction coefficients. The decrease of emission intensity is in accordance with the argument of DMPS DTC formation, as no luminescence at the near infrared wavelength range was detected from the as-synthesized DMPS DTCs of several different sizes (Au_4 up to a few nanometers in core diameter).

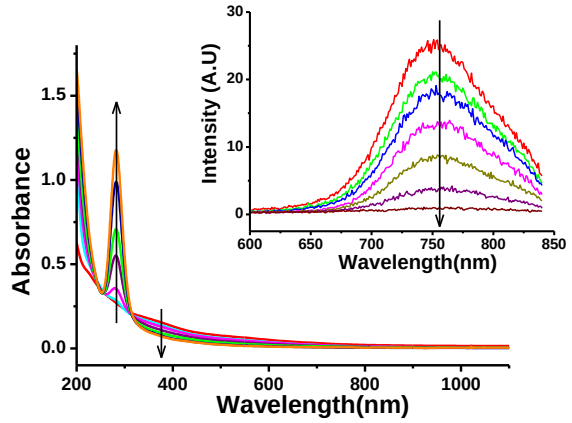

Figure 3.1. Absorbance and luminescence spectra of monolayer reaction of tiopronin MPCs with DMPS molecules. The concentration of tiopronin Au MPCs was *ca.* 1.00×10^{-7} M. The ligand mole ratio (R) of DMPS/Tiopronin was 10:1. The reaction was performed at room temperature in aqueous solution. Absorbance spectra from bottom to top at 282 nm: Tiopronin MPCs only, 3 h, 15 h, 50 h, 114 h, 258 h, and 426 h. Emission Spectra (Inserted plot, excited at 450 nm) from top to bottom at 760 nm: Tiopronin MPCs only, 5 min, 1 h, 15 h, 26 h, 50 h and 114h). Note the luminescence diminished within days and the absorption of 282 nm peak kept increasing over ~3 weeks.

Near IR luminescence has been observed from several types of Au MPCs with core diameter smaller than 2 nm and attributed to d-sp band transition.[382] A threshold size has been accurately charac-

terized to be *ca.* 2.2 nm using hexanethiolates as the sole protecting ligands.[383,384] The emission is significantly enhanced by the introduction of various polar monothiol ligands in MPC monolayer, with quantum efficiency up to *ca.* 10^{-2} observed.[116,385] For MPCs with drastically different energetics revealed by absorbance and electrochemistry,[386] the emission energy, however, displays weak dependence on the overall MPC energy states. On the basis of those observations, the physical origin of the emission was attributed to not just pure atomic energy levels, but certain localized states at core-monolayer interface.[116,385] It is therefore very interesting to notice the novel thiol-bridging bond structures predicted by density function theory calculation and elucidated by X-ray crystallography.[108,138,297] Note in each thiol-bridging structure, one Au atom is uniquely positioned away from all other core atoms. The optical features in the monothiol-dithiol exchange suggest that the luminescence be correlated with those Au-tiopronin surface interactions not available upon DMPS dithiol replacements.

3.2.2 Characterization of Monolayer Reaction Products of Tiopronin MPC with DMPS Ligands

After the absorbance transition was finished, the monolayer reaction products were analyzed by MALDI MS. Under negative reflectron mode, both Au_4L_3 (1344.6) and Au_4L_4 (1530.5) were found to be the major species in the mass spectrum presented in **Figure 3.2**. This is further confirmed by the absorbance signatures and non-invasive NMR characterization measured in solution shown next. The isotope pattern of 32S and 34S can be clearly seen in the two inserted panels. The signals below 1000 m/z are not included due to the overlapping with the matrix background. No detectable peak is observed above 5000 m/z. Other m/z signals, summarized in **Table 3.1**, are attributed to the residual intermediates of the incomplete reaction and their fragmentation in MS analysis. Note the mass spectra of tiopronin MPCs and large DMPS Au DTCs have been previously reported with rich fragmentations at wide m/z ranges.[16,350] The normalized absorbance spectra of the synthesized and exchanged products can be

found in **Figure 3.3**. Besides the 282 nm absorption band intensity, two absorbance curves overlap very well, supporting the existence of Au4 DTCs in both systems. The polydispersity of the exchange products contributes to the higher baseline therefore the less defined 282 nm absorbance band. The reaction was not monitored by MS, as direct correlation to the physical properties could not be achieved by the invasive measurements. Further MS analysis of the reaction intermediates and the corresponding fragmentations could offer insights of the reaction mechanism.

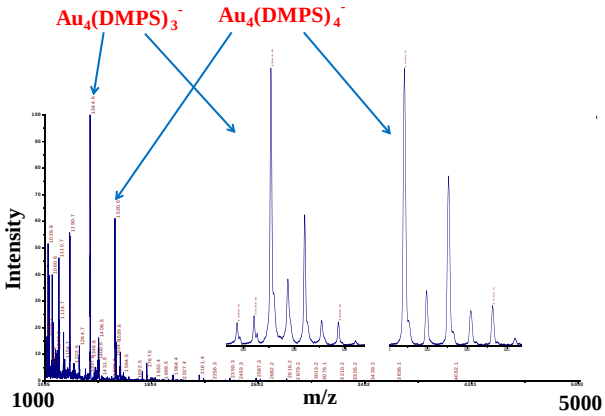

Figure 3.2. MALDI MS spectrum of DMPS DTCs formed by monolayer reaction of tiopronin MPCs with DMPS. The spectrum was collected with CHCA (α-cyano-4-hydroxycinnamic acid) as matrix under negative reflectron mode. No appreciable signal was detected in higher m/z region. The two labeled peaks correspond to $Au_4(DMPS)_3$ and $Au_4(DMPS)_4$ respectively. Other less abundant m/z peaks display similar pattern as those shown in **Figure 3.14**.

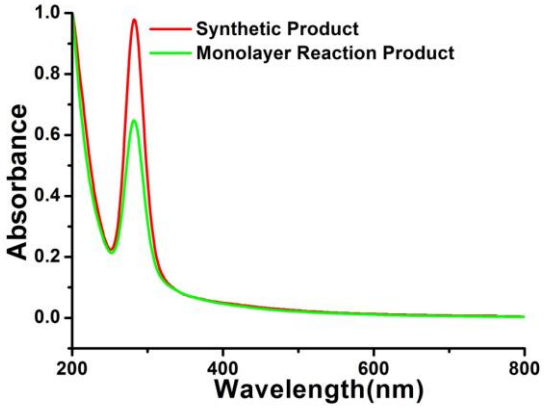

Figure 3.3. Comparison of normalized absorbance spectra of the synthesized DMPS Au_4DTCs and the products of tiopronin Au MPC-DMPS monolayer reaction. DMPS Au_4DTCs were synthesized as reported[350] with DMPS:Au mole ratio being 3.

3.2.3 NMR Studies of Reaction Process of Tiopronin MPCs with DMPS

To understand the reaction mechanism and to correlate the transition of the optical features with the dithiol-monothiol exchange process, the reaction was monitored in-situ by proton NMR. In comparison to optical studies, a much higher concentration was used to detect respective proton signals. Upon attachments to the Au core, the sharp proton peaks of unbound ligand molecules in NMR spectra are broadened and lose the fine structures, known as line-broadening effects. The effect has been employed to signal the presence of free ligands in the purification and to monitor the electron and ligand exchange reactions of Au MPCs.[78,326,361,362] The proton NMR signal changes in the process of monolayer reaction of tiopronin MPCs at *ca.* 5.0×10^{-5} M concentration with DMPS (R=10) are presented in **Figure 3.4**. The broad peaks at *ca.* 1.5-2 ppm and 3.5-4 ppm in the top spectrum represent the methyl and methylene groups of tiopronin MPCs. The sharp spikes at *ca.* 2.4 and 2.7 ppm, unchanged during the reaction process and presumably the impurities, conveniently serve as the internal standard for quantification purpose.

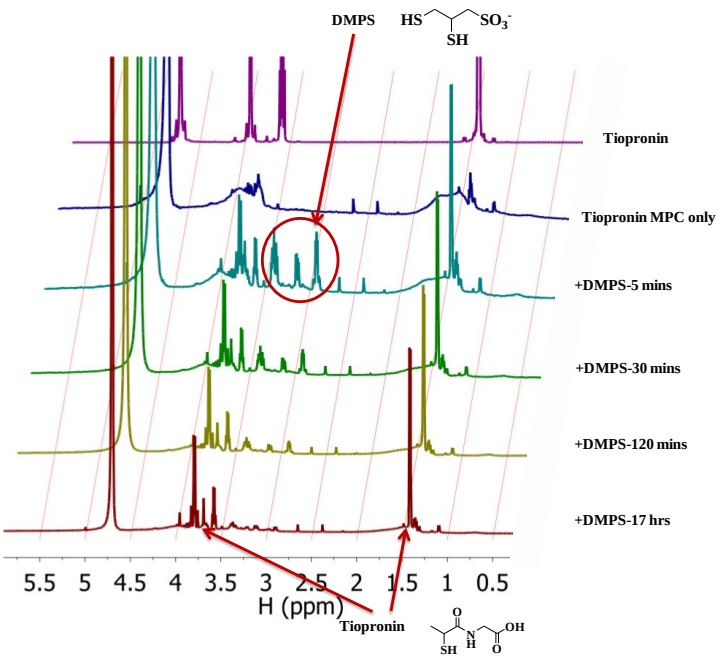

Figure 3.4. ^{1}H NMR spectra of monolayer reaction of tiopronin MPCs with DMPS. From top to bottom: Tiopronin molecule, Tiopronin MPCs only, Tiopronin MPC + DMPS 5 min, 30 minutes, 120 minutes, and 17 hours. The concentration of tiopronin MPCs is *ca.* 5.0×10^{-5} M with ligand mole ratio R of 10:1 in solvent D_2O.

With the addition of DMPS ligand, the sharp signals of free DMPS can be observed as indicated in the second spectrum collected immediately after the addition and mixing process (5 mins). The sharp features from free tiopronin ligands develop over the broad peaks, indicating gradual release of tiopronin ligands. Meanwhile, the intensities of the DMPS proton peaks decrease over time, due to the line broadening and overlapping with tiopronin signals upon binding to Au. By comparing the decrease of free DMPS proton peaks at *ca.* 2.9 ppm and the increase of free tiopronin signal at *ca.* 3.8 ppm over time, calibrated with the unchanged signal at 2.4 ppm or HOD signal at *ca.* 4.7 ppm in D_2O, it is estimated that each DMPS releases two tiopronin molecules. The ligand reaction kinetics studied by NMR reveals an initial fast step, plotted in supporting information **Figure 3.5**., and a subsequent slower process at much longer time (not shown). The percentage of the liberated over the total number of tiopronin ligands in

the monolayer is ca. 30% during the initial step. The exchange kinetics is in agreement with those reported in the case of monothiol exchange reactions.[361,362] Previous NMR studies revealed a two step reaction process with *ca.* 20-30% of the total surface ligands being replaced efficiently while the rest display sluggish kinetics. The heterogeneous exchange reactivity has been attributed to the surface locations such as vertex, edge and terrace sites on the Au core. The monothiol replacement by dithiol is comparable to those observed by luminescence, suggesting the luminescence is ligand dependent. During the review process, it caught our attention that a structurally constrained multidentate ligand was found to exchange only with monomeric staple motif but not extended units (dimer) on Au38 and Au40 clusters.[387] Considering the smaller dithiol molecules used in this study that do not have the intramolecular structural constraint, the steric hindrance effect is not expected to be significant.

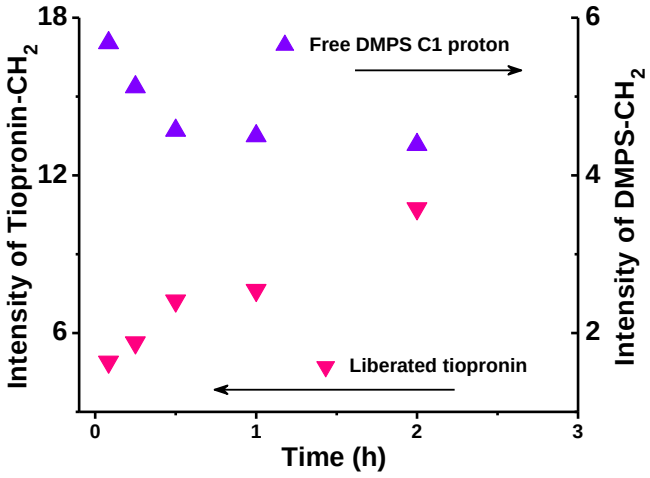

Figure 3.5. Monolayer reaction kinetics of tiopronin Au MPCs with DMPS studied by ^{1}H NMR. The increase of tiopronin methylene proton intensity (left axis) and the decrease of DMPS C1 proton intensity (right axis) display a *ca.* 2:1 correlation in the first 2 hours calculated from **Figure 3.4**.

It is well known in core etching studies that core size changes feature a sluggish kinetics and require harsh conditions such as elevated temperature and huge excess of thiols.[120] The core size change

during the fast ligand replacement monitored by luminescence and NMR is therefore considered negligible, attested by the much slower absorbance changes observed in **Figure 3.1**.

3.2.4 Kinetics of Monolayer Reaction of Tiopronin MPCs with DMPS

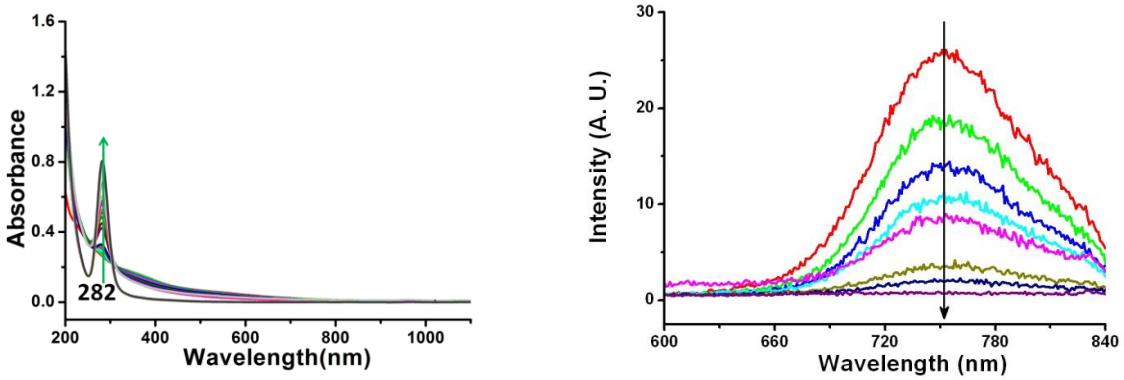

Figure 3.6. Absorbance and luminescence spectra of tiopronin MPCs reaction with DMPS. The concentration of tiopronin MPCs is 1.00×10^{-6} M. The ligand mole ratio DMPS/Tiopronin (R) = 10:1. The absorbance spectra at 282 nm from bottom to top: Tiopronin MPCs only, 5 min, 30 min, 1 h, 2 h, 4 h, 6 h, 21 h, 29 h, 45 h, 53 h, 69 h, 94 h, 113 h, 121 h, 137 h, 145 h, and 161 h. Emission Spectra excited at 450 nm from top to bottom: Tiopronin MPC only, 5 min, 30 min, 1 h, 2 h, 4 h, 6 h, and 21 h. The fluorescence diminishes in ~ 1 day, and the 282 nm peak absorption keeps increasing in ~3 weeks. Each spectrum was collected by taking a certain amount of reaction mixture and diluted by a factor of 10 immediately before the measurement at the indicated time.

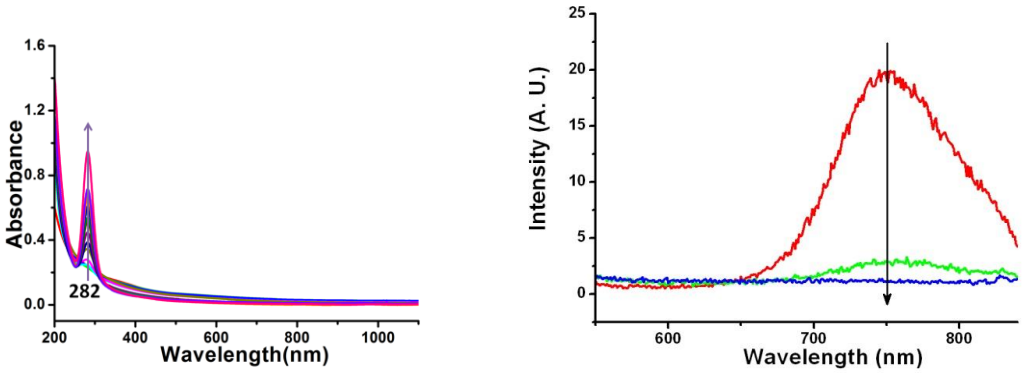

Figure 3.7. Absorbance and luminescence spectra of tiopronin MPCs reaction with DMPS. The concentration of tiopronin MPCs is 1.00×10^{-5} M. The ligand mole ratio DMPS/Tiopronin (R) = 10:1. The absorbance spectra at 282 nm from bottom to top: Tiopronin MPCs only, 5 min, 30 min, 2 h, 4 h, 7 h, 23 h, 32 h, 47 h, 55 h, 71 h, 79 h, 95 h, 120 h, 191 h. Emission Spectra excited at 450 nm from top to bottom: Tiopronin MPC only, 5 min and 30 min. The fluorescence diminishes in ~ 30 minutes, and the 282 nm peak absorption keeps increasing in ~3 weeks. Each spectrum was collected by taking a certain amount of reaction mixture and diluted by a factor of 100 immediately before the measurement at the indicated time.

The reaction mechanism is further studied by varying the concentration and ratio of the reactants. Representative luminescence emission and absorbance spectra can be found in supporting information **Figure 3.6** and **Figure 3.7**, which display similar features as shown in Figure 1. Summarized in **Figure 3.8**, the emission maxima at ca. 760 nm and the absorbance values at 282 nm of the corresponding reactions are plotted against reaction time in panel A and B respectively. Luminescence displays strong concentration dependence of both reactants, indicating the signal being affected by a single step process involving both reactants. In each reaction, the changes of luminescence intensity are much faster compared to the absorbance changes. With MPC concentration at 1×10^{-5} M and dithiol: monothiol ligand ratio (R) being 10, the luminescence disappears within 30 minutes, shown in **Figure 3.7**. The luminescence kinetics is apparently in accordance with the initial fast stage in NMR measurements, which indicates heterogeneous contribution of tiopronin ligands in the monolayer to the Au MPC luminescence. In other words, those tiopronin ligands being efficiently released correlate to the luminescence intensity decrease while those being replaced slower are less involved in the emission related process. Note the ligand molecules and Au(I) species are known to be non-luminescent.[341]

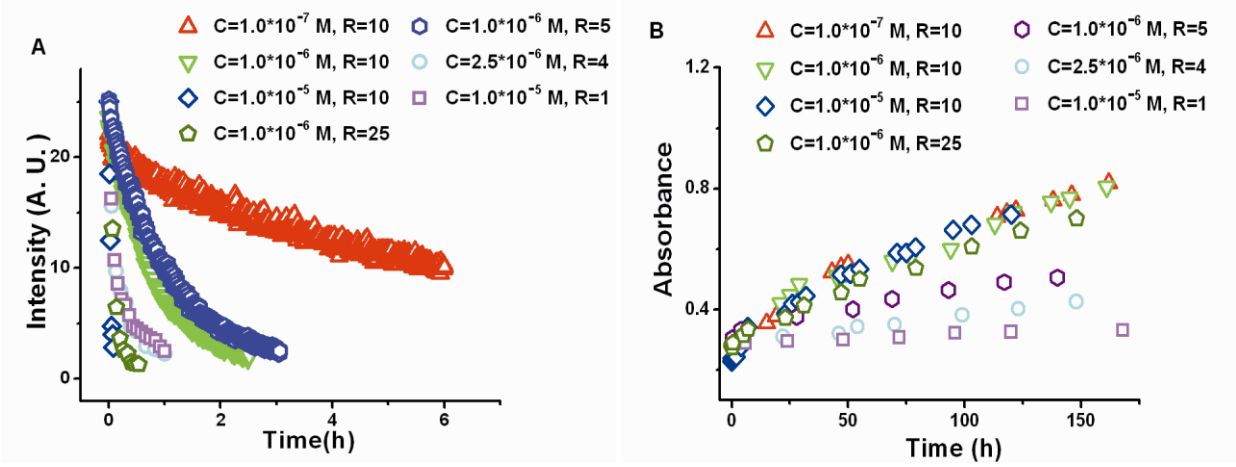

Figure 3.8. Kinetics of monolayer reactions at different reactant Au MPC concentration and ligand mole ratio R (DMPS:tiopronin). A: Emission intensity changes at 760 nm (excited at 450 nm); B: Absorbance changes at 282 nm.

Monitored at 282 nm, the absorbance changes reflect the combined effects of Au DTC formation and tiopronin Au MPC consumption. The isosbestic point indicates the conversion of chemical species with different extinction coefficients. It is interesting to notice that the absorbance changes are independent of reactant concentration with R values at 10 or larger. At lower R values (1-5) at which the pseudo-first order condition could not be assumed, the absorbance transition features a more sluggish kinetics and deviates from the overlapped trends. The independence of absorbance changes with respect to initial reactant concentration at high R values in **Figure 3.8.B** suggests zero order kinetics. The zero order kinetics indicates a self reorganization process, presumably involving the intermediate species formed after luminescence transition. At high R values, sufficient dithiol molecules will increase the possibility of the dithiols occupying adjacent sites on the Au surface, which facilitates the surface reorganization and Au4DTC formation. Correspondingly, the Au4DTC absorbance increases much slower at low dithiol ratios. The deviation from linearity in **Figure 3.8.B** is attributed to the dissociation of

Au4DTCs, which will change the extinction coefficient of the remaining Au MPC. The absorbance changes are qualitatively in accordance with the core etching behaviors.[120]

The representative fitting of the reaction kinetics is presented in **Figure 3.9**. As the DMPS Au DTCs are non-luminescent in the wavelength range, the emission intensity changes over time in panel A directly reflect the rate of the forward reaction, or the disappearance of luminescence energy states on Au MPCs. All luminescence curves in **Figure 3.8.A** can be excellently fitted with second order reaction kinetics. The results suggest that the rate determining reaction step related to the luminescence energy states is an associative bimolecular reaction. At high dithiol: monothiol ratios (R>1) at which the pseudo-first order condition is met, the facile extinction of luminescence can be reasonably fitted with a first order kinetic equation. Representative fitting displays a single linear line shown in panel A of **Figure 3.9**. The fitted first order rate constants display nicely defined concentration dependence with respect to the excess DMPS ligands, shown in panel B of **Figure 3.9**, confirming the reaction is first order for either reactant, or second order overall. The rate constant is found to be ca. 73.5 $M^{-1}s^{-1}$, faster that the kinetics observed in monothiol place exchange reactions.[361] The observation further supports that dithiols preferentially bind to Au over monothiols, as much lower concentration and ratio were employed in the current studies in comparison to the monothiol exchanges.[361,362]

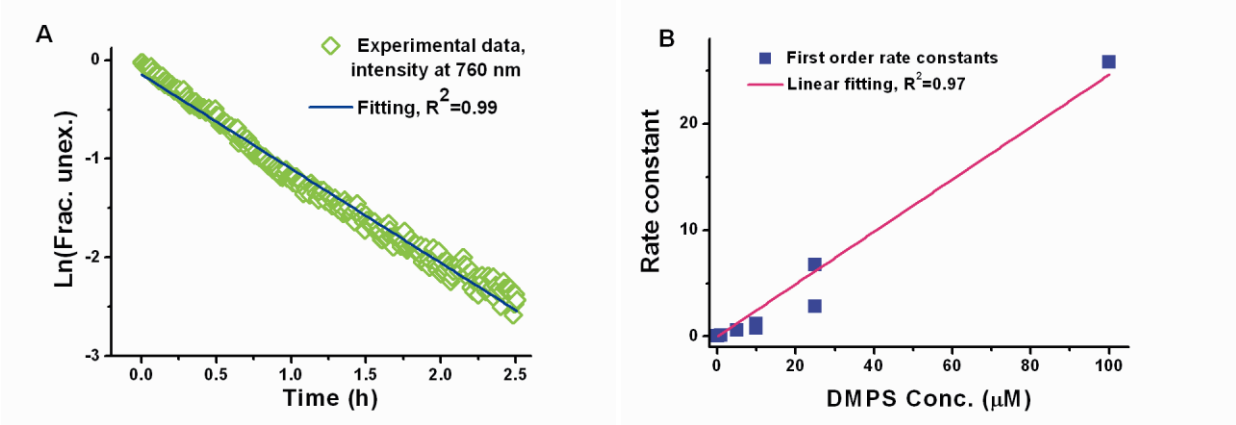

Figure 3.9 A: Representative first order fitting of luminescence changes. The y axis is the natural logarithm of the intensity at time *t* over the original intensity at *ca.* 760 nm excited at 450 nm; B: Linear correlation of fitted first order rate constants of luminescence changes with DMPS concentration.

3.2.5 Proposed Mechanism of Monolayer Reaction of Tiopronin MPCs with DMPS

The results suggest a consecutive reaction pathway, with the signal transitions originated at different reaction processes: a fast ligand exchange process followed by a zero order reorganization process (core etching) that leads to the formation of the Au4DTCs. The proposed mechanism is presented in **Scheme 3.1**. In the first step, each DMPS ligand efficiently replaces two tiopronin molecules on the surface of the MPCs due to the entropy gain characterized by NMR results. As the surface bonding changes from Au-monothiolate to Au-dithiolate, the luminescence is efficiently quenched. The main differences between the monothiol and dithiol surface attachments would be the structural constraint imposed by the 2, 3-dithiol DMPS. Meanwhile, the gold core change is considered negligible, evidenced by the less affected absorbance features. The second step corresponds to the core etching and Au4DTC formation, shown as the slow enhancement of the 282 nm absorption band and confirmed in the mass spectrum. It is well known that the Au core etching by monothiols is a much slower process at room temperature.[120] At this step, those adjacent DMPS ligands on gold core surface are expected to be the

prerequisites for the formation of the DMPS Au4 DTCs. Dithiol surface reorganization is much slower therefore slower kinetics is detected.

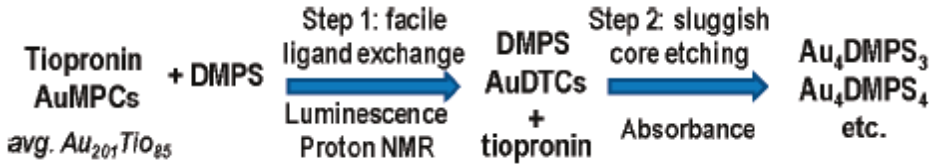

Scheme 3.1. Proposed reaction mechanism of tiopronin MPCs with DMPS.

3.2.6 UV-Visible Absorbance and Luminescence Features of DMPS DTCs with Tiopronin Molecules

To confirm the proposed reaction mechanism, and specifically the correlation of near IR luminescence to the Au-monothiol surface bonding unavailable in the Au-dithiol system, the reverse reaction of DMPS DTCs with tiopronin was performed. Considering the reported core size dependence at *ca.* 2.2 nm in monothiol MPC luminescence,[156,388] two types of DMPS Au DTCs were selected with the average sizes at ca. 1.5 nm and 2-5 nm respectively, characterized by AFM.[350] The absorbance and emission spectra of the monolayer reaction of 1.5 nm DMPS DTCs with tiopronin ligands are shown in **Figure 3.10**. No emission at 700-1000 nm range is observed from the original DTCs. After the addition of free tiopronin molecules, the near IR emission intensifies gradually. The results strongly suggest that unique Au-tiopronin monothiol interactions are the origin of the near IR emission. Meanwhile, the absorbance band at 282 nm intensifies slightly upon the addition of tiopronin monothiols. As thiolates are known to be mobile on Au, the presence of excess thiols (tiopronin) presumably facilitates the dithiol surface motion/reorganization and lead to the formation of Au_4DTCs.

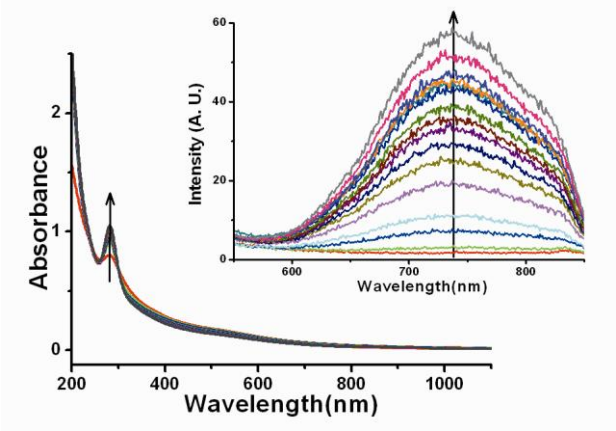

Figure 3.10. Monolayer reaction of 1.5 nm DMPS DTCs with tiopronin molecules monitored by absorbance and luminescence. The ligand mole ratio of tiopronin:DMPS is ca. 2:1 with the concentration of DMPS DTCs at *ca.* 1×10^{-5} M. From bottom to top, the absorbance band at 282 nm and emission intensity were collected from: DMPS DTCs only, 5 min, 4 h, 5 h, 28 h, 48 h, 72 h, 96 h, 120 h, 144 h, 168 h, 193 h, 216 h, 264 h, 312 h, and 360 h. Emission spectra were recorded with excitation wavelength at 450 nm.

To further demonstrate the core size impacts on the luminescence, the reaction of larger DMPS Au DTCs (2-5 nm) with tiopronin molecules was studied. Presented in supporting information **Figure 3.11**, the original Au DTCs display a slight SP band at 520 nm. The luminescence increased but at much less extent, attributed to the low population of smaller DTCs in the ensemble of larger Au cores. Again the Au4 absorbance band at 282 nm increased while the lower energy absorbance decreased over time, corresponding to the Au_4DTCs formation.

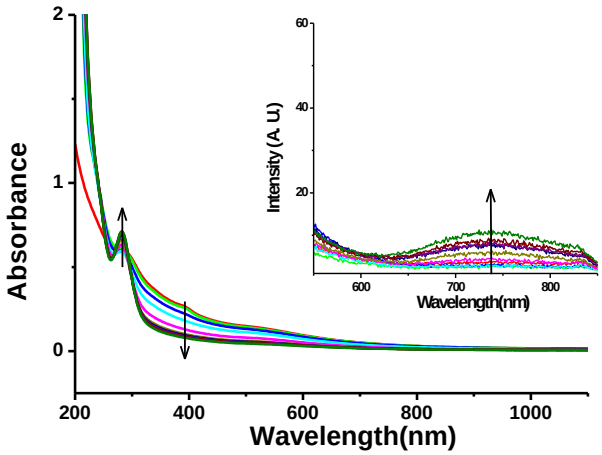

Figure 3.11. Absorbance and luminescence spectra of 2-5 nm DMPS Au DTC (0.5X) reaction with tiopronin molecules. The absorbance spectra at 400 nm from top to bottom: DMPS DTCs-0.5X only, 5 min, 1 h, 5 h, 24 h, 48 h, 72 h, 96 h, 120 h, and 144 h. Corresponding emission spectra excited at 450 nm were inserted. The emission intensity at ca. 730 nm increases from bottom to top. The concentration of DMPS DTCs (0.5X) is estimated to be 1.00×10^{-5} M and the mole ratio of tiopronin: DMPS of 2: 1. (Considering the weak surface plasmon band at 520 nm in absorbance spectra and assuming both thiol groups attached to the gold core, the composition is assumed to be $Au_{314}(DMPS)_{45}$ as a primary estimate based on the reported composition of large tiopronin Au MPCs.)

3.2.7 Characterization of DMPS DTCs with Tiopronin Molecules

Interestingly, the addition of excess tiopronin ligands did not liberate DMPS ligands. The proton NMR spectra of monolayer reaction of 1.5 nm DMPS DTCs with tiopronin are presented in **Figure 3.12**. The NMR spectrum of 1.5 nm DMPS DTCs displays more significant line-broadening effects compared to free DMPS ligand or Au_4DTCs (ca. 1.0 nm).[350] Upon the addition of tiopronin ligands, the broad proton signals from DMPS DTCs became better resolved, approaching the Au_4DTC features. More importantly, no released free DMPS signal is detected, as it would be an entropy loss process. The sharp features from free tiopronin appeared diminished due to the broadening effect, corresponding to surface at-

tachment to the gold core. Similar trends can also be observed from the reaction of 2-5 nm DMPS DTC with tiopronin, which is presented in supporting information **Figure 3.13**. The reaction also leads to the addition of tiopronin ligands into the DTC monolayer instead of a ligand exchange process. The formation of Au_4DTCs is therefore resulted from surface reorganization of DMPS ligands in the presence of excess tiopronin binding to the gold core. During the process, mixed monthiol tiopronin and dithiol DMPS stabilized clusters have been formed. The ligand addition process is illustrated in **Scheme 3.2**.

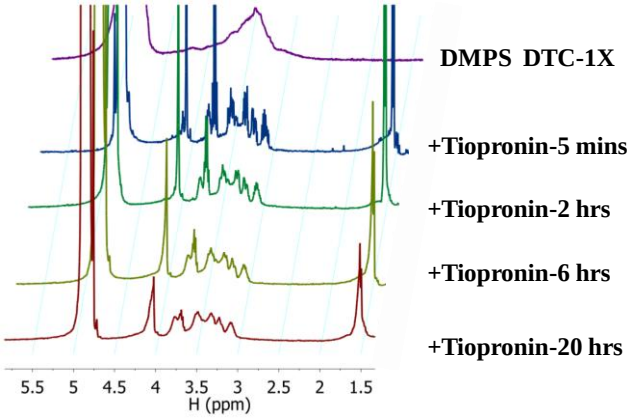

Figure 3.12. ^{1}H NMR spectra of monolayer reaction of 1.5 nm DMPS DTCs with tiopronin. From top to bottom: 1.5 nm DMPS DTCs only, DMPS DTC-1X + Tiopronin-5 min, 2 hrs, 6 hrs, and 20 hrs. Tiopronin: DMPS molar ratio *ca.* 2: 1, in solvent D_2O.

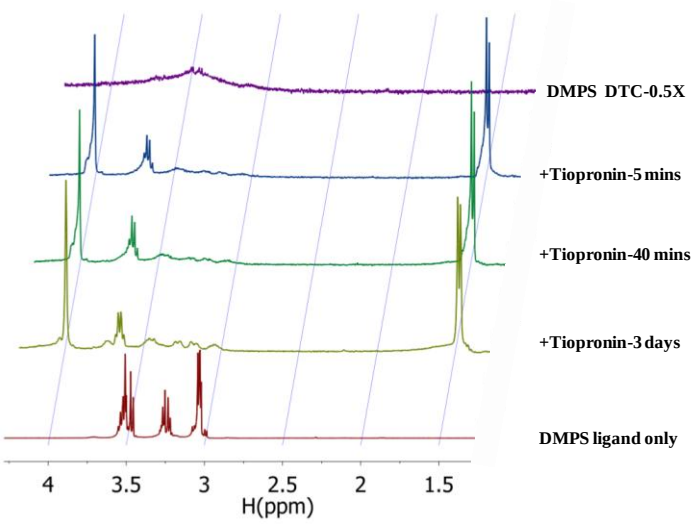

Figure 3.13. ^{1}H NMR spectra of monolayer reaction of 2-5 nm DMPS DTCs (0.5X) with tiopronin. Tiopronin: DMPS= 2:1. From top to bottom: DMPS DTCs-0.5X only, DMPS DTCs-0.5X + DMPS after 5 minutes, DMPS DTCs-0.5X + DMPS 40 minutes, DMPS DTCs-0.5X + DMPS 3 day, DMPS ligand only.

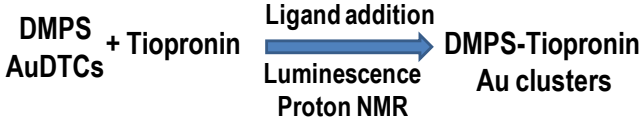

Scheme 3.2. Reaction route of DMPS DTCs with tiopronin. The core etching process is not included.

The composition of the reaction products of 1.5 nm DMPS DTCs with tiopronin was analyzed by MALDI MS. A mixture of m/z peaks can be identified with composition up to $Au_{20}S_{10}$ with reasonable intensity in **Figure 3.14** and listed in **Table 3-1**. While the laser intensity was continuously varied following the reported procedure,[27] significant fragmentation was consistently observed with well defined Au_xS_y patterns illustrated in the inserted panel. Therefore, the assigned m/z peaks are believed from ionization/fragmentation, which suggests the presence of corresponding large species in the reaction products. The peak at m/z of 1344.6, corresponding to Au_4L_3 (L=DMPS) anion (losing one proton) can be easily identified. However, the Au_4L_4 signal is much weaker. As no extra DMPS was available in the reaction

mixture, Au_4L_3 was more favored over Au_4L_4 as the final product. Therefore, the less abundant Au_4L_4 supports the proposed surface reorganization process induced by the addition of tiopronin. As both Au_4L_3 and Au_4L_4 are present at comparable abundance in the MS spectrum collected under similar conditions (**Figure 3.2** and previous report[350]), fragmentation of Au_4L_4 is not expected. The expanded view of the Au_4L_3 m/z signal is included in **Figure 3.15**, in which the isotope pattern similar to that shown in **Figure 3.2** can be observed. Other than the Au_4L_3, the Au_6S_5 (1341.5 **Figure 3.15**) and Au_7S_5 (1539.5) anions are notable favorable fragments detected. Periodic patterns of Au_xS_y are observed. Similar behaviors were obtained from the reaction products of 2-5 nm DMPS DTCs with tiopronin (**Figure 3.16**). Further analysis of the intriguing mass fragments and reaction kinetics are underway.

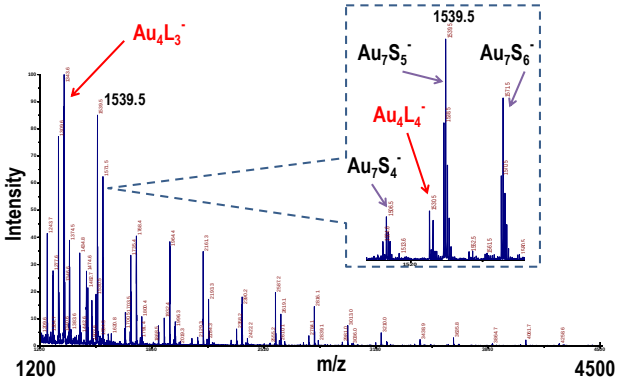

Figure 3.14. MALDI MS characterization of monolayer reaction product of 1.5 nm DMPS Au DTCs with tiopronin. L represents DMPS ligands. The spectrum was collected with CHCA matrix under negative reflectron mode.

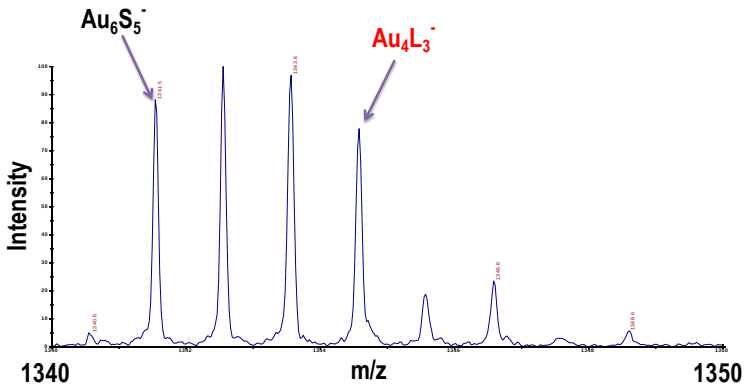

Figure 3.15. Expanded view of m/z patterns of Au_4L_3 and Au_6S_5 anions that display isotope peaks.

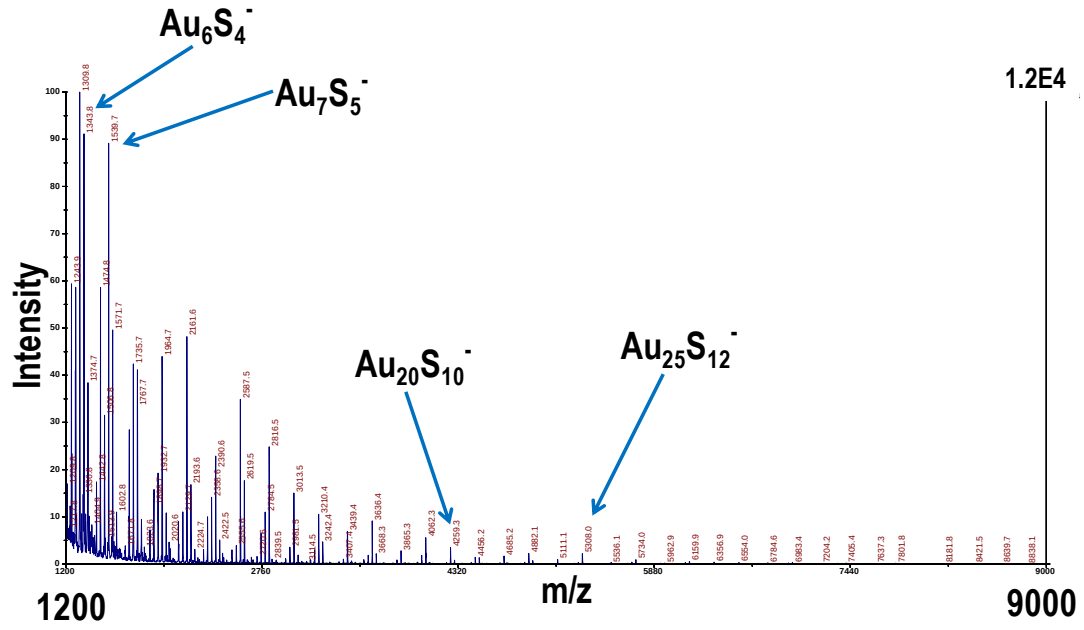

Figure 3.16. MALDI MS results of monolayer reaction product of 2-5 nm DMPS Au DTCs with tiopronin. CHCA (α-cyano-4-hydroxycinnamic acid) matrix was used.

Table 3.1. Mass spectrometric peak assignments of **Figure 3.2**, **Figure 3.15** and **Figure 3.16**. The larger deviations of the calculated values versus the experimental results at higher m/z are attributed to the instrumental calibration (note the deviation and m/z values displays a linear correlation).

Tiopronin MPC +DMPS Experimental m/z	DTC-1X+Tiopronin Experimental m/z	DTC-0.5X+Tiopronin Experimental m/z	Calculated m/z	Peak assignment

1344.6	1343.6		1345 (Au:197; S:32; minus H)	$Au_4(DMPS)_3^-$
1530.5	1530.5		1531 (Au:197; S:32; minus H)	$Au_4(DMPS)_4^-$
	1539.5		1539.1	$Au_7S_5^-$
1570.5	1571.5	1571.7	1571.2	$Au_7S_6^-$
1703.5	1703.5		1704.0	$Au_8S_4^-$
1767.4	1768.4	1767.7	1768.1	$Au_8S_6^-$
1799.4	1800.4		1800.2	$Au_8S_7^-$
1932.5	1932.4	1932.7	1933.0	$Au_9S_5^-$
1964.4	1964.4	1964.7	1965.1	$Au_9S_6^-$
1996.4	1996.3		1997.2	$Au_9S_7^-$
	2129.3	2129.7	2130.0	$Au_{10}S_5^-$
2161.4	2161.3	2161.6	2162.1	$Au_{10}S_6^-$
2193.3	2193.3	2193.6	2194.1	$Au_{10}S_7^-$
	2326.3		2327.0	$Au_{11}S_5^-$
2390.3	2390.2	2390.6	2391.1	$Au_{11}S_7^-$
2422.2	2422.2	2422.5	2423.2	$Au_{11}S_8^-$
2555.3	2555.2	2555.6	2556.0	$Au_{12}S_6^-$
2587.2	2587.2	2587.5	2588.1	$Au_{12}S_7^-$
	2752.1		2753.0	$Au_{13}S_6^-$
2816.1	2816.1	2816.5	2817.1	$Au_{13}S_8^-$
3013.1	3013.0	3013.5	3014.1	$Au_{14}S_8^-$
3210.0	3210.0	3210.4	3211.0	$Au_{15}S_8^-$
3438.9	3438.9	3439.4	3440.0	$Au_{16}S_9^-$
3635.9	3635.8	3636.4	3637.0	$Au_{17}S_9^-$
3864.8	3864.7	3865.3	3866.1	$Au_{18}S_{10}^-$
4061.7	4061.7	4062.3	4063.0	$Au_{19}S_{10}^-$
4258.6	4258.6	4259.3	4260.0	$Au_{20}S_{10}^-$
		5308.0	5309.0	$Au_{25}S_{12}^-$

3.3 Experimental Section

3.3.1 Chemicals

Tetrachloroauric acid ($HAuCl_4 \cdot 3H_2O$, >99.99% metals basis), sodium borohydride ($NaBH_4$, 99%), sodium 2, 3-dimercaptopropanesulfonate monohydrate ($C_3H_7O_3S_3Na \cdot H_2O$, ~95%), N-(2-Mercaptopropionyl)-glycine (Also named tiopronin, $C_5H_9NO_3S$, >98.0%), and solvents were used as received from Aldrich. Water (18.2 MΩ·cm) was purified by Barnstead Nanopure system.

3.3.2 Measurements

UV-Visible absorbance spectra were recorded with a Shimadzu UV-1700 spectrophotometer. Mass spectrometry (MS) spectra were acquired with ABI 4800 matrix assisted laser desorption ionization (MALDI) TOF-TOF analyzer. Aqueous soluble α-Cyano-4-hydroxycinnamic acid (CHCA) was used as the matrix. Luminescence was measured with a Horiba Jobin-Yvon Fluorolog 311 spectrometer with T channel, through which a PMT detector in visible range and an InGaAs near IR detector can be used. Proton NMR spectra were acquired on a Bruker Avance 400 MHz spectrometer in deuterated water.

3.3.3 Synthesis of Tiopronin Au MPCs and DMPS Au DTCs

Tiopronin MPCs were synthesized and purified following the reported procedure.[88] At thiol:Au mole ratio of 3 in the synthesis, the synthesized Au MPCs with average composition of $Au_{201}Tio_{85}$ was used in the exchange reactions. Dithiol DMPS clusters were synthesized via modified Brust reaction.[350] Briefly, dithiol ligands and $HAuCl_4$ were dissolved in nanopure water separately at respective amount and mixed under stirring. $NaBH_4$ was added to reduce those Au-dithiol intermediate species, followed by dialysis over 3-5 day period in nanopure water. The purified products were characterized by proton NMR, with broadened proton NMR signals confirming the removal of unbound DMPS molecules. No further separation was performed. The sizes of the clusters have been characterized to be 1.5±0.6 nm di-

ameter (1X DTC) and 2-5 nm diameter (0.5X DTC) by atomic force microscopy (AFM) imaging as recently reported, with X representing the initial DMPS-to-gold ratio during the synthesis.[350]

3.3.4 Monolayer Reactions of Au Clusters –Monothiol Tiopronin versus Dithiol DMPS

In a typical exchange reaction, aqueous solutions of Au clusters and incoming thiols were mixed at designed concentration and mole ratio. The reaction was monitored by absorbance and luminescence measurements, either directly from the reaction mixture or with the mixture diluted to proper concentration immediately before optical measurements. The ratio of incoming ligand molecules to original ligands was varied. Note the cluster:thiol ratio will differ by the number of ligands in the original monolayer. The overall concentration of Au clusters ranged from 10^{-8} to 10^{-5} M. The reactions at higher concentration were also monitored by proton NMR.

After the reaction was finished, confirmed by optical changes, the solution was acidified to pH=1 with hydrochloric acid and dialyzed with membrane (MWCO= 500). The dialyzed sample was confirmed free of unbound ligands by proton NMR and analyzed by MALDI MS.

3.4 Summary

In conclusion, the monothiol-dithiol monolayer reactions of Au clusters are studied. With DMPS dithiol molecules added, tiopronin molecules were efficiently liberated from Au MPC monolayer followed by a much slower core etching process with DMPS Au_4DTCs formed. Monolayer addition was observed in the reaction of DMPS DTCs with tiopronin molecules. The reaction kinetics was analyzed by UV-Visible absorbance, fluorescence, ^{1}H NMR spectroscopy. The near IR luminescence of Au MPCs is correlated with Au-monothiol interactions unavailable with the structurally constrained DMPS dithiols. The study also suggests that interfacial bonding, in addition to the nature of the materials and quantum

confinement, could dominate the physical properties of nanomaterials that have a significant amount of atoms participating in surface bonding.

This chapter is adapted with permission from Langmuir, 2011, 27, 2989-2996.

4 MIXED DITHIOLATE DURENE-DT AND MONOTHIOLATE PHENYLETHANETHIOLATE PROTECTED AU130 NANOPARTICLES WITH DISCRETE CORE AND CORE-LIGAND ENERGY STATES

4.1 Background and Research Strategy

Small gold nanoparticles stabilized by thiolates, often referred as monolayer protected clusters (MPC), have attracted extensive research interests due to their rich optical, electrochemical and other physiochemical properties.[1,3,4] Those fundamental properties, together with their favorable small dimension and non-toxic chemical components, lead to broad applications in biomedicine, sensing, optoelectronics and catalysis.[4,188,195,199] Breakthroughs have been achieved recently in the composition and structure elucidation of Au MPCs at atomic and molecular level, including $Au_{25}(SR)_{18}$, $Au_{38}(SR)_{24}$, and $Au_{102}(SR)_{44}$ by X-ray crystallographic studies[107,108,110,138,389] and theoretical calculations.[111,113,126,298,349] A novel interfacial bond structure, the RS-Au-SR "staple" motif, has been discovered in the form of single or extended units (e.g. RS-Au-SR-Au-SR), coping with different core surface curvatures.[107,108,110,111,113,126,138,298,349,389] Super-atom theory has been proposed, through which the underlying electronic structure corresponding to the absorbance features of these molecular gold clusters has been theoretically described.[112]

Nanomaterials with desired physiochemical properties are needed for targeted applications. It is important to correlate the composition and structure of the nanoclusters with their properties for application design. Toward that aim, extensive research efforts have been devoted to control the size, composition and shape of nanomaterials.[1,3,4] With the recent discovery of the "staple" motif at core-ligand interface of the Au MPCs,[107,108,138,389] interfacial bonding structures are believed to play an important role in the properties of nanoclusters, in addition to the well-known quantum confinement factors such as shape and size/composition.[350] Dithiolate-protected Au nanoclusters with 2, 3-dimercaptopropane-1-sulfonate (DMPS, a 1, 2-dithiol ligand) have been created.[350]

The Au-S bond formation with multidentate dithiols is determined by two factors: the structural constraint imposed on the surface bond formation by two thiol groups of one dithiol molecule, and the entropy gain of one dithiol over two monothiol molecules upon binding to gold. The favored composition and structure, in turn, affect the physical properties of the gold nanoclusters. The chemical reactivity, specifically the monolayer reactions between monothiol and dithiol molecules, has been explored.[343] The near IR luminescence is correlated to nanocluster composition and Au-thiolate interactions.[343] Dithiols and other multithiol ligands have also been employed in the stabilization of larger Au nanoparticles,[376,377,390] in the synthesis of Ag nanoclusters,[391] and targeted biointeractions.[378,379,392] Interesting phase segregation has been observed from the Au clusters stabilized by mixed monothiols of different polarities.[359,360] To the best of our knowledge, heterogeneous monothiolate and dithiolate ligands have not been employed in the nanocluster synthesis.

In this chapter, a new type of molecular gold nanocluster is created by employing mixed aromatic thiols, monothiol ligand phenylethanethiol (PhC2S) and dithiol ligand durene-α1, α2-dithiol (Durene-DT, a 1, 4-dithiol). The impacts of dithiol molecular structure and dithiol:monothiol:Au ratio on the cluster formation and properties are studied. The rationale is that the dithiols preferentially bind to Au due to entropy gain.[390,393] Meanwhile, monothiols fill into those sites inaccessible by the dithiols due to molecu-

lar structure constraint and core surface curvature. The mixed thiolate clusters (MTC) display discrete absorption bands and rich electrochemical properties. Near IR luminescence is reported. The average composition is characterized as $Au_{130}(Durene\text{-}DT)_{29}(PhC2S)_{22}$ at ±1-2 resolution. An energy diagram is proposed to correlate the energetics measured by optical and electrochemical methods.

4.2 Results and Discussion Results and Discussion

4.2.1 UV-Visible Absorbance of Mixed Thiolate Au Clusters

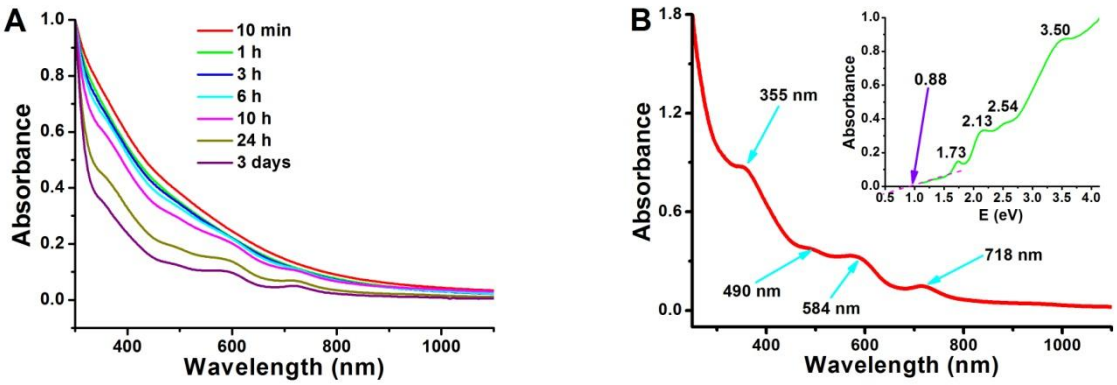

Figure 4.1. A. The absorbance change during the reduction. An aliquot of the reaction mixture in toluene phase was diluted to proper absorbance range for each measurement. The spectra were normalized at 300 nm. B. Absorbance spectrum of the purified product in methylene chloride. The spectrum plotted in energy axis is inserted.

The formation of Au MTCs after the reduction by $NaBH_4$ was monitored by UV-Visible absorbance measurements shown in **Figure 4.1**A. The absorbance of the reaction mixture displays a featureless decay upon reduction initially, e.g. at 10 minutes. Multiple discrete absorption bands intensified over 24 hrs and became slightly better defined in ~3 days. The transition suggests the formation of thermodynamically favored or kinetically trapped species. Similar "size focusing" process associated with absorbance conversion was also observed in the one phase synthesis of $Au_{25}(PhC2S)_{18}$.[31,394] The final products

were collected after the absorbance transition is finished in 1-3 days. The absorbance features of the purified product can be seen in **Figure 4.1**B. Four discernible bands at *ca.* 355 nm (3.50 eV), 490 nm (2.54 eV), 584 nm (2.13 eV), and 718 nm (1.73 eV) can be observed in the spectrum. An optical band gap of ca. 0.88 eV is extrapolated as indicated for this MTC sample.

It is well-known that various gold nanoclusters have discrete absorption bands. Au25 nanoparticle with ~1.33 eV band gap shows pronounced absorbance bands at ca. 400 nm (3.11 eV), 450 nm (2.76 eV), and 670 nm (1.86 eV).[97,104,108,119,395] Au38 nanoclusters stabilized by glutathione,[97] PhC2S, hexanethiolate or dodecanethiolate, have ~0.92 eV band gap and displays discrete absorption bands at *ca.* 520 nm (2.39 eV), 560 nm (2.21 eV), 620 nm (2.00 eV), 750 nm (1.66 eV), and 1050 nm (1.18 eV).[121,123,124] Recent reports show that the absorbance spectrum of highly monodisperse larger Au144 nanoclusters, previously considered featureless, displays absorbance bands at *ca.* 510 nm (2.44 eV) and 700 nm (1.78 eV).[92] The absorbance features of the Au MTCs suggest different core size and interfacial bonding that are characterized next.

It is worth noting that the ligands employed in monothiolate Au MPC literatures do not have accessible energy states in optical absorbance and electrochemistry studies. Correspondingly, the optical bands and the electrochemical features are solely correlated with the Au core. In Au MTCs, Durene-DT (or dithiolate-Au) does have accessible states in the energy range of electrochemical and optical measurements. Analogous to the metal-ligand charge transfer process in classic inorganic complexes, core-ligand interactions induce the deviation from the size dependent trend observed in monothiol Au MPCs, which is further addressed in electrochemistry section.

4.2.2 Molecular Ion Identification by MALDI-MS

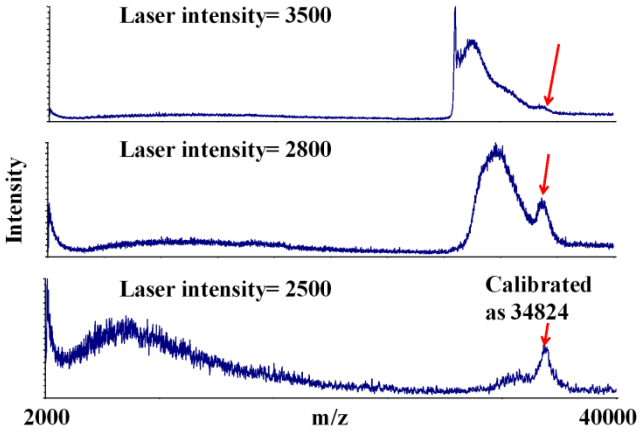

Figure 4.2. MALDI mass spectra of Au MTCs at different laser intensities. The spectra were collected under linear positive mode with DCTB (trans-2-[3-(4-tert-butylphenyl)-2-methyl-2-propenyldidene]) as matrix. No discernible signal was detected above 40000. The m/z value was calibrated with doubly charged bovine serum albumin (BSA) as external standard (**Figure 4.3**).

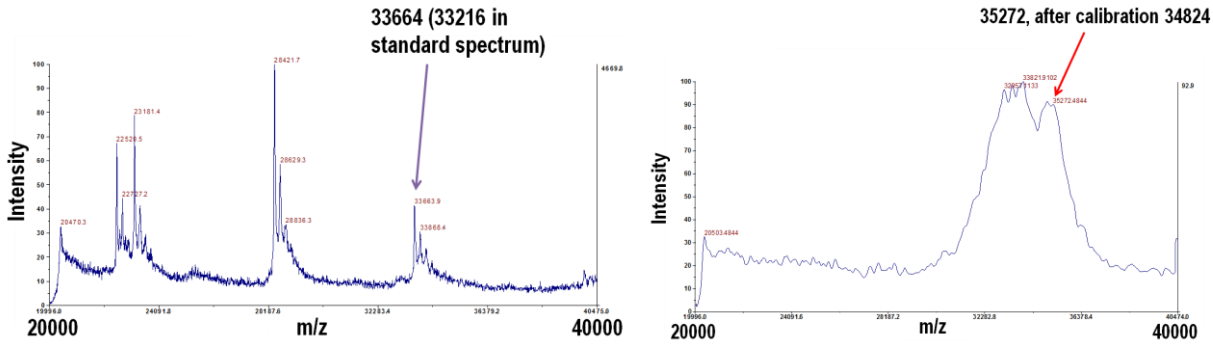

Figure 4.3. Left: MALDI mass spectrum of external standard Bolvine Serum Albumin (BSA) in sinapinic acid matrix. In the standard mass spectrum of BSA (see: http://www3.appliedbiosystems.com/cms/groups/psm_marketing/documents/generaldocuments/cms_041996.pdf), MW= 33216, based on this, our instrument has 33664-33216=448 difference in this measurement. Right: MALDI mass spectrum of MTC-1-2-1-X. The spectrum was collected immediately after the BSA analysis (on the same plate but different spot), with laser intensity being the only parameter changed. Note this spectrum was collected from a different batch of sample as those presented in the main text. The MW of 35272, based on calibration, is calculated to be 35272-448= 34824.

Since both Durene-DT and PhC2S ligands have phenyl group in their molecular structures that facilitate ionization, the MTCs were analyzed by MALDI-MS with DCTB as matrix.[27,30] The laser intensity was systematically varied to identify molecular ions. Representative mass spectra at different laser intensities under linear positive mode are presented in **Figure 4.2**. By increasing the laser intensity, a single dominant m/z peak at 34824 was identified at sufficiently low laser intensity at 2500. If the sample is a mixture of Au MTCs with multiple size/compositions, smaller MTCs should be identified at lower or comparable laser intensities. The m/z peak of 34824 is assigned to be the molecular ion species. At higher laser intensities (2800, 3500 or higher), lower m/z peaks, notably a sharp peak corresponding to mass loss of 6.11k, and broad peaks corresponding to mass loss of 5.25k and 3.09k, were observed. Due to the similar mass of Durene-DT (198) and Au (197), and linear mode used in the detection of high m/z

molecular ion species, other analytical methods are necessary for the interpretation of MTC composition. Full interpretation of the fragmentation patterns, and the MS analysis of MTC formation kinetics in the synthesis, are under further analysis and will be separately reported.

No low m/z peaks could be detected until molecular ion species is observed. The total ion flux signal decreases as laser intensity decreases, corresponding to the higher baseline noise. An expanded view of the distorted baseline at the low m/z range (e.g. 8 KD) at higher laser intensity is shown in **Figure 4.4**. Under negative mode, only well defined Au_XS_Y fragment patterns were observed at low m/z range. Again, smaller MTCs at lower m/z range were not observed, suggesting that the proposed molecular ion species correspond to the interesting absorbance features.

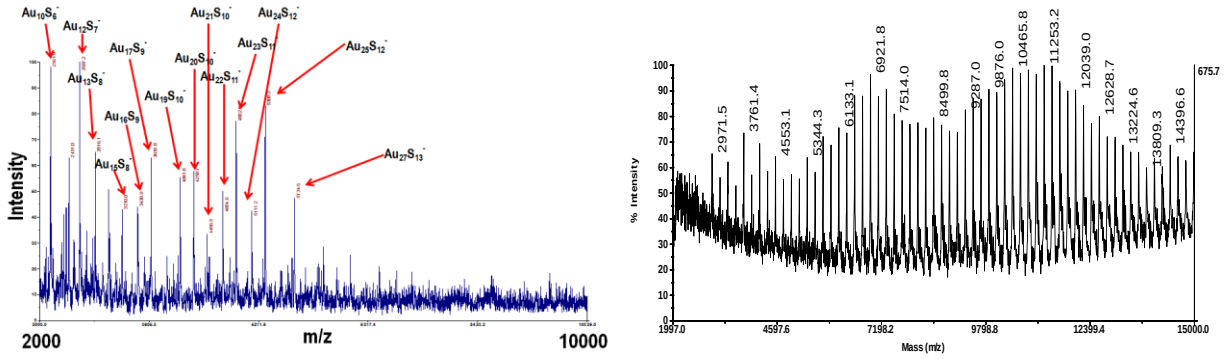

Figure 4.4. The MALDI mass spectra of the Au MTCs with reflectron negative mode (Left), and representative fragments observed in linear positive mode (Right). DCTB was used as matrix. In the reflectron negative mode, well defined Au_xS_y pattern was observed, while in the linear positive mode, fragments of the Au MTCs can be obtained.

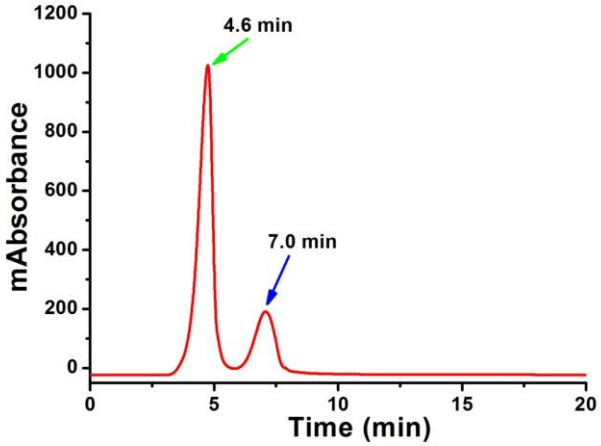

Figure 4.5. The representative chromatogram of Au MTCs separated by HPLC. A phenyl column was used. The mobile phase was 60% toluene plus 40% acetone, and the flow rate was 0.4 mL. Multiple wavelength detection was employed, and this data was recorded with detection wavelength of 360 nm.

The monodispersity of Au MTCs is confirmed by HPLC. Better separation was achieved after systematic variation of mobile phases (toluene and acetone, toluene and acetonitrile, chloroform and acetone) and stationary phase (phenyl, C18, and cyano column). Representative results are shown in supporting information, **Figure 4.5**. Two main peaks were consistently observed, with the dominate species accounting for *ca.* 80% of total sample injected. Interestingly, both species display similar absorbance features compared to the original MTC (**Figure 4.6**). The two eluates are believed to have the same composition but at different charge states. The assignment is further elaborated in the correlation of electrochemical and optical energetics. Similar behaviors have also been observed in the separation of Au25 nanoclusters at -1 and 0 charge states.[396] While the separation results confirm the monodispersity of the MTCs being analyzed, it is important to point out that the column materials, presumably the functional groups on unmodified silica, are known to oxidize Au nanoclusters.[353] Rest potential results before

and after HPLC separation confirmed the oxidation effect, which complicates the characterization of the two species eluted (**Figure 4.7**).

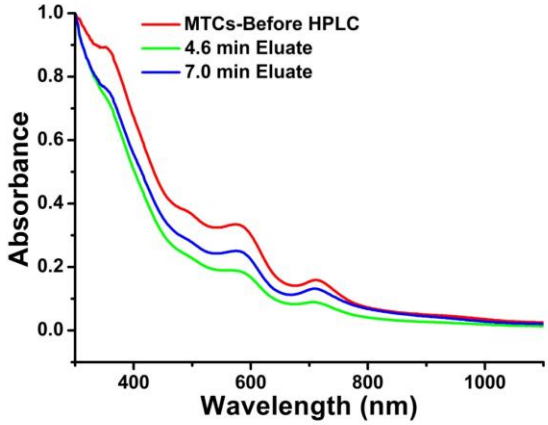

Figure 4.6. Normalized absorbance spectra of original injected Au MTC sample, 4.6 min eluate and 7.0 min eluate.

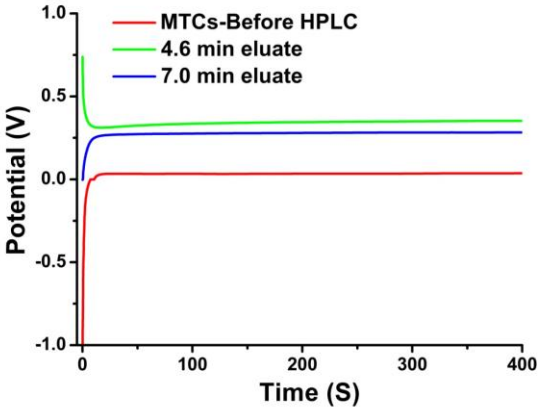

Figure 4.7. Rest potential comparison of original MTCs and HPLC collected eluates. Initial potential drift due to double layer effects should be ignored.

4.2.3 Ligand Composition in the Monolayer Determined by ^{1}H NMR

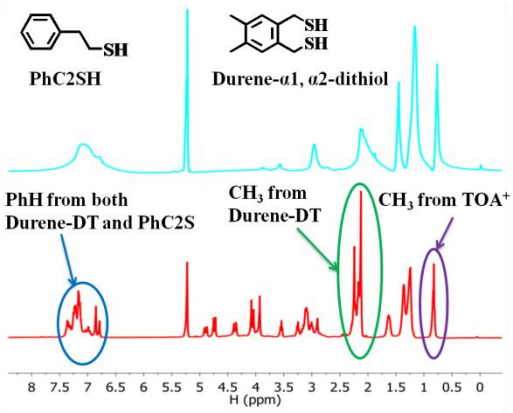

Figure 4.8. NMR spectra of Top: the purified MTCs and Bottom: the decomposed products. The purified MTCs (top panel) were decomposed in the same NMR tube without purification, from which the bottom spectrum was collected. The two spectra were aligned based on the sharp peak at 5.24 ppm with CD_2Cl_2 as solvent. The same figures can also be found in **Figure 4.9**, with detailed integration included.

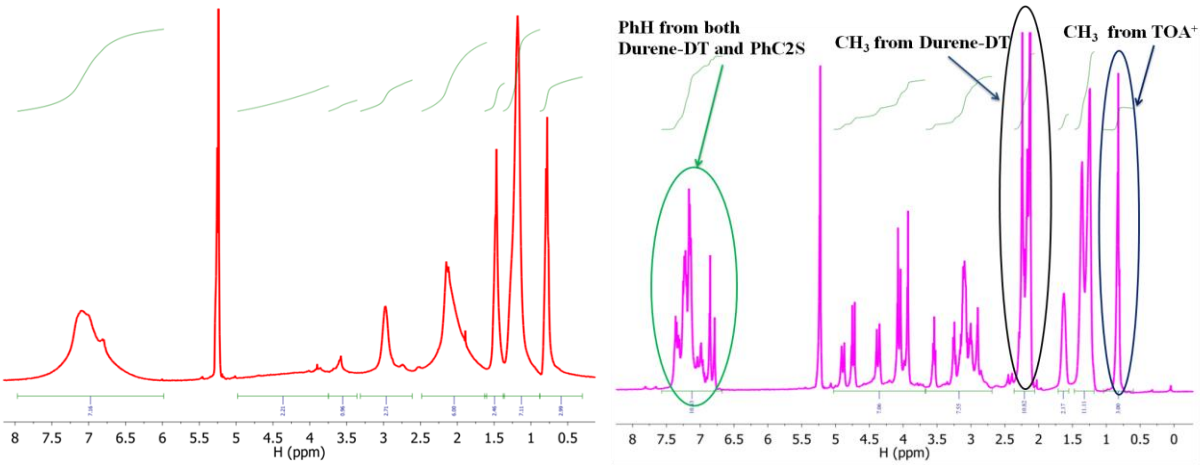

Figure 4.9. Enlarged view of 1H NMR spectrum of the purified MTCs (Left) and decomposed sample (Right), CD_2Cl_2 as solvent, R. T., detailed integration included in both spectrum.

Strong line broadening can be observed in the 1D proton NMR spectrum shown in **Figure 4.8**, a well known effect resulted from the motion restriction and heterogeneity of proton chemical environ-

ment upon cluster formation.[70] This effect suggests the presence of unbonded free ligands or smaller clusters being negligible. Otherwise, both would generate sharper features on top of the broad peaks.[326,361,362] The extent of the peak broadening of the purified MTCs is comparable to those observed from $Au_{144}(SR)_{60}$ MPCs (M. W. ca. 37k), and is much more significant than that of $Au_{25}(PhC2S)_{18}$ (M. W. 7.39k).[104,353,361] The observation is in agreement with the MS finding of a large nanocluster with M. W. at ca. 35k.

The ligand attachments on the final MTCs are analyzed by proton NMR. The phenyl proton peaks of PhC2S and Durene-DT partially overlap in the MTC spectrum, with the methyl proton from Durene-DT at *ca.* 2.2 ppm being the main signal readily identifiable for individual ligand species. Those methylene protons of both ligands are indiscernible in the 1D MTC spectrum due to the proximity to the Au core, therefore significantly broadened at 2.8-5 ppm. The peak at *ca.* 3 ppm and those below 2 ppm indicate the presence of TOA^+, being either residue from the synthesis or part of the final MTCs as counter ions addressed in the electrochemistry discussion. Note it is a well known challenge to fully remove the TOA^+ in the synthesis and purification of Au MPCs. Furthermore, the disappearance of the thiol proton signal suggests that both thiol groups of the Durene-DT ligands bind to Au, supported by the disappearance of the thiol stretching signal in the infrared (IR) spectrum (**Figure 4.10**).

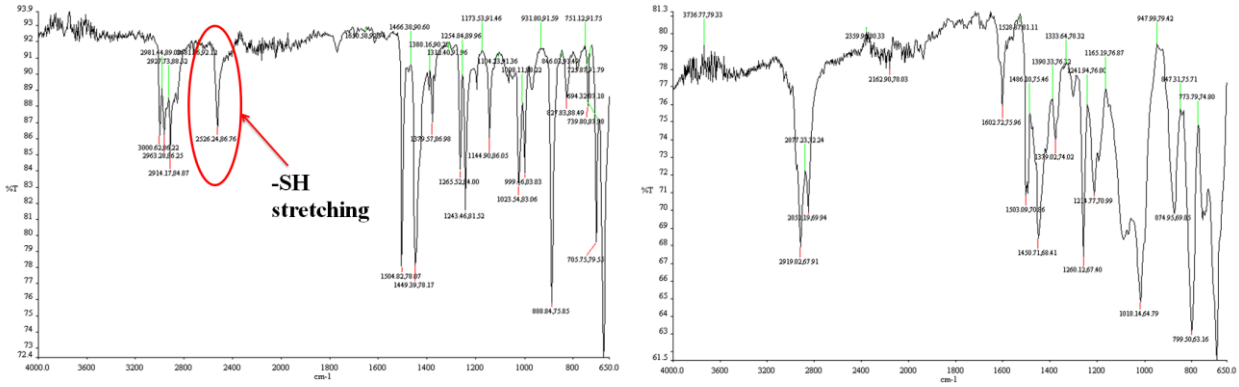

Figure 4.10. Infrared spectra, Left: Durene-α1, α2-dithiol ligand only, Right: Au MTCs, thiol stretching peak (~2526.24 cm^{-1}) signal disappears upon the formation of the clusters.

The mass differences of Durene-DT and Au could not be resolved by MALDI MS under linear mode. To quantify the mole ratio of Durene-DT and PhC2S in the monolayer, the purified MTCs confirmed by the proton NMR spectrum in the top panel were decomposed by iodine death reaction.[397] The same sample was directly used to collect the bottom spectrum. The liberated Durene-DT and PhC2S, generally in the form of disulfide, display sharp NMR peaks that allow quantitative analysis. Full assignment of the proton signals based on Total Correlation NMR Spectroscopy (**Figure 4.11**) can be found in **Figure 4.12**. The methylene proton signals are complicated, especially those of Durene-DT for potential reactions elaborated in electrochemistry section. To achieve best resolution, the mole ratio of the organic components is calculated based on the integrated peak intensities of the methyl group of TOA^+ (12H), methyl group of Durene-DT (6H) and phenyl groups of PhC2S (5H). Therefore, the amount of PhC2S was calculated from the total phenyl proton intensity subtracted by the Durene-DT phenyl proton contribution, which is 1/3 of the intensity of the Durene-DT methyl group based on the proton ratio of 2:6. The calculated mole ratio of Durene-DT: PhC2S: TOA^+ is 1.0: 0.76: 0.14. While the amount of TOA^+ varies slightly for different samples from repeated syntheses, the ratio of the two thiols is consistent at *ca.* 5% uncertainty determined by the NMR peak analysis.

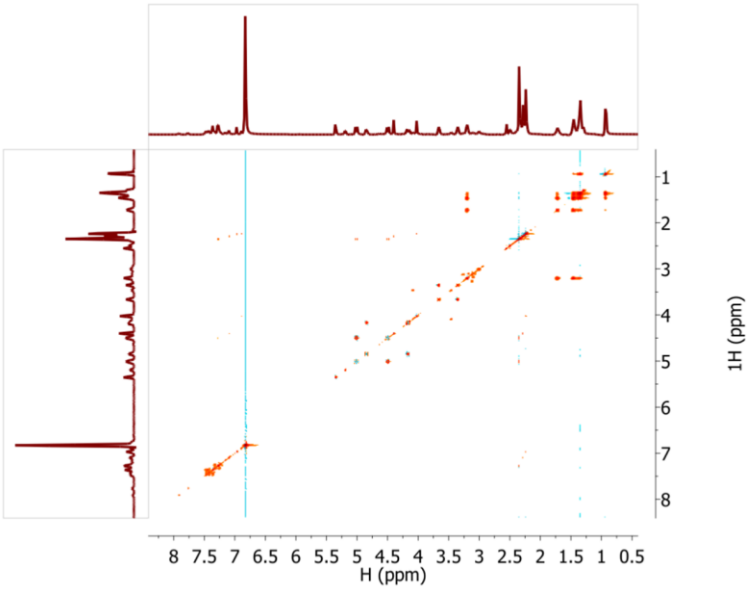

Figure 4.11. ^{1}H -^{1}H TOCSY spectrum of decomposed MTCs, CD_2Cl_2 as solvent, R. T.

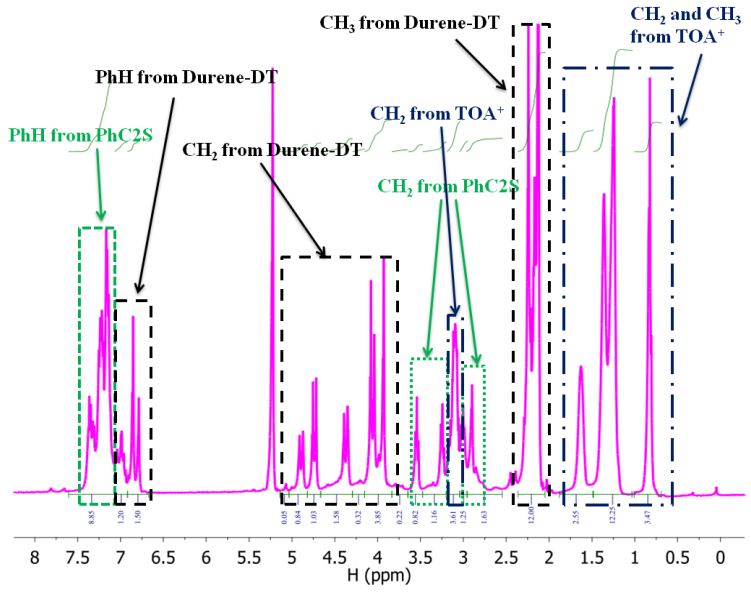

Figure 4.12. Full peak assignment of protons in the decomposed sample in ^{1}H NMR spectrum, CD_2Cl_2 as solvent, R. T. The correlation is based on the TOCSY spectrum in **Figure 4.11**.

4.2.4 Diffusion Coefficient and Monodispersity Probed by Diffusion–Ordered NMR Spectroscopy (DOSY)

The nanoparticle size and monodispersity are further characterized by diffusion-ordered NMR spectroscopy (DOSY). Two dimensional (2D) NMR techniques have been used in structural determination, surface compositional analysis, and in ligand exchange kinetic studies of Au nanoparticles.[77,398] Compared with invasive mass spectrometry and surface techniques such as transmission electron microscopy (TEM), NMR techniques directly characterize the hydrodynamic states of gold nanoparticles in solution,[85] knowledge directly relevent for biological and other applications.

The DOSY spectrum of the Au MTCs is presented in **Figure 4.13**. One group of Au MTC proton signals with the same diffusion coefficient (Log(D) at -9.5) could be found. Based on the diffusion coefficent of $Au_{25}(SC2Ph)_{18}$ reported previously,[350] as marked in the oval region, no signal from smaller clusters (e.g. Au25 or Au38) were detected. As additional reference points, trace amount of fast diffusing molecules are also observed at Log(D) between -8.2 and -8.8, including solvent peak (CD_2Cl_2), water, and the two types of ligands. It is interesting to notice that TOA^+ ions diffuse much slower than other small molecules. This suggests that TOA^+ ions are associated with the MTCs as counter ions, which also explains its presence after extensive purification. These results attest high monodispersity of the larger MTC sample, which diffuse much slower than the well established $Au_{25}(PhC2S)_{18}$ nanoclusters.

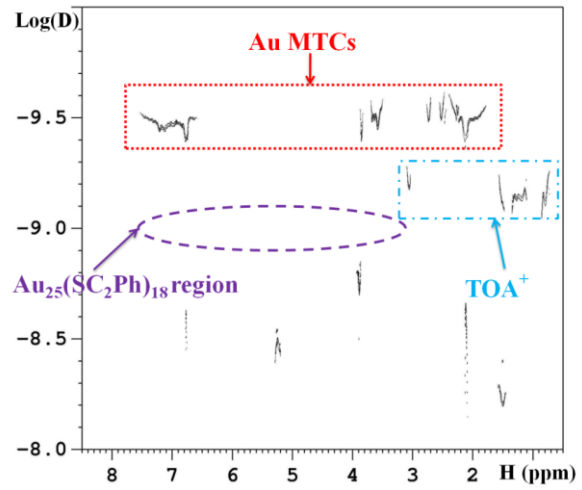

Figure 4.13. DOSY spectrum of Au MTCs in CD_2Cl_2 at R. T. X axis represents the chemical shift of the protons, while y axis is the logathrim of the calculated diffusion coefficients. The 1D spectrum can be refereed from the top panel in **Figure 4.8**.

4.2.5 Thermogravimetric Analysis (TGA)

Due to the similarity of mass between Au and Durene-DT for MS analysis, the gold-to-organic mass ratio is determined to be ca. 70.7: 29.3 by thermogravimetric analysis (TGA) (**Figure 4.14**). In conjunction with the mole ratio of Durene-DT: PhC2S: TOA+ obtained from NMR analysis, the final mole ratio of Au: Durene-DT: PhC2S: TOA^+ is calculated to be 4.5: 1.0: 0.76: 0.14. The amount of TOA^+ in different MTC samples was calculated by the respective NMR peak intensity in the composition analysis.

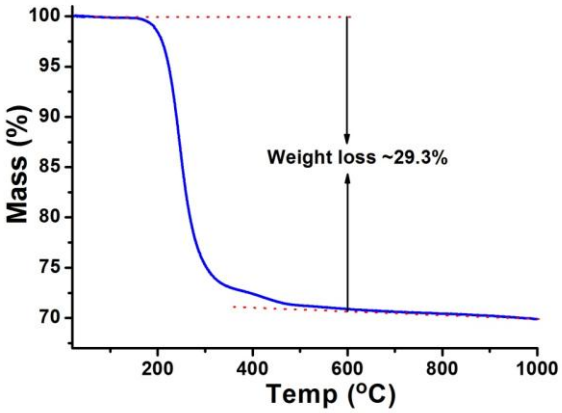

Figure 4.14. Thermogravimetric analysis (TGA) of the MTCs, the calculated metal/organic mass ratio is 70.7:29.3.

4.2.6 Molecular Composition of the Au MTCs

The "molecular formula" of these intact nanoclusters is elucidated. The molecular ion observed in MALDI-MS under positive mode is assigned to be a singly charged cationic species with one TOA^+ associated as a counter ion. This argument is supported by the rest potential measurements addressed in the electrochemistry discussion. Therefore, the molecular mass at 34824 corresponds to Au_x(Durene-DT)$_y$(PhC2S)$_z$(TOA^+)$_1$. The uncertainty of TOA^+ amount observed in solution NMR measurements is not expected to affect the MS analysis, which is recorded in gas phase under ionization. The final values of x, y and z are then calculated to be 130, 29 and 22 respectively determined by NMR and TGA. The composition of the MTCs is proposed to be Au_{130}(Durene-DT)$_{29}$(PhC2S)$_{22}$, with varied charge states as characterized by rest potential measurements. Considering the measurement error associated with the techniques, specifically the NMR peak intensity integration, TGA calculation, and linear mode used due to the high mass range, the error is estimated to be at ±1-2 resolution. The comparison of those possible compositions with experimental results is summarized in supporting information, **Table 4.1**. Further

computational and crystallographic studies would offer valuable knowledge of the bond structures and confirm the elucidated composition and energetics.

Table 4.1. The comparison of experimental data and the representative compositions proposed of the Au MTCs.

Composition Au: Durene-DT:PhC2S	Molar ratio of Durene-DT: PhC2S by NMR (0.71-0.76)	M. W. (calculated)	Deviation from experimental m/z value (34824)
$Au_{130}(Durene\text{-}DT)_{29}(PhC2S)_{22}$	1: 0.76	34774 (One TOA^+)	50
$Au_{130}(Durene\text{-}DT)_{30}(PhC2S)_{21}$	1: 0.70	34833 (One TOA^+)	9
$Au_{130}(Durene\text{-}DT)_{31}(PhC2S)_{23}$	1: 0.74	34837 (No TOA^+)	13

4.2.7 Near Infrared (IR) Luminescence of Au130 MTCs

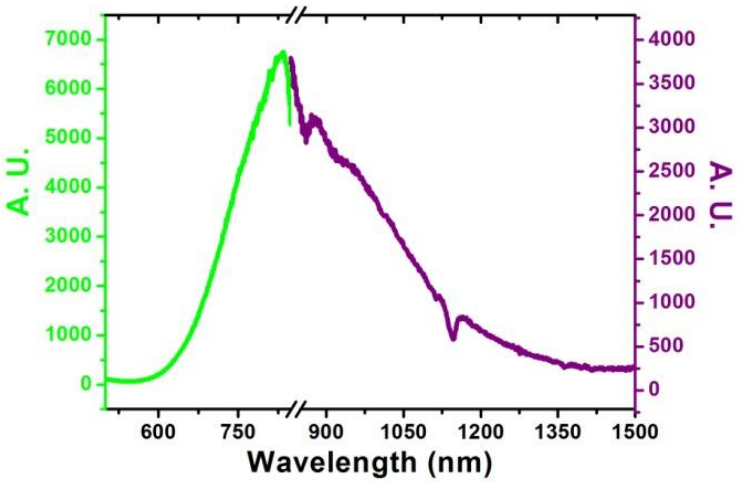

Figure 4.15. Luminescence of dilute Au130 MTCs at R. T. in CH_2Cl_2, excited at 400 nm. The left and right emission spectra were collected by the visible (up to 850 nm) and near IR detector (from 850 nm) separately. The distortion near the break on wavelength axis is limited by the detector correction file. Individual emission spectra without correction can be found in **Figure 4.16**.

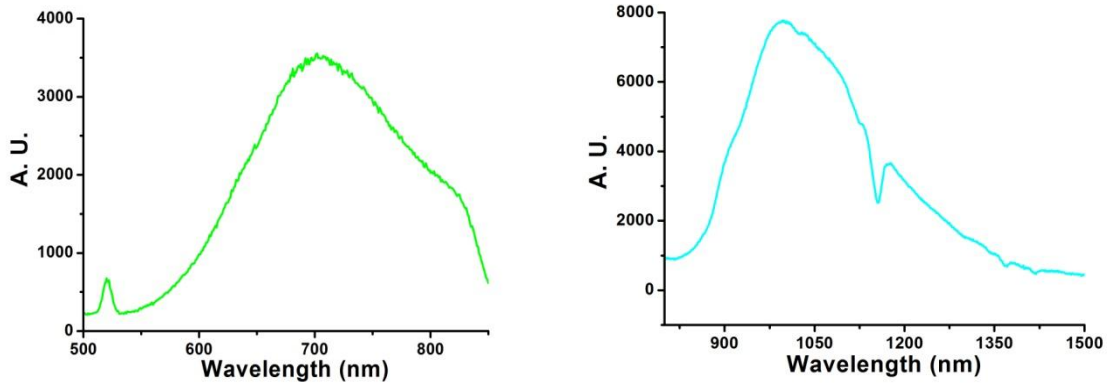

Figure 4.16. Original emission spectra of the Au130 MTCs at 450-850 nm (excited at 450 nm), and 850-1500 nm (excited at 400 nm) without correction.

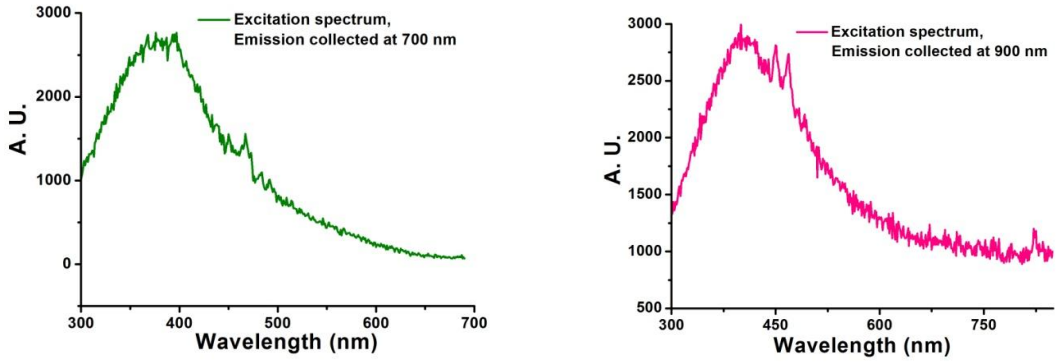

Figure 4.17. Excitation spectra of MTCs, emission collected at 700 nm (by visible detector) and 900 nm (by near IR detector).

Broad luminescence was observed spanning from visible to near IR range as shown in **Figure 4.15**. The corresponding excitation spectrum displays a broad excitation ranging from 300 nm to 500 nm with a maximum at ca. 400 nm (**Figure 4.17**). Significant energy relaxation exists between the excitation and emission maximum. The absorbance features are absent in the excitation spectrum. The luminescence properties are reminiscent of those from various Au MPCs: near IR emission at a common energy with featureless excitation regardless of absorbance features.[116,339-341] The observation is attributed to the

presence of Au(0) core, through which those excitons are effectively relaxed into common states defined at the Au-thiolate interface. The relaxation mechanism through Au(0) core distinguish these nanoclusters from conventional Au(I) inorganic complexes, in which the absorbance, luminescence excitation and emission correlates well in a similar fashion as organic dye molecules.[338,374]

In monothiol Au MPCs, luminescence quantum efficiency (QE) increases significantly (up to ca. 10^{-2}) upon the polarization of ligand monolayer and Au core, by ligand exchange reaction or by electrochemical charging.[115,116,118] Using tiopronin Au MPCs (Average composition $Au_{201}(tiopronin)_{85}$, QE at *ca.* 0.10%) as standard materials,[116] the quantum yield of the Au MTCs is calculated to be *ca.* 0.35% based on the integrated area ratio. The thiol bridging motif (RS-Au-SR) suggests the physical origin of the unique common energy states, as the Au atom embedded between the two thiolates has different chemical environments from other Au atoms. The dithiol ligands in 1, 2-dithiol DMPS stabilized Au-dithiol nanoclusters have been found to impose structural constraint on the Au-thiolate bond formation and efficiently eliminate the luminescence.[350] Monolayer reactions between monothiol tiopronin and 1, 2-dithiol DMPS were found to effectively switch the luminescence on and off.[343,350] The 1, 4-dithiol, Durene-DT apparently has more flexible structures compared to 1, 2-dithiol DMPS. The high surface coverage by Durene-DT and the presence of monothiolate PhC2S also contributed to the high QE observed from these MTCs.

4.2.8 Binding Energy by X-ray Photoelectron Spectroscopy (XPS) Studies

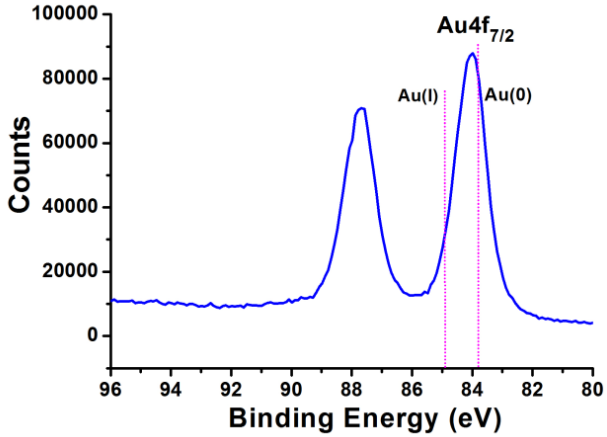

Figure 4.18. Au XPS spectrum of the Au130 MTCs. Dash lines illustrate the previously reported Au (0) and Au(I)-thiolate binding energies. The binding energy is calibrated by C 1S at 284.6 eV shown in **Figure 4.19**.

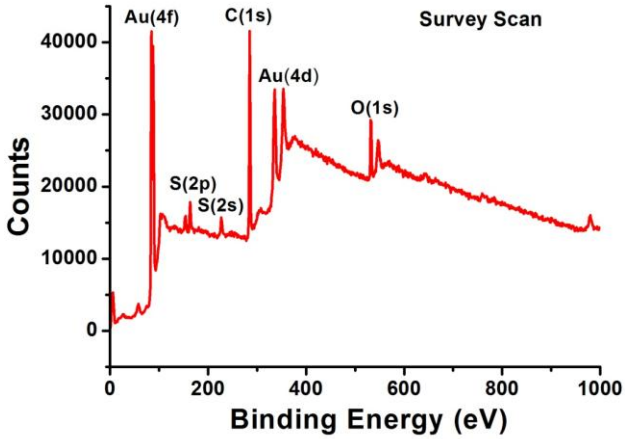

Figure 4.19. The survey scan of the Au130 MTCs XPS spectrum. In the survey scan, the signal of Cl (2s: ~270.0 eV; 2p: ~198.0 eV), Br (3s: 256 eV; 3p: ~182.5 eV; 3d: ~69.0 eV) could not be found. The binding energy of O(1s) with ~532.0 eV originates from the aluminum substrate used in the measurements. The binding energy was calibrated based on C 1S peak at 284.6 eV.

The high thiol:Au ratio is approaching the theoretical limit of full surface passivation of a packed Au core.[70] The charge states of Au and S, especially the presence of Au(0) core, are evaluated by XPS. The binding energy (BE) of Au($4f_{7/2}$) is measured to be 84.0 eV shown in **Figure 4.18**. It has been reported in Au MPC studies that, the Au($4f_{7/2}$) BE increases as the particle size decreases, within the range from Au(0) film at ~83.8 eV to Au(I) thiolate species at *ca.* 84.5-86.0 eV.[70,97,101,334] The BE of these Au130 MTCs agrees with the reported results but appears to be very close to Au(0). The observation confirms our characterization of a relatively large Au130 core. Among several factors previously proposed,[101] the initial charge states of the Au MTC are believed to be the main reason for the low Au(I) signal detected. The high thiolate:Au ratio, therefore S-Au interactions in the Au MTCs, is confirmed by the S(2p) spectrum in **Figure 4.20**. The BE of S(2p) at 162.5 eV is similar to that of Au(I) complexes and *ca.* 0.5 eV more positive than those from larger Au nanoparticles.[99,101] No Br or Cl signal is observed in survey scan (**Figure 4.19**). The XPS results confirm the presence of Au(0) core, which allow the relaxation of luminescence excitation, and the quantized charging behaviors observed in electrochemistry.

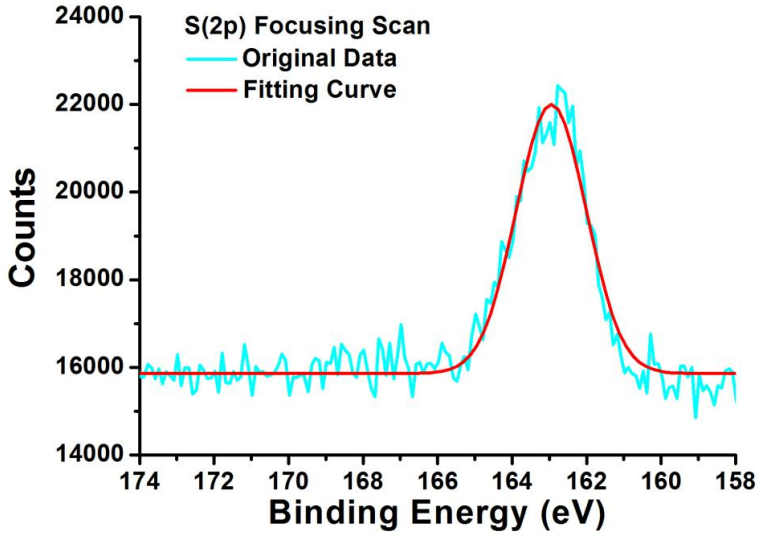

Figure 4.20. S(2p) focusing scan XPS spectrum of the Au130 MTCs.

4.2.9 Electrochemical Properties of Au130 MTCs

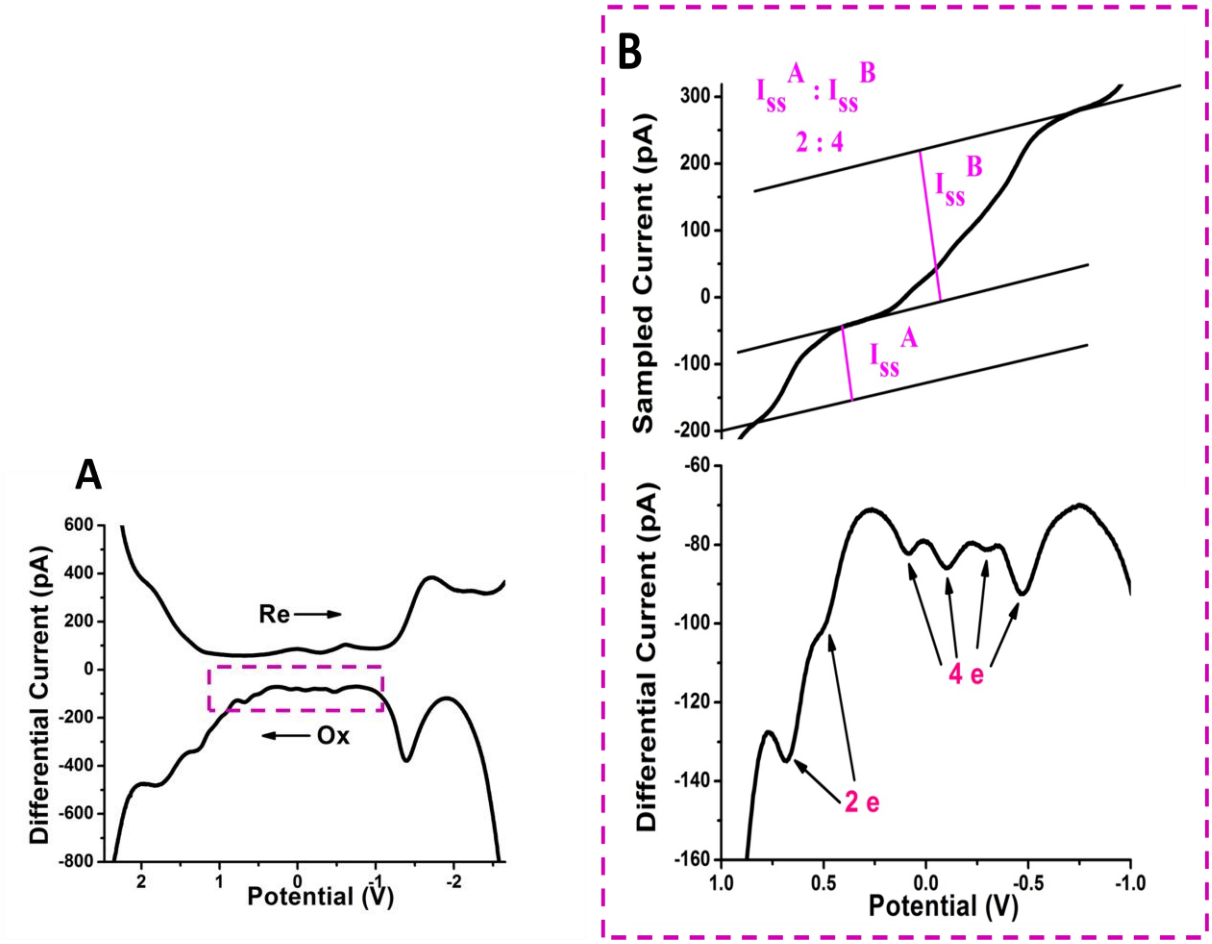

Figure 4.21. A: Square wave voltammogram (SWV) of Au MTCs, recorded in 0.1 M TBAP in CH_2Cl_2 solvent at -70°C. B: Zoom in of oxidation scan in SWV with one corresponding sampled current shown above. Step amplitude was at 25 mV with 4 mV increments. Frequency was 15 Hz. The working electrode was a 20 micron Pt disk electrode. An Ag/AgCl wire as reference electrode was calibrated in 2 mM ferrocene with 0.1 M TBAP solution prior to use. The sample solution, in CH_2Cl_2 at *ca.* 3 mM, was degassed under argon prior to the measurements.

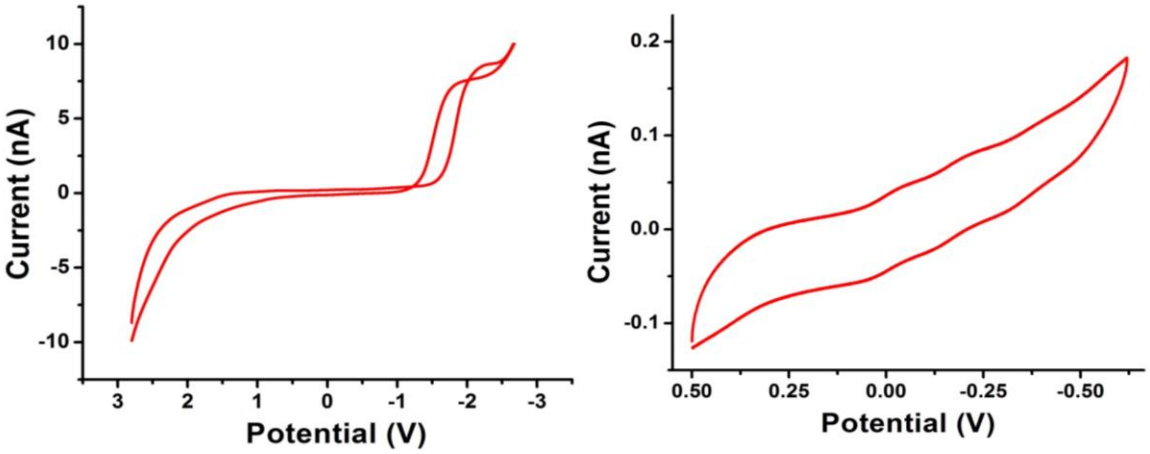

Figure 4.22. Cyclic voltammograms of the Au130 MTCs in CH_2Cl_2 with 0.1 M TBAP. The measurements were taken at low temperature (-70 ^{o}C) at 100 mV/s scan rate.

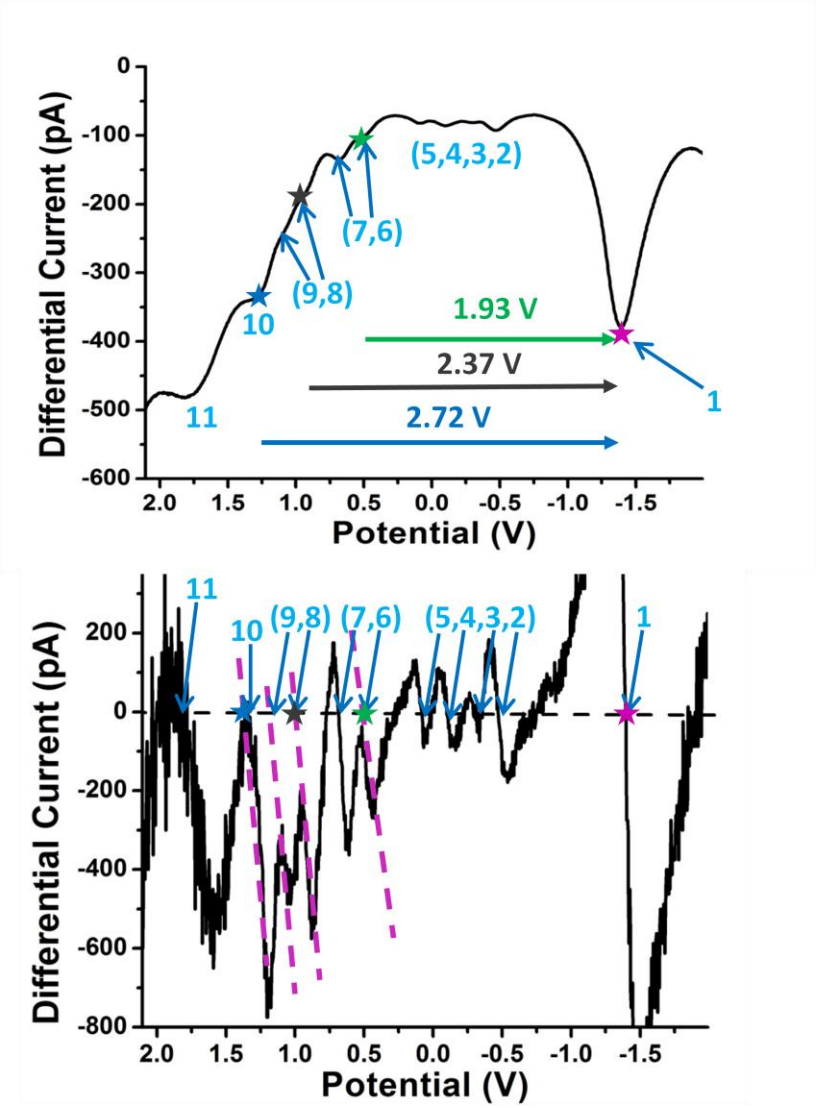

Figure 4.23. SWV oxidation scan of the Au130 MTCs from **Figure 4.21** with 1st derivative plot shown in bottom panel. Stars indicate peaks used for optical correlation.

Square wave voltammograms (SWV) shown in **Figure 4.21** were collected at low temperature for better peak resolution at broad potential window. Cyclic voltammograms (CV) are provided in **Figure 4.22**. Precise peak potentials were measured by differentiating the data and extrapolating the derivative plot to cross zero (**Figure 4.23**). Those values corresponding to the notable SWV peaks were listed in **Table 4.2** for the calculation of electrochemical energetics. Four uniformly spaced peaks (#2-5) near zero

potential were well-resolved, with the oxidation scan shown in panel B. This corresponds to four continuous quantized charging events. A differential pulse voltammogram at room temperature is provided in **Figure 4.24**, clearly showing the regular peak spacing between each of the four peaks. The continuous quantized charging behaviors of Au130 MTCs are similar with those observed from large monothiol Au MPCs such as $Au_{140\text{-}147}$.[148,149]

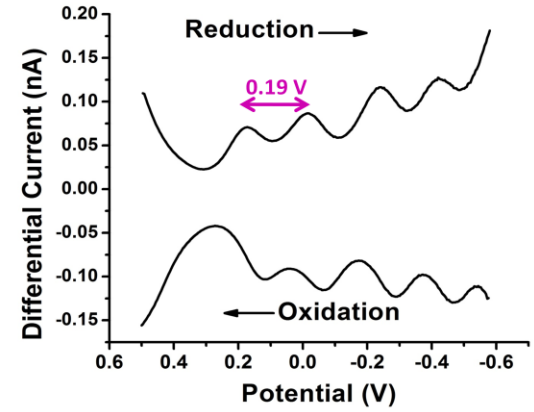

Figure 4.24. Differential pulse voltammogram of the Au130 MTCs in CH_2Cl_2 with 0.1 M TBAP, measurement was taken at narrow potential range, room temperature.

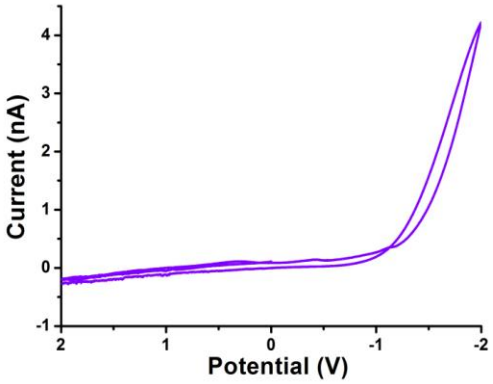

Figure 4.25. Cyclic voltammogram of Durene-DT ligand at room temperature in CH_2Cl_2 with 200 mV/s scan rate. Note the electron transfer process appears to be irreversible and adsorption on the Pt microdisk electrode was observed. The Durene-DT sample was confirmed free of disulfide by proton NMR.

Importantly, the electrochemical behaviors are fundamentally different from those of small monothiol Au MPCs such as Au25 that display electron transfer (ET) activities at discrete energy states.[3,119,121,137,399] One dominant irreversible peak at -1.4 V is observed upon reduction (note the high current in cyclic voltammogram, **Figure 4.22**). Free durene-dithiol molecules undergo irreversible reduction at ca. -1.6 V (**Figure 4.25**), corresponding to one electron reduction to the corresponding anionic radicals.[400-403] The major peak at -1.4 V is attributed to the radical formation upon reduction. The reduction potential is lower than free dithiol molecules, suggesting the stabilization by the interaction with Au core. The electron could therefore be delocalized between the Au core and the attached Durene-DT ligands. Unlike those monothiol ligands that do not have accessible energy states, the energy states of Durene-DT ligands and Au core will hybridize, leading to the quantized Au core charging at lower potentials and ligand reactions at higher potentials. To clarify, the apparent gap between major peaks in voltammogram is not from the core HOMO-LUMO energy states observed in small monothiol Au MPCs such as Au25 or Au38. Those apparent LUMO states are rather dominated by Durene-DT ligands.

Table 4.2. Potential and peak spacing of the Au MTCs in the square wave voltammogram. Data calculated from Figure **4.21**.

Peak #	11	10	9	8	7	6	5	4	3	2	1
Potential (V)	1.84	1.32	1.14	0.97	0.68	0.53	0.09	-0.10	-0.30	-0.47	-1.40
Peak Spacing		11-10	10-9	9-8	8-7	7-6	6-5	5-4	4-3	3-2	2-1
Energy (V)		0.52	0.18	0.17	0.29	0.15	0.44	0.19	0.20	0.17	0.93

The charging energy of Au130 MTCs is determined by the average peak spacing as 0.19 V. This value is slightly smaller than that observed in PhC2S or hexanethiolate stabilized Au25 and Au144

MPCs.[85,148,334,339] Durene-DT has one instead of two methylene groups between the Au core and phenyl group compared to PhC2S, therefore slightly less monolayer thickness and larger dielectric constant. Furthermore, TOA^+ ions have been found to be associated with the MTCs in solution by NMR DOSY measurements. Based on concentric sphere model and optimization,[404] those effects will lead to smaller charging energy. Separated by a 0.44 V gap (peak # 6-5), another pair of ET peaks reveals one energy state below the frontier states. The current ratio is found to be 2:4 from one scan of the square wave data (comparable to cyclic voltammogram current). Therefore, all six differential current peaks are attributed to single electron transfer activities. The baseline distortion in sampling current prohibits similar interpretation at higher potentials/energies.

4.2.10 The Correlation of Electrochemical and Optical Energetics: Core Charging and Core-Ligand Charge Delocalization

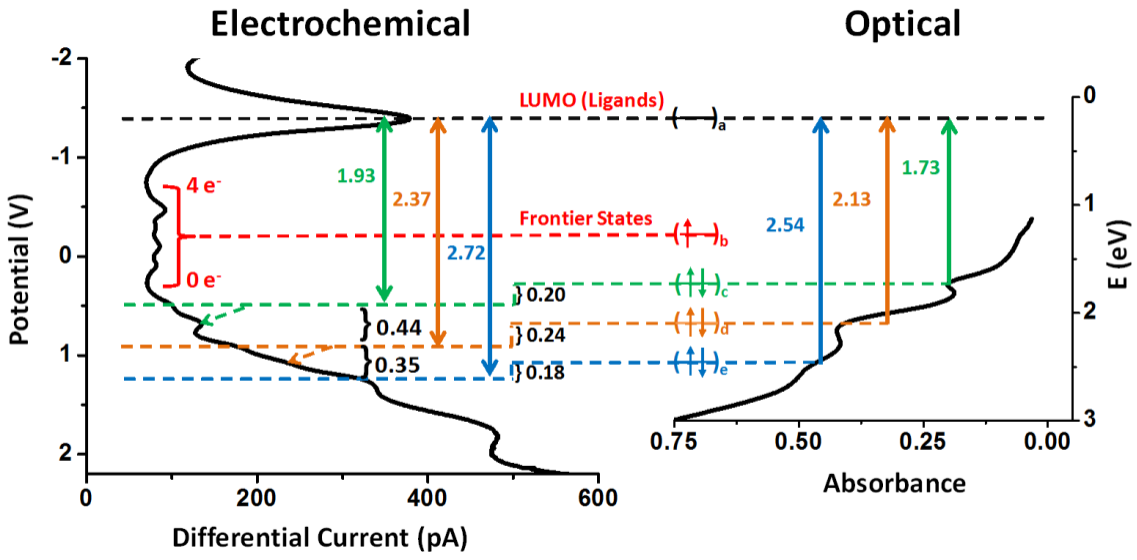

Figure 4.26. Energy diagram that correlates optical and electrochemical features. The oxidation scan (left) and absorbance spectrum (right) are aligned based on the energy stated shown in the middle. The undetermined degeneracy of those states are denoted x, y and z.

In classic inorganic metal-ligand complexes, the charge transfer between metal center and stabilizing ligands is known to generate rich optical and electrochemical features. For the Au MTCs, the core-ligand interaction, analogous to those metal-ligand charge transfer effects, is found to significantly affect the energetics. Shown in **Figure 2.26**, the absorbance bands and electrochemical activities are correlated using oxidation scan that generally offers better resolved features. Starting from the middle of the diagram, the frontier states (degenerated orbitals) could hold multiple electrons and display continuous peaks separated by quantized charging energy, with four continuous peaks resolved from this specific MTC sample. With ca. 29 Durene-DT ligands in the monolayer, multiple LUMO states are accessible for electrochemical reduction or optical excitation at the same energy states. Note this is different from the charging of core energy states, which requires charging energy for each additional electron transfer activity.

With the distinct LUMO as reference point (mainly contributed from Durene-DT ligands), electrochemical and optical transitions are correlated. The first three optical absorption bands at 1.73, 2.13 and 2.54 eV are matched with corresponding electrochemical peaks as indicated. Note the first of the two ET peaks in each energy state (corresponding to 1.73 and 2.13 optical bands) is used in the comparison. The second ones are indicated by the arrow, requiring additional charging energy compared to the first ones. The average differences between measured optical and electrochemical transitions (0.2 V) are approximately equivalent to the measured charging energy (0.19 V). The high background signal at high potentials and potential structure/composition changes of MTC at high charge states in electrochemistry prohibit the precise correlation of the 3.50 eV optical band, as well as the degeneracy of those energy states.

The optical band gap is extrapolated to be *ca.* 0.88 eV from the absorbance spectrum, but varies from sample to sample and is not as well-defined as the other bands. With 0-4 electrons filling the fron-

tier energy states, the Fermi level will shift accordingly, which will cause the absorption band gap to vary. Indeed, the rest potential of the sample used here is ~0.09 V with Ag/AgCl wire as quasi reference electrode. Typical rest potentials vary from -0.05 V to +0.10 V for different batches of Au130 MTC samples. For an ideal neutral MTC sample, the HOMO-LUMO gap is predicted to be 0.74 V from electrochemistry, calculated from the gap between the LUMO peak and the last charging peak of the HOMO (0.93 V) with one charging energy value (0.19 V) subtracted.

4.3 Experimental Section

4.3.1 Chemicals

Tetrachloroauric acid trihydrate ($HAuCl_4 \cdot 3H_2O$, >99.99% metals basis), sodium borohydride ($NaBH_4$, 99%), 2-Phenylethanethiol (>99%), tetrabutylammonium perchlorate (TBAP, >99%), tetraoctylammonium bromide (TOABr, 98%), trans-2-[3-(4-tert-butylphenyl)-2-methyl-propenylidene]-malononitrile (DCTB, >99%) and organic solvents (HPLC grade) were used as received from Sigma-Aldrich. Durene-α1, α2-dithiol (>95%) was purchased from TCI-America.

4.3.2 Measurements

UV-Visible absorbance spectra were recorded with a Shimadzu UV-1700 spectrophotometer. Luminescence was measured with a Horiba Jobin-Yvon Fluorolog 311 spectrometer with T channel, through which a visible PMT detector and a near IR InGaAs detector were attached. MALDI mass spectra were acquired with ABI 4800 matrix assisted laser desorption ionization (MALDI) TOF-TOF analyzer, with DCTB as matrix. Proton NMR spectra were acquired on a Bruker Avance 400 MHz spectrometer in CD2Cl2. A CH instrument 700C electrochemical workstation was used in electrochemical measurements. An Agilent technologies HPLC 1200 series with multiple wavelength detectors was used. X-ray Photoe-

lectron Spectroscopy (XPS) analysis was conducted with a SSX-100 (Surface Science laboratories Inc.) using an Al K-alpha X-ray source (1486.6 eV) with the analysis chamber pressure lower than 1×10^{-8} Torr.

4.3.3 Synthesis and Purification

The mixed thiolated clusters (MTCs) were synthesized via a modified two phase Brust-Schiffrin method.[9] In a typical experiment, gold salt ($HAuCl_4 \cdot 3H_2O$) was first phase-transferred from an aqueous solution to a toluene solution with TOABr. The organic layer was separated, and then a mixed thiol solution (Durene-DT: PhC2S: Au= 1: 2: 1) was added in at moderate magnetic stirring. The solution color changed from gold yellow to colorless in ~30 mins. Then freshly prepared $NaBH_4$ (20 equivalents of gold) aqueous solution was added quickly while vigorously stirring. The solution turned black immediately. After the reaction was completed in 1-3 days monitored by absorbance transition, the organic layer was separated and washed by water 3-5 times. The solvent was removed by rotary evaporator, and the product was first precipitated by methanol, while the methanol solution was filtered away. The black solid was further rinsed with copious acetonitrile (stirring overnight) to remove the extra free ligand molecules. The leftover black solid is collected as final MTCs product.

4.3.4 Iodine Death Reaction

In the NMR tube, Au MTCs were dissolved in CD_2Cl_2, and the 1D proton NMR spectrum was acquired. The MTCs were then decomposed by adding iodine,[397] and the NMR tube was shaken vigorously for a while. The color changed from black to violet. Meanwhile brown precipitate formed at the bottom of the tube. The proton NMR spectrum was recorded after the reaction was complete (several hours later).

4.4 Summary

In summary, interesting energetics is observed from a new type of molecular gold cluster protected by mixed monothiol ligand and dithiol ligand. The molecular ion at *ca.* 34.8 KD was detected by MALDI-MS. The mole ration of Au: Durene-DT: PhC2S was determined by TGA and NMR techniques. The Au-S bond formation and charge states were studied by XPS and IR spectroscopy. The average composition of the Au MTCs is determined as $Au_{130}(Durene\text{-}DT)_{29}(PhC2S)_{22}$ at ±1-2 resolution. The MTCs display multiple discrete absorption bands, originated from core-ligand charge delocalization. Quantized double charging behaviors are observed at lower potentials in voltammetric measurements. Ligand reaction is observed at higher potential ranges. An energy diagram has been proposed to correlate the optical and electrochemical energetics of this molecular nanocluster. The interesting energetics is attributed to the unique structural constraints imposed by the dithiolate ligand on the interfacial bonding structures at the gold core surface that demand further investigation.

5 NEAR INFRARED LUMINESCENCE OF GOLD NANOCLUSTERS AFFECTED BY THE BONDING OF 1, 4-DITHIOLATE DURENE AND MONOTHIOLATE PHENYLETHANETHIOLATE

5.1 Background and Research Strategy

Optical activities in near IR range are highly favorable for biomedical applications because the tissues are most transparent within the spectrum range of ca. 650-900 nm.[405] Imaging and hyperthermia therapeutics are two major applications that benefit from the deep penetration of photons. Extensive

research efforts have been focused on the development of luminescent probes that have maximum emission in near IR range with high quantum efficiency (QE). Some classic organic dye molecules with extended conjugation such as cyanine derivatives are commercially available. Their photostability needs to be improved while maintaining reasonable aqueous solubility and high QE.[406] In the past decades, semiconductor quantum dots have emerged as promising candidates for optical imaging due to their size dependent emission with high quantum yield.[407] The semiconductor materials suffer from the fundamental concerns of toxicity in the composition and the technical limits such as photoblinking.[405]

Small thiolated gold nanoparticles, often referred as monolayer protected gold clusters (Au MPCs),[3-5] are another category of materials that displays intriguing near IR luminescence,[115-118,156,372] as well as other optical and electrochemical activities.[105,121,148,149] Because of those properties, Au MPCs have found versatile applications in bioscience and materials science.[186,197] Unlike the band gap fluorescence, the emission displays a very broad peak, with the maximum wavelength found to be insensitive to the size of the Au core and weakly depend on ligand and solvent environment. The QE, on the other hand, increases with the decrease of core size from ca. 2.2 nm.[156] Furthermore, the QE is found to increase with the increase in ligand and core polarity (i.e. charge state).[115] Since Au (I)-thiolates does not have detectable near IR emission, those observations suggest the near IR luminescence originates from some common "surface states" on Au core, supported by the significant energy relaxation of the visible excitation. The "surface states" are mainly composed of the atomic orbitals from Au and S, while the bonding structures were postulated to the vertex and edges on a truncated octahedron Au core.[339] The non-toxic components, excellent photostability and aqueous solubility, and reasonable QE (10^{-3} to 10^{-2}) already make the Au nanoclusters competitive with currently available near IR dyes and allow single particle imaging. It is still desired but challenging to further enhance the QE, which requires fundamental understanding of the nature of those surface states.

It is well-known that the properties and functions of broadly defined nanomaterials depend on their size, shape and composition. However, those atoms at the surface of the nanomaterials obviously have different chemical environment (chemical bonding) compared with those inside, therefore would lead to different properties and functions. Due to the limited knowledge of the exact surface chemical bonding structure and energetics, the impacts of surface on the overall properties are in general poorly understood and vaguely referred as surface (defect) effects. Au nanoclusters with core diameter less than a few nanometers have high ratio of surface atoms versus interior ones. Correspondingly, their fundamental physiochemical properties and potential applications heavily depend on the surface contribution. It is imperative to understand the surface bonding structures and to establish the correlation between the property and surface structure. Important breakthroughs have been achieved recently on the crystal structure determination of $Au_{102}(SR)_{44}$,[138] $Au_{25}(SR)_{18}$[107,108] and $Au_{38}(SR)_{24}$.[389] An interesting five atom "Au-S-Au-S-Au" thiol-bridging staple motif on the core-ligand interface has been revealed at the core-ligand interface. It is especially exciting to notice the unique chemical environment of the Au atom in the middle, which could correspond to the much better structurally defined "surface defect sites".

To explore the correlation of the near IR luminescence and other physiochemical properties with the novel thiol-bridging staple motif, dithiolate-protected Au clusters with 2, 3-dimercaptopropane-1-sulfonate (DMPS, a 1, 2-dithiol ligand) have been directly synthesized.[350] The binding of two thiolate groups of the dithiol molecule in the place of two monothiols to gold is favored by the gain of entropy. Meanwhile, the molecular constraint between the two thiol group (C-C in the case of 1, 2-dithiol) limits the insertion of one Au atom for the formation of the intramolecular staple motif. No near IR emission was detected from a series of different sized nanoclusters synthesized. Furthermore, the near infrared luminescence is shown to switch "on" by introducing monothiols into non-emitting DMPS Au DTCs, and switch "off" by replacing the monothiolates with the 1, 2-dithiolates accordingly.[343] The study further illustrates the importance of the interfacial Au-thiolate bonding on the QE of the near IR emission.

To identify an interfacial bonding motif that further enhance the QE, the monolayer reactions of Au nanoclusters between a 1, 4-dithiol (durene-DT) and a widely used monothiol (PhC2S) are studied in this report. Two types of reactions have been performed. With the addition of durene-DT, PhC2S stabilized Au25 MPCs undergo ligand exchange reaction. The exchange process is accompanied with the gradual enhancement of near-IR luminescence and the loss of well-defined absorbance bands. In the second approach, the addition of PhC2S monothiols to the durene-DT protected Au DTCs resulted in the formation of mixed thiolate nanoclusters, characterized by the gradual decrease of near-IR luminescence. The study demonstrates that the luminescence QE of the Au nanoclusters can be further enhanced by the optimization of 1, 4-dithiolate-Au bonding.

5.2 Results and Discussions

5.2.1 Optical Properties of the Reaction between Monothiolate Au MPCs with Durene-DT 1, 4-Dithiols

In the presence of extra durene-DT molecules, the absorbance and luminescence spectra of $Au_{25}(SC2Ph)_{18}$ MPCs change over time as presented in **Figure 5.1**. The characteristic absorbance bands at ca. 400 nm, 450 nm and 670 nm from Au25 MPCs gradually diminish. Those absorbance bands from Au25 MPCs arise from the energetics established by the Au core and RS-Au-SR 'staple bonding motif'.[107,108,138] The durene-DT ligands change the Au: thiolate bonding and the stoichiometry ratio during the reaction process, therefore change the corresponding energy states and the corresponding absorbance transition. Furthermore, the formation of the polydispersed products will also lead to the loss of the discrete absorbance bands.

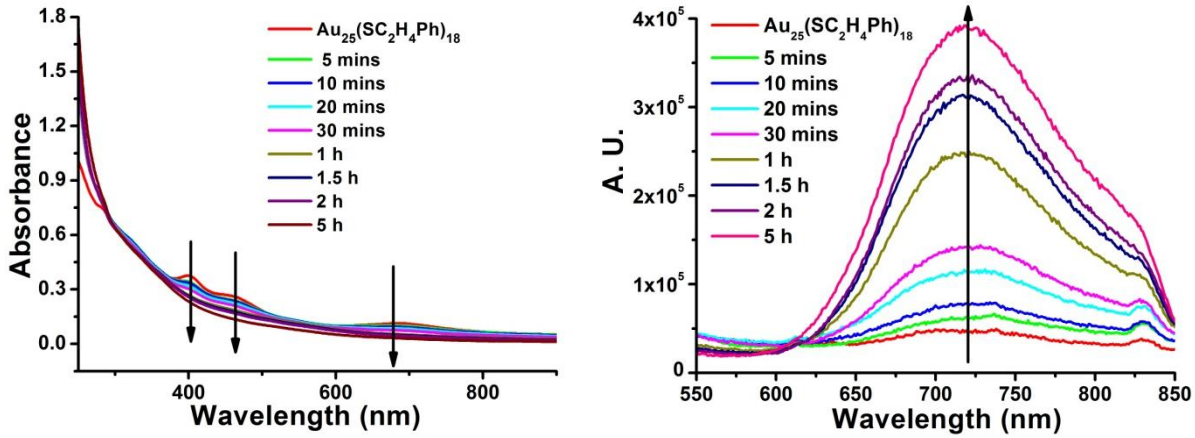

Figure 5.1. The spectrum changes of absorbance (Left) and luminescence (Right) in the reaction between $Au_{25}(SC2Ph)_{18}$ with durene-DT. The ligand ratio is ca. 4: 1 (durene-DT: PhC2S). The reaction was performed in CH_2Cl_2 at room temperature.

The increase in emission intensity suggests exciting trend to enhance the QE. The luminescence of Au25 has been reported in the literature with the QE at the order of 10^{-4} to 10^{-3} depending on the ligands and core charge states.[105,118] The QE of $Au_{25}(SC2Ph)_{18}$ increased upon oxidation as reported by Jin's group, being approximately $1*10^{-4}$ at -1 core charge states and $4*10^{-4}$ at 0 charge states. Limited by the responsive wavelength range of the detector used (up to ca. 840 nm), the numbers are ca. one half of the total emission QE that spans over to ca. 1000 nm. Therefore, the QEs of Au_{25}^{-} and Au_{25}^{0} would be $2*10^{-4}$ and $8*10^{-4}$ respectively.

For the reaction of neutral $Au_{25}(SC2Ph)_{18}$ with durene-DT in this report, the luminescence enhancement factor is about 10 times upon ligand displacement. The QE of the final product is therefore ca. $8*10^{-3}$. In an earlier report, the luminescence of Au MPCs is found to decrease upon the exchange with a 1, 2-dithiol DMPS.[343] In terms of improving the QE of the Au nanoclusters, the combined studies suggest a qualitative order of 1, 4-dithiolate-Au over monothiolate-Au over 1, 2-dithiolate-Au. The underlying assumption is that the core size and ligand/core polarity are comparable during the ligand ex-

change reaction (i.e. within 5-10 hours). This can be justified by the rich literature of ligand exchange reactions and the ligand molecular structures of the monothiolate-dithiolate system selected.

The ligand exchange reactions of various monothiol Au MPCs have been widely studied, pioneered by Murray's group.[2] The ligand exchange process generally follows second-order reaction kinetics. Importantly, the Au core size is found to remain unchanged during the reaction at early stage. At longer reaction time (days) with excess of thiols and/or elevated temperature, core etching or annealing reaction could occur.[120] In the specific case of dithiol-monothiol exchange in $Au_{25}(PhC2S)_{18}$,[361] the conservation of Au25 core with 18 ligand sites (S bonding) is reported in the exchange of toluene-3, 4-dithiol (1, 2-dithiol) with $Au_{25}(PhC2S)_{18}$.[28] Furthermore, the combined mass spectrometric and computational studies implied that for the reaction of $HS\text{-}(CH_2)_n\text{-}SH$ with $Au_{25}(PhC2S)_{18}$, propane and butane dithiols have ideal chain length for inter-semi-ring cross-linking.[408] No optical transition was reported.

It is worth pointing out that the determination of the exact Au-S interfacial bond structure remains challenging for either as-synthesized or ligand exchanged nanoclusters. The polydispersity nature of the exchange reaction products further complicates the situation. Based on the above discussion, the physical origin of the changes in optical properties is attributed to the differences in Au-S interfacial bonding structure introduced by the dithiolate ligands. Further experimental or theoretical structural determination will offer additional insights.

5.2.2 Dithiol-Monothiol Exchange Monitored by Proton NMR

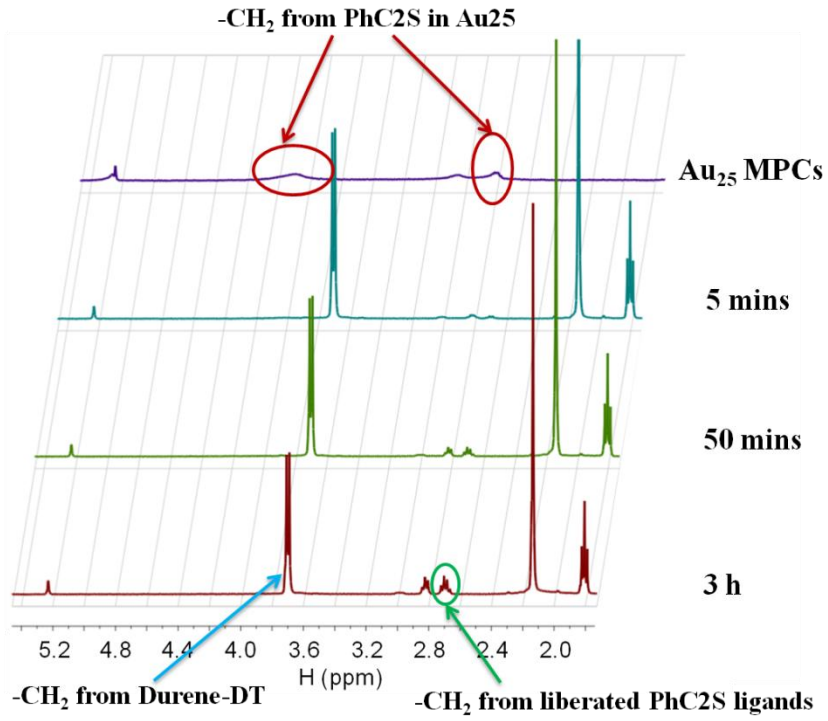

Figure 5.2. The proton NMR spectra of the reaction between $Au_{25}(SC2Ph)_{18}$ with durene-DT. The mole ratio of durene-DT: PhC2S was 4:1. The reaction was in CD_2Cl_2 at room temperature. The peak intensity in each spectrum was calibrated by the solvent proton signal at 5.24 ppm.

To confirm the correlation of optical transitions to the ligand exchange process, the reaction of durene-DT with $Au_{25}(PhC2S)_{18}$ was monitored by proton NMR. **Figure 5.2** presents the proton NMR signal changes. The peak intensity in each spectrum was calibrated with the solvent peak at ca. 5.24 ppm. Upon binding to the bulky nanoclusters, sharp proton peaks from free ligand molecules will be broadened, known as line-broadening effect.[361,362] The broad peaks denoted in the top spectrum corresponds to the CH_2 groups on $Au_{25}(PhC2S)_{18}$. Based on the reported charge dependence of the chemical shifts and line shapes, the original Au MPCs are partially oxidized (neutral species).[104,326]

The sharp peaks at ca. 3.8 ppm, 2.2 ppm and 1.9 ppm in the lower spectra are from the CH_2, CH_3 and SH groups of the added durene-DT molecules. The intensity of those sharp peaks decreases over time due to the broadening effects, indicating the attachment on Au nanoclusters. Meanwhile, the PhC2S monothiol is liberated from the nanoclusters, reflected by the growth of the sharp features at 2.75-2.95 ppm. The stoichiometry of durene-DT and PhC2S reaction is calculated based on the changes in the integrated peak intensity from the 5- and 50-minute spectra. The CH_2 peak at 3.8 ppm from durene-DT and one CH_2 peak at 2.8 ppm from the liberated PhC2S ligands were used. The ratio suggests that one durene-DT molecule replaces two PhC2SH molecules, which corresponds well with previous reports.[343] The stoichiometry and the reaction kinetics strongly support the mechanism of luminescence enhancement by the introduction of 1, 4-dithiolate durene-DT in the monolayer.

5.2.3 Proton NMR Characterization of Durene-DT Au DTCs and the Reaction with PhC2S Monothiols

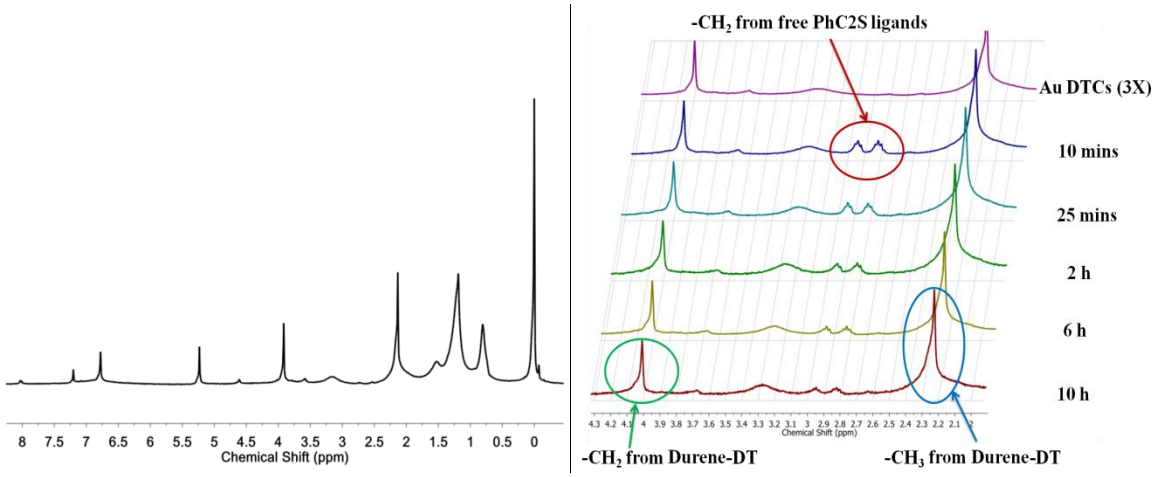

Figure 5.3. Left: Proton NMR spectrum of as-synthesized durene-DT Au DTCs. Right: Proton NMR spectra of the reaction between durene-DT Au DTCs and PhC2S monothiols. The reaction was in $CDCl_3$ solvent (7.2 ppm) at room temperature. Trace amount of CD_2Cl_2 was added as internal reference (5.3 ppm) for intensity calibration. The mole ratio of PhC2SH: durene-DT is estimated to be ca. 2: 1. The spectra were calibrated by the CH_2 signal of durene-DT at 4.05 ppm.

To further validate the proposed mechanism of luminescence enhancement by the interaction between Au and durene-DT ligands, monolayer reaction of durene-DT Au DTCs with PhC2S monothiols is studied. The NMR spectrum of the as-synthesized durene-DT Au DTCs is shown in the panel A of **Figure 5.3**. Repeated and systematic variations of the synthetic conditions suggest that durene-DT Au DTCs are unstable under ambient conditions. Full removal of the excess durene-DT and TOA^+ from the reaction mixture leads to the decomposition of the freshly prepared samples. Therefore, the broadened durene-DT ligand signals, better seen in panel B, coexist with the excess TOA^+ (signals below 2 ppm, and at 3.2 ppm) and trace amount of free durene-DT molecules. As reported in our earlier paper, highly stable Au nanoclusters can only be synthesized with mixed durene-DT and PhC2S ligands.[409] The binding of PhC2S was not excluded by the excess durene-DT molecules during the synthesis, suggesting that some sites within the monolayer are only accessible to the monothiols instead of dithiols.

The proton signals from the added phenylethanethiols decrease over time primarily due to the broadening effects, shown in **Figure 5.3**. The proton signals of durene-DT basically remain unchanged. Since the sharp peaks corresponding to the free durene-DT molecules in the reaction mixture do not change within the reaction period, we believe that the newly added PhC2S bind to the Au nanoclusters in an association mechanism instead of place exchange. Similar reaction mechanism has been reported in the reaction of DMPS DTCs with tiopronin.[343] The quantification of this reaction process is dampened by the needs to maintain the stability of the as-synthesized Au DTCs with excess durene-DT molecules and TOA ions. As the PhC2S monothiols gradually attach to the Au core, the surface ligand density increases and improves the stability of the Au nanoclusters. Note the reaction products would have a mixed monolayer composed of durene-DT and PhC2S ligands, in a similar rationale to the direct synthesis employing both monothiols and dithiols. The final products of this kinetic process are expected to be polydispersed as characterized by mass spectrometry discussed at the end.

5.2.4 Optical Properties of Durene-DT Au DTCs with PhC2S Monothiols

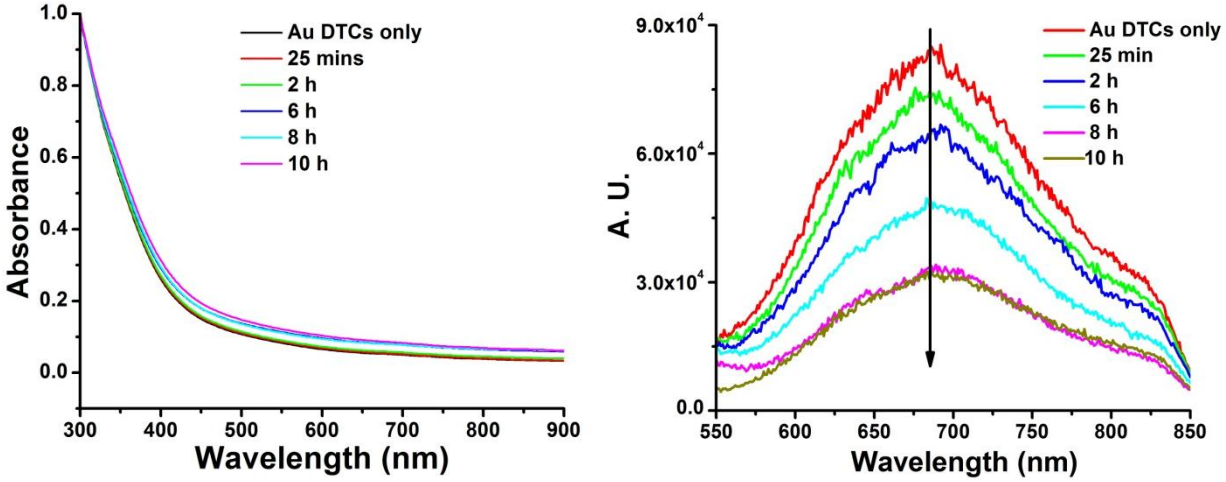

Figure 5.4. The absorbance (Left) and luminescence (Right) change of Durene DTCs reacted with phenylethanethiol. The reaction was in CH_2Cl_2 solvent at room temperature. The mole ratio of PhC2S: durene-DT is 2:1.

Representative absorbance and luminescence changes during the reaction between Au DTCs and PhC2S monothiols are presented in **Figure 5.4**. Upon the addition of PhC2S monothiols to the durene-DT Au DTCs, the absorbance spectra remain basically unchanged. This is an indication of less significant change, if any, of core size and core energy states. With durene-DT in the nanocluster monolayer, it is unlikely that Au25 remains to be a favorable core composition in the original polydispersed nanoclusters. Under the ligand addition mechanism, the core size is unlikely to change during this process. Therefore, the core size and energetics of the durene-DT Au nanoclusters, upon the addition of PhC2S ligands, did not display the Au25 absorbance signatures.

However, the near-IR luminescence gradually decreases upon the attachment of PhC2S confirmed in NMR studies. The monothiolate-Au bonding would lower the percentage of interfacial 1, 4-dithiolate-Au interactions. The luminescence QE decreases accordingly. The spectra at 8 and 10 hours overlap, suggesting a steady-state of the surface reaction. The QE of the final product is calculated to be ca. $4*10^{-}$

^{3}, slightly lower that the products from Au25 MPCs with durene-DT at $8*10^{-3}$. The difference can be attributed to the differences in the abundance and the respective QE of the luminescent species in the two polydispersed samples. Though the poor stability limits the precise characterization of the as-synthesized Au DTCs, similar absorbance and luminescence transitions have been observed from different Au DTCs from repeated synthesis, and from the synthetic products under systematically varied conditions (Au: dithiol ratio, reaction time, etc.). The observation suggests that the 1, 4-dithiolate-Au interactions offer improved QE in comparison with the staple bonding motif found in monothiolate-Au interactions. Interestingly, the Au DTCs stabilized by 1, 2-dithiol DMPS are non-luminescent.[350] The near IR luminescence can be reinstalled by the introduction of monothiol tiopronin.[343] Therefore, the improved QE from 1, 4 durene-DT interactions with Au offer another promising route to further enhance the near IR luminescence, in addition to the known factors of core size and core/ligand polarities. At longer reaction time, the luminescence will intensify, indicating an etching/annealing mechanism that leads to core size change. The interesting transition has been reported in similar studies of monothiol Au MPCs thus not further elaborated in this report.

5.2.5 Mass Spectrometry Characterization of the Reaction Products

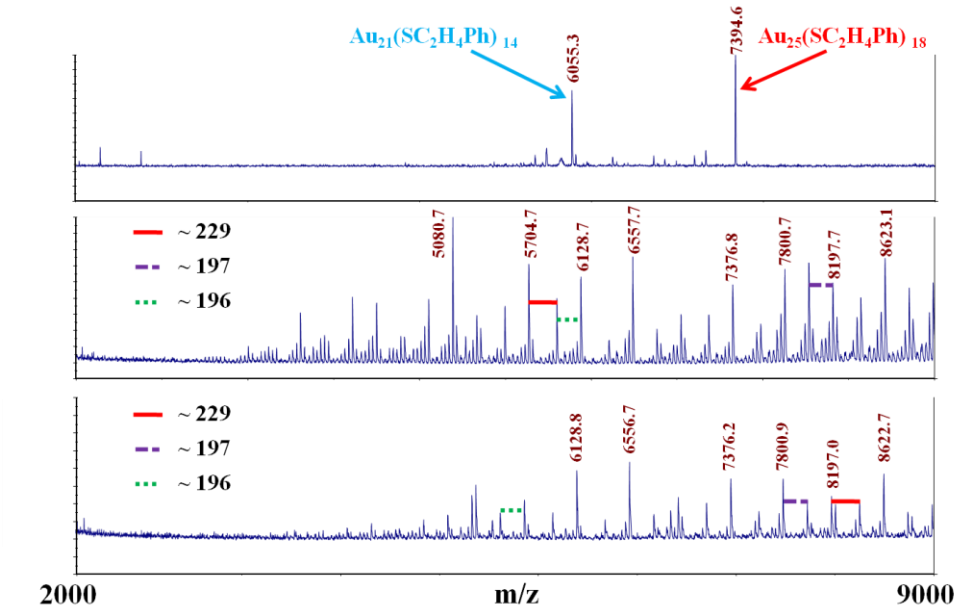

Figure 5.5. Mass spectra of $Au_{25}(PhC2S)_{18}$ (Top), the final products of Au25 MPCs with Durene-DT (Middle) and the final products of Au DTCs with PhC2SH (Bottom). The spectra were collected under reflectron positive mode with DCTB as matrix. (229: Au+S; 197: Au; 196: Durene-DT minus 2H).

The final products of both reactions have mixed durene-DT and PhC2S ligands in the monolayer. The stability of durene-DT Au DTCs is therefore improved, which allows further characterization. The results presented in **Figure 5.5** were collected under positive mode in matrix assisted laser desorption ionization mass spectrometry (MALDI-MS) analysis. Under negative mode, no significant peak was detected other than the Au_xS_y patterns at low m/z range (not shown). The spectrum of $Au_{25}(SC2Ph)_{18}$ is shown on top, in which intact molecular ion of $Au_{25}(SC2Ph)_{18}$ and the major fragment of $Au_{21}(SC_2H_4Ph)_{14}$ can be seen as reference points for the comparison with the reaction products.[27] The m/z value of the molecular ion is found to be ca. 3 Da higher than the theoretical values, attributed to the instrument calibration. The final products of both types of reactions display similar m/z patterns in the mass range under reflectron mode. The major peaks are labeled in the two bottom spectra. Some of those m/z

peaks are obviously the fragments formed during the MS analysis. To guide the observation, a few representative mass losses are indicated in the spectra. Though the MS analysis has been successfully employed in many Au MPC studies, the similarity in mass (i.e. Au at 197, durene-DT at 198, durene-DT minus H at 197 (losing one –SH), and durene-DT minus 2H at 196 (losing both -SH)) makes it highly challenging to conclude on a definitive solution. We offer the composition as (Au + Durene-DT)$_{x+y}$(PhC2S)$_z$S$_m$, with x ranges from 18 to 34, y ranges from 2 to 8, z ranges from 5 to 10, and m ranges from 1 to 2. Two representative peaks at 6557.7 and 7376.8 m/z values can be described as Au_{25}(Durene-DT)$(PhC2S)_{10}S_2$ and $Au_{27}(Durene\text{-}DT)_7(PhC2S)_5$ respectively. The compositions of other peaks can be derived by the variation of x, y, z and m values. Since the exchange products are generally known to be polydispersed, it is reasonable to notice that the mass peaks are distributed around the original Au25MPC molecular ion signal. It has also been reported that the recombination process during MS analysis could also lead to the increase of m/z peak values. Further studies are needed to validate the tentative molecular formula assignments. Furthermore, no discernible signal can be observed above 9000 Da from the products of DTCs – monothiols reaction. For MPCs - dithiols products, a series of relatively weak peaks near 9.9-10.3 kDa with mass differences of ca. 196-197 were detected under linear mode (not shown). The mass differences between those peaks correspond to either one Au or one durene-DT (196-198). Representative compositions of those peaks could be described as $Au_{38}(Durene\text{-}DT)_{6\text{-}8}(PhC2S)_9$, which has very similar Au-S composition to the reported $Au_{38}(PhC2S)_{24}$ MPCs[389] and could be favorable based on super atom theory (i.e. 38-2*6-9=17).[112] Regardless, it is interesting to notice the similarity in the spectra of the two reaction products. The results strongly indicate the similarity and the improved stability of those mixed thiolate clusters.

5.3 Materials and Method

5.3.1 Chemicals

Tetrachloroauric acid trihydrate ($HAuCl_4 \cdot 3H_2O$, >99.99% metals basis), sodium borohydride (NaBH4, 99%), 2-Phenylethanethiol (>99%), tetraoctylammonium bromide (TOABr, 98%), *trans*-2-[3-(4-tert-butylphenyl)-2-methyl-propenylidene]-malononitrile (DCTB, >99%) and organic solvents (HPLC grade) were used as received from Sigma-Aldrich. Durene-α1, α2-dithiol (>95%) (durene-DT) was purchased from TCI-America.

5.3.2 Methods

UV-Visible absorbance spectra were recorded with a Shimadzu UV-1700 spectrophotometer. Luminescence was measured with a Horiba Jobin-Yvon Fluorolog 311 spectrometer with T channel, through which a visible PMT detector and a near IR InGaAs detector were attached. Mass spectra were acquired with ABI 4800 matrix assisted laser desorption ionization (MALDI) time-of –flight (TOF) analyzer, with DCTB as matrix.

5.3.3 Synthesis and Purifications

The synthesis of $Au_{25}(SC2Ph)_{18}$ follows the kinetic controlled approach developed by Jin's group.[301] Durene-DT protected Au DTCs were synthesized using a one-phase procedure. Briefly, $HAuCl_4 \cdot 3H_2O$ (0.1 mmol, 39.4 mg) was dissolved in 10 mL of water. TOABr (0.12 mmol, 66 mg) in 10 mL toluene was used to transfer Au(III) into the organic phase to form TOA-$AuCl_4$. The toluene phase was isolated and cooled over a dry ice/acetone bath. Meanwhile, a solution of durene-DT (0.3 mmol, ~60 mg) in 10 mL toluene was added to a solution of TBA-BH_4 (1 mmol, 258 mg, in 10 mL toluene) at rapid stirring. This solution was also chilled over the dry ice/acetone bath. The two suspensions were mixed together at rapid stirring. Dry ice was gradually removed from acetone bath and the reaction was allowed to proceed for several hours at room temperature. The reaction was stopped after the absorbance transition stabilized.

The solution was rinsed with water 3-5 times prior rotary evaporation of toluene. The Au DTCs are then sequentially washed with methanol, ethanol, and hexane until the filtrates became clear. The leftover products were collected as final product.

5.4 Summary

The near-IR luminescence of Au nanoclusters is found to strongly depend on the interfacial bonding at core-ligand interface. Qualitatively, the 1, 4-dithiolate-Au bonding offers more intense near IR emission over the monothiolate-Au interaction that is known to have the staple bonding motif. Combined with the previous studies that no detectable luminescence could be observed from 1, 2-dithiolate-Au interactions on Au nanoclusters, we propose that the core-ligand interfacial bonding is a promising factor that could further enhance the quantum yield of the near IR luminescence of Au nanoclusters for biomedical applications.

This chapter is reproduced from Nanoscale/DOI:10.1039/C2NR30504F, by the permission from The Royal Society of Chemisrtry.

6 CONCLUSIONS AND MAJOR DISCOVERY

In conclusion, the dissertation work of my PhD is centered on the synthesis, characterizations and properties of gold nanoclusters tuned by interfacial bonding structure and their energetic studies. By introducing DMPS 1, 2-dithiol ligands on the gold surface, Au4 complexes with characteristic absorption feature at 282 nm have been created. Near infrared luminescence “switch” of gold nanoclusters based on the monolayer ligand exchange reaction has been fabricated. By employing mixed durene-dt 1,4-

dithiol and phenylethanethiol ligands, Au130 nanoparticle with multiple absorption bands at ~355 nm, ~490 nm, ~584 nm and ~718 nm and rich electrochemistry features (continuous quantized double-layer charging peaks at lower potentials and radical anion or cation peak at higher potentials) has been synthesized. The correlation between the optical and electrochemical energetics has been successfully correlated. Further work on the electro-paramagenitic behaviors of the Au130 nanoparticle is underway in our group. Moreover, the impacts of the 1, 4-dithiolate-Au bonding on the near infrared luminescence of the gold nanoclusters have been investigated. We found that 1, 4-dithiolate-Au bonding offers intense near IR emission than monothiolate-Au and 1, 2-dithiolate-Au. All those results confirmed our previous hypothesis, that is, interfacial bonding structure is an important factor that does affect the property of gold nanoclusters. We envision that the interfacial bonding structure will play an important role in other nanoparticle property and eventually trigger more research efforts in the near future.

7 REFERENCES

(1) Daniel, M.-C.; Astruc, D. *Chem. Rev.* **2004**, *104*, 293.

(2) Templeton, A. C.; Wuelfing, M. P.; Murray, R. W. *Acc. Chem. Res.* **2000**, *33*, 27.

(3) Murray, R. W. *Chem. Rev.* **2008**, *108*, 2688.

(4) Sardar, R.; Funston, A. M.; Mulvaney, P.; Murray, R. W. *Langmuir* **2009**, *25*, 13840.

(5) Jin, R. *Nanoscale* **2010**, *2*, 343.

(6) Turkevitch, J.; Stevenson, P. C.; Hillier, J. *Discuss. Farady Soc.* **1951**, *11*, 55.

(7) Yao, T.; Sun, Z.; Li, Y.; Pan, Z.; Wei, H.; Xie, Y.; Nomura, M.; Niwa, Y.; Yan, W.; Wu, Z.; Jiang, Y.; Liu, Q.; Wei, S. *J. Am. Chem. Soc.* **2010**, *132*, 7696.

(8) Polte, J.; Ahner, T. T.; Delissen, F.; Sokolov, S.; Emmerling, F.; Thunmann, A. F.; Kraehnert, R. *J. Am. Chem. Soc.* **2010**, *132*, 1296.

(9) Brust, M.; Walker, M.; Bethell, D.; Schiffrin, D. J.; Whyman, R. *J. Chem. Soc., Chem. Comm* **1994**, 801.

(10) Brust, M.; Fink, J.; Bethell, D.; Schiffrin, D. J.; Kiely, C. *J. Chem. Soc.; Chem. Comm* **1995**, 1655.

(11) Goulet, P. J. G.; Lennox, R. B. *J. Am. Chem. Soc.* **2010**, *132*, 9582.

(12) Li, Y.; Zaluzhna, O.; Xu, B.; Gao, Y.; Modest, J. M.; Tong, Y. J. *J. Am. Chem. Soc.* **2011**, *133*, 2092.

(13) Kanehara, M.; Sakurai, T.; Sugimura, H.; Teranishi, T. *J. Am. Chem. Soc.* **2009**, *131*, 1630.

(14) Mpourmpakis, G.; Caratzoulas, S.; Ulachos, D. G. *Nano Lett.* **2010**, *10*, 3408.

(15) Negishi, Y.; Takasugi, Y.; Sato, S.; Yao, H.; Kimura, K.; Tsukuda, T. *J. Am. Chem. Soc.* **2004**, *126*, 6518.

(16) Gies, A. P.; Hercules, D. M.; Gerdon, A. E.; Cliffel, D. E. *J. Am. Chem. Soc.* **2007**, *129*, 1095.

(17) Tracy, J. B.; Kalyuzhny, G.; Crowe, M. C.; Balasubramanian, R.; Choi, J. P.; Murray, R. W. *J. Am. Chem. Soc.* **2007**, *129*, 6706.

(18) Tracy, J. B.; Crowe, M. C.; Parker, J. F.; Hampe, O.; Fields-Zinna, C. A.; Dass, A.; Murray, R. W. *J. Am. Chem. Soc.* **2007**, *129*, 16209.

(19) Fields-Zinna, C. A.; Crowe, M. C.; Dass, A.; Weaver, J. E. F.; Murray, R. W. *Langmuir* **2009**, *25*, 7704.

(20) Fields-Zinna, C. A.; Sardar, R.; Beasley, C. A.; Murray, R. W. *J. Am. Chem. Soc.* **2009**, *131*, 16266.

(21) Gutienez, E.; Powell, R. D.; Furuya, F. R.; Hainfeld, J. F.; Schaaff, T. G.; Shafigllin, M. N.; Stephens, P. W.; Whetten, R. L. *Eur. Phys. J. D* **1999**, *9*, 647.

(22) Schaaff, T. G.; Knight, G.; Shafigullin, M. N.; Borkmann, R. F.; Whetten, R. L. *J. Phys. Chem. B* **1998**, *102*, 10643.

(23) Schaaff, T. G. *Anal. Chem.* **2004**, *76*, 6187.

(24) Schaaff, T. G.; Whetten, R. L. *J. Phys. Chem. B* **2000**, *104*, 2630.

(25) Schaaff, T. G.; Shafigullin, M. N.; Khoury, J. T.; Vezmar, I.; Whetten, R. L. *J. Phys. Chem. B* **2001**, *105*, 8785.

(26) Dass, A.; Holt, K.; Parker, J. F.; Feldberg, S. W.; Murray, R. W. *J. Phys. Chem. C* **2008**, *112*, 20276.

(27) Dass, A.; Stevenson, A.; Dubay, G. R.; Tracy, J. B.; Murray, R. W. *J. Am. Chem. Soc.* **2008**, *130*, 5940.

(28) Fields-Zinna, C. A.; Parker, J. F.; Murray, R. W. *J. Am. Chem. Soc.* **2010**, *132*, 17193.

(29) Wu, Z.; Gayathri, C.; Gil, R. R.; Jin, R. *J. Am. Chem. Soc.* **2009**, *131*, 6535.

(30) Qian, H.; Zhu, Y.; Jin, R. *J. Am. Chem. Soc.* **2010**, *132*, 4583.

(31) Dharmaratne, A. C.; Krick, T.; Dass, A. *J. Am. Chem. Soc.* **2009**, *131*, 13604.

(32) Dass, A. *J. Am. Chem. Soc.* **2009**, *131*, 11666.

(33) Dass, A.; Dubay, G. R.; Fields-Zinna, C. A.; Murray, R. W. *Anal. Chem.* **2008**, *80*, 6845.

(34) Harkness, K. M.; Fenn, L. S.; Cliffel, D. E.; Mclean, J. A. *Anal. Chem.* **2010**, *82*, 3061.

(35) Angel, L. A.; Major, L. T.; Dharmaratne, A. C.; Dass, A. *ACS Nano* **2010**, *4*, 4691.

(36) Fields-Zinna, C. A.; Sampson, J. S.; Crowe, M. C.; Tracy, J. B.; Parker, J. F.; Deney, A. M.; Muddiman, D. C.; Murray, R. W. *J. Am. Chem. Soc.* **2009**, *131*, 13844.

(37) Giersig, M.; Mulvaney, P. *Langmuir* **1993**, *9*, 3408.

(38) Hasan, M.; Bethell, D.; Brust, M. *J. Am. Chem. Soc.* **2003**, *125*, 1132.

(39) Knake, R.; Fahmi, A. W.; Tofail, S. A. M.; Clohessy, J.; Mihov, M.; Cunnane, V. J. *Langmuir* **2005**, *21*, 1001.

(40) Azzam, T.; Eisenberg, A. *Langmuir* **2007**, *23*, 2126.

(41) Chen, C., -C.; Hsu, C.-H.; Kuo, P.-L. *Langmuir* **2007**, *23*, 6801.

(42) Wang, Y.; Neyman, A.; Arkhangelsky, E.; Gitis, V.; Meshi, L.; Weinstock, I. A. *J. Am. Chem. Soc.* **2009**, *131*, 17412.

(43) Qu, W.-G.; Wang, S.-M.; Hu, Z.-J.; Cheang, T.-Y.; Xing, Z., -H.; Zhang, X., -J.; Xu, A.-W. *J. Phys. Chem. C* **2010**, *114*, 13010.

(44) Shumaker-Parry, J. S.; Sadar, R. *J. Am. Chem. Soc.* **2011**, *133*, 8179.

(45) Maye, M. M.; Lim, I. S.; Luo, J.; Rab, Z.; Rabinovich, D.; Liu, T.; Zhong, C.-T. *J. Am. Chem. Soc.* **2005**, *127*, 1519.

(46) Dai, X.; Nekrassova, O.; Hyde, M. E.; Compton, R. G. *Anal. Chem.* **2004**, *76*, 5924.
(47) Wanunu, M.; Popovitz-Biro, R.; Cphen, H.; Vaskevich, A.; Rubinstein, I. *J. Am. Chem. Soc.* **2005**, *127*, 9207.
(48) Kim, Z. H.; Leone, S. R. *J. Phys. Chem. B* **2006**, *110*, 19804.
(49) Tong, L.; Li, Z.; Zhu, T.; Xu, H.; Liu, Z. *J. Phys. Chem. C* **2008**, *112*, 7119.
(50) Jensen, P. S.; Chi, Q.; Zhang, J.; Ulstrup, J. *J. Phys. Chem. C* **2009**, *113*, 13993.
(51) Xu, Q.; Kang, X.; Bogomolni, R. A.; Chen, S. *Langmuir* **2010**, *26*, 14923.
(52) Chaikin, Y.; Leader, H.; Popovitz-Biro, R.; Vaskevich, A.; Rubinstein, I. *Langmuir* **2011**, *27*, 1298.
(53) Plaza, J. L.; Chen, Y.; Jacke, S.; Palmer, R. E. *Langmuir* **2005**, *21*, 1556.
(54) Palgrave, R. G.; Parkin, I. P. *J. Am. Chem. Soc.* **2006**, *128*, 1587.
(55) Diao, P.; Guo, M.; Zhang, Q. *J. Phys. Chem. C* **2008**, *112*, 7036.
(56) Miyazaki, T.; Hasegawa, R.; Yamaguchi, H.; Oh-oka, H.; Nagato, H.; Amemiya, I.; Uchikoga, S. *J. Phys. Chem. C* **2009**, *113*, 8484.
(57) Santosh, G.; Shirman, E.; Weissman, H.; Shimoni, E.; Pinkas, I.; Rudich, Y.; Rybtchinski, B. *J. Phys. Chem. B* **2010**, *114*, 14389.
(58) Adam, K. L.; Jena, B. K.; Percival, S. J.; Zhang, B. *Anal. Chem.* **2011**, *83*, 920.
(59) Yang, T.; Zhang, Y.; Li, Z. *Biomacromolecules* **2011**, *12*, 2027.
(60) Bhargava, S. K.; Booth, J. M.; Agrawal, S.; Coloe, P.; Kar, G. *Langmuir* **2005**, *21*, 5949.
(61) Polte, J.; Emmerling, F.; Radtke, M.; Reinholz, U.; Riesemeier, H.; Thunemann, A. F. *Langmuir* **2010**, *26*, 5889.
(62) Abecassis, B.; Testard, F.; Kong, Q.; Francois, B.; Spalla, O. *Langmuir* **2010**, *26*, 13847.
(63) Boye, D. M.; Wang, Z.; Huang, J. Y.; Fan, H. *J. Am. Chem. Soc.* **2010**, *132*, 12826.
(64) Gole, A.; Dash, C.; Soman, C.; Sainkar, S. R.; Rao, M.; Sastry, M. *Bioconjugate Chem.* **2001**, *12*, 684.
(65) Stoeva, S. I.; Prasad, B. L. V.; Uma, S.; Stoimenov, P. K.; Zaikovski, V.; Sorensen, C. M.; Klabunde, K. J. *J. Phys. Chem. B* **2003**, *107*, 7441.
(66) Sajanlal, P. R.; Screeprasad, T. S.; Nair, A. S.; Pradeep, T. *Langmuir* **2008**, *24*, 4607.
(67) Kim, J.-H.; Bryn, W. W.; Lee, T. R. *Langmuir* **2008**, *24*, 11147.
(68) Han, J.; Li, L.; Guo, R. *Macromolecules* **2010**, *43*, 10636.
(69) Mayer, C. *Annu. Rep. NMR Spectrosc* **2005**, *55*, 205.
(70) Hostetler, M. J.; Wingate, J. E.; Zhong, C. J.; Harris, J. E.; Vachet, R. W.; Clark, M. R.; Londono, J. D.; Green, S. J.; Stokes, J. J.; Wignall, G. D.; Glish, G. L.; Porter, M. D.; Evans, N. D.; Murray, R. W. *Langmuir* **1998**, *14*, 17.
(71) Zelakiewicz, B.; de Dios, A. C.; Tong, Y. *J. Am. Chem. Soc.* **2003**, *125*, 18.
(72) Song, Y.; Huang, T.; Murray, R. W. *J. Am. Chem. Soc.* **2003**, *125*, 11694.
(73) Song, Y.; Harper, A. S.; Murray, R. W. *Langmuir* **2005**, *21*, 5492.
(74) Dass, A.; Guo, R.; Tracy, J. B.; Balasubramanian, R.; Douglas, A. D.; Murray, R. W. *Langmuir* **2008**, *24*, 310.
(75) Shon, Y. S.; Mazzitelli, C.; Murray, R. W. *Langmuir* **2001**, *17*, 7735.
(76) Shon, Y. S.; Wuelfing, W. P.; Murray, R. W. *Langmuir* **2001**, *17*, 1255.
(77) Kohlmann, O.; Steinmetz, W. E.; Mao, X. A.; Wuelfing, W. P.; Templeton, A. C.; Murray, R. W.; Johnson, C. S. *J. Phys. Chem. B* **2001**, *105*, 8801.
(78) Donkers, R. L.; Song, Y.; Murray, R. W. *Langmuir* **2004**, *20*, 4703.
(79) Bhaltacharya, S.; Srivastava, A. *Langmuir* **2003**, *19*, 4439.
(80) Dorris, A.; Rucareanu, S.; Reven, L.; Barrett, C. J.; Lennox, R. B. *Langmuir* **2008**, *24*, 2532.
(81) Badia, A.; Gao, W.; Singh, S.; Demers, L.; Guccia, L.; Reven, L. *Langmuir* **1996**, *12*, 1262.
(82) Shaffer, A. W.; Worden, J. G.; Huo, Q. *Langmuir* **2004**, *20*, 8483.

(83) Sharma, R.; Holland, G. P.; Solomon, V. C.; Zimmermann, H.; Schiffenhaus, S.; Amin, S. A.; Buttry, D. A.; Yarger, J. L. *J. Phys. Chem. C* **2009**, *113*, 16387.

(84) Sharma, R.; Taylor, R. E.; Bouchard, L.-S. *J. Phys. Chem. C* **2011**, *115*, 3297.

(85) Canzi, G.; Mrse, A. A.; Kubiak, C. P. *J. Phys. Chem. C* **2011**, *115*, 7972.

(86) Calzolai, L.; Franchini, F.; Gililand, D.; Rossi, F. *Nano Lett.* **2010**, *10*, 3101.

(87) Zhou, H.; Du, F.; Li, X.; Zhang, B.; Li, W.; Yan, B. *J. Phys. Chem. C* **2008**, *112*, 19360.

(88) Templeton, A. C.; Chen, S. W.; Gross, S. M.; Murray, R. W. *Langmuir* **1999**, *15*, 66.

(89) Kell, A. J. A., A.; Yang, L.; Workentin, M. S. *Langmuir* **2005**, *21*, 9741.

(90) Huang, C.-M.; Wei, K.-H.; Jeng, U.-S.; Liang, K. S. *Macromolecules* **2007**, *40*, 5067.

(91) Coutts, M. J.; Coritie, M. B.; Ford, M. J.; McDonagh, A. M. *J. Phys. Chem. C* **2009**, *113*, 1325.

(92) Qian, H.; Jin, R. *Nano Lett.* **2009**, *9*, 4083.

(93) Zhu, M.; Qian, H.; Jin, R. *J. Am. Chem. Soc.* **2009**, *131*, 7220.

(94) Moulder, J. F.; Stickle, W. F.; Sobol, P. E.; Bomben, K. D. *Handbooks of X-ray Photoelectron Spectroscopy* **1992**, *published by Perkin-Elmer Corp*, MN.

(95) Crist, B. V. *Handbooks of Monochromatic XPS Spectra* **2004**, *published by XPS International LLC*, CA.

(96) Tanaka, A.; Takeda, Y.; Imamura, M.; Sato, S. *Phys. Rev. B* **2003**, *68*, 195415.

(97) Negishi, Y.; Nobusada, K.; Tsukuda, T. *J. Am. Chem. Soc.* **2005**, *127*, 5261.

(98) Shibu, E. S.; Muhammed, M. A. H.; Tsukuda, T.; Pradeep, T. *J. Phys. Chem. C* **2008**, *112*, 12168.

(99) Shon, Y. S.; Gross, S. M.; Dawson, B.; Porter, M.; Murray, R. W. *Langmuir* **2000**, *16*, 6555.

(100) Cecchet, F.; Pilling, M.; Hevesi, L.; Schergna, S.; Wong, J., K. Y.; Clarkson, G. J.; Leigh, D. A.; Rudolf, P. *J. Phys. Chem. B* **2003**, *107*, 10863.

(101) Bourg, M.-C.; Badia, A.; Lennox, R. B. *J. Phys. Chem. B* **2000**, *104*, 6562.

(102) Kaciulis, S.; Caro, T. D.; Ingo, G. M.; Padeletti, G. *J. Phys. Chem. C* **2009**, *113*, 12772.

(103) Parker, J. F.; Fields-Zinna, C. A.; Murray, R. W. *Acc. Chem. Res.* **2010**, *43*, 1289.

(104) Donkers, R. L.; Lee, D.; Murray, R. W. *Langmuir* **2004**, *20*, 1945.

(105) Lee, D.; Donkers, R. L.; Wang, G.; Harper, A. S.; Murray, R. W. *J. Am. Chem. Soc.* **2004**, *126*, 6193.

(106) Shichibu, Y.; Negishi, Y.; Tsukuda, T.; Teranishi, T. *J. Am. Chem. Soc.* **2005**, *127*, 13464.

(107) Heaven, M. W.; Dass, A.; White, P. S.; Holt, K. M.; Murray, R. W. *J. Am. Chem. Soc.* **2008**, *130*, 3754.

(108) Zhu, M.; Aikens, C. M.; Hollander, F. J.; Schatz, G. C.; Jin, R. *J. Am. Chem. Soc.* **2008**, *130*, 5883.

(109) Negishi, Y.; Chaki, N. K.; Shichibu, Y.; Whetten, R. L.; Tsukuda, T. *J. Am. Chem. Soc.* **2007**, *129*, 11322.

(110) Zhu, M.; Eckenhoff, W. T.; Pintauer, T.; Jin, R. *J. Phys. Chem. C* **2008**, *112*, 14221.

(111) Akola, J.; Walter, M.; Whetten, R. L.; Hakkinen, H.; Gronbeck, H. *J. Am. Chem. Soc.* **2008**, *130*, 3756.

(112) Walter, M.; Akola, J.; Lopez-Acevedo, O.; Jadzinsky, P. D.; Calero, G.; Ackerson, C. J.; Whetten, R. L.; Gronbeck, H.; Hakkinen, H. *Proc. Nat. Acad. Sci. USA* **2008**, *105*, 9157.

(113) Hakkinen, H.; Walter, M.; Gronbeck, H. *J. Phys. Chem. B* **2006**, *110*, 9927.

(114) Jiang, D.-e.; Tiago, M. L.; Luo, W.; Dai, S. *J. Am. Chem. Soc.* **2008**, *130*, 2777.

(115) Wang, G.; Guo, R.; Kalyuzhny, G.; Choi, J. P.; Murray, R. W. *J. Phys. Chem. B* **2006**, *110*, 20282.

(116) Wang, G.; Huang, T.; Murray, R. W.; Menard, L.; Nuzzo, R. G. *J. Am. Chem. Soc.* **2005**, *127*, 812.

(117) Xie, J.; Zheng, Y.; Ying, J. Y. *J. Am. Chem. Soc.* **2009**, *131*, 888.
(118) Wu, Z.; Jin, R. *Nano Lett.* **2010**, *10*, 2568.
(119) Donil Lee, R. L. D., Gangli Wang, Amanda S. Harper, Royce Murray *J. Am. Chem. Soc.* **2004**, *126*, 6193.
(120) Schaaff, T. G.; Whetten, R. L. *J. Phys. Chem. B* **1999**, *103*, 9394.
(121) Toikkanen, O.; Ruiz, V.; Ronnholm, G.; Kalkkinen, N.; Liljeroth, P.; Quinn, B. M. *J. Am. Chem. Soc.* **2008**, *130*, 11049.
(122) Chaki, N. K.; Negishi, Y.; Tsunoyama, H.; Shichibu, Y.; Tsukuda, T. *J. Am. Chem. Soc.* **2008**, *130*, 8608.
(123) Qian, H.; Zhu, Y.; Jin, R. *ACS Nano* **2009**, *3*, 3795.
(124) Qian, H.; Zhu, M.; Andersen, U. N.; R., J. *J. Phys. Chem. A* **2009**, *113*, 4281.
(125) Wijngaarden, J. T.; Toikkanen, O.; Liljeroth, P.; Quinn, B. M.; Meijerink, A. *J. Phys. Chem. C* **2010**, *114*, 16025.
(126) Jiang, D.-e.; Luo, W.; Tiago, M. L.; Dai, S. *J. Phys. Chem. C* **2008**, *112*, 13905.
(127) Lopez-Acevedo, O.; Tsunoyama, H.; Tsukuda, T.; Hakkinen, H.; Aikens, C. M. *J. Am. Chem. Soc.* **2010**, *132*, 8210.
(128) Pei, Y.; Gao, Y.; Zeng, X. C. *J. Am. Chem. Soc.* **2008**, *130*, 7830.
(129) Shichibu, Y.; Konishi, K. *Small* **2010**, *6*, 1216.
(130) Wu, Z.; MaDonald, M. A.; Chen, J.; Zhang, P.; Jin, R. *J. Am. Chem. Soc.* **2011**, *133*, 9670.
(131) Pei, Y.; Gao, Y.; Shao, N.; Zeng, X. C. *J. Am. Chem. Soc.* **2009**, *131*, 13619.
(132) Nimmala, P. R.; Dass, A. *J. Am. Chem. Soc.* **2011**, *133*, 9175.
(133) Knoppe, S.; Boudon, J.; Dolamic, I.; Dass, A.; Burgi, T. *Anal. Chem.* **2011**, *83*, 5056.
(134) Tsunoyama, H.; Negishi, Y.; Tsukuda, T. *J. Am. Chem. Soc.* **2006**, *128*, 6036.
(135) Schmid, G.; Pfeil, F.; Boese, R.; Bandermann, F.; Meyer, S.; Calias, G. H. M.; van der Velden, J. W. A. *Chem. Ber.* **1981**, *114*, 3634.
(136) Schmid, G. *Inorg. Synth.* **1990**, *27*, 214.
(137) Balasubramanian, R.; Guo, R.; Mills, A. J.; Murray, R. W. *J. Am. Chem. Soc.* **2005**, *127*, 8126.
(138) Jadzinsky, P. D.; Calero, G.; Ackerson, C. J.; Bushnell, D. A.; Kornberg, R. D. *Science* **2007**, *318*, 430.
(139) Levi-Kalisman, Y.; Jadzinskey, P. D.; Kalisman, N.; Tsunoyama, H.; Tsukuda, T.; Bushnell, D. A.; Kornberg, R. D. *J. Am. Chem. Soc.* **2011**, *133*, 2976.
(140) Pei, Y.; Gao, Y.; Zeng, X. C. *ACS Nano* **2008**, *2*, 1497.
(141) Li, Y.; Galli, G.; Gygi, F. *ACS Nano* **2008**, *2*, 1896.
(142) Reimers, J. R.; Wang, Y.; Cankurtaran, B. O.; Ford, M. J. *J. Am. Chem. Soc.* **2010**, *132*, 8378.
(143) Hulkko, E.; Lopez-Acevedo, O.; Koivisto, J.; Levi-Kalisman, Y.; Kornberg, R. D.; Pettersson, M.; Hakkinen, H. *J. Am. Chem. Soc.* **2011**, *133*, 3752.
(144) Schaaff, T. G.; Shafigullin, M. N.; Khoury, J. T.; Whetten, R. L.; Cullen, W. G.; First, P. N.; Gutierrez-Wing, C. A. J.; Jose-Yacaman, M. J. *J. Phys. Chem. B* **1997**, *101*, 7885.
(145) Chen, S. I., R. S.; Hostetler, M. J.; Pietron, J. J.; Murray, R. W. Schaaff, T. G.; Khoury, J. T.; Alvarez, M. M.; Whetten, R. L. *Science* **1998**, *280*, 2098.
(146) Hicks, J. F.; Templeton, A. C.; Chen, S. W.; Sheran, K. M.; Jasti, R.; Murray, R. W.; Debord, J.; Schaaf, T. G.; Whetten, R. L. *Anal. Chem.* **1999**, *71*, 3703.
(147) Chen, S. W.; Murray, R. W.; Feldberg, S. W. *J. Phys. Chem. B* **1998**, *102*, 9898.
(148) Hicks, J. F.; Miles, D. T.; Murray, R. W. *J. Am. Chem. Soc.* **2002**, *124*, 13322.
(149) Quinn, B. M.; Liljeroth, P.; Ruiz, V.; Laaksonen, T.; Kontturi, K. *J. Am. Chem. Soc.* **2003**, *125*, 6644.

(150) Wuelfing, W. P.; Gross, S. M.; Miles, D. T.; Murray, R. W. *J. Am. Chem. Soc.* **1998**, *120*, 12696.

(151) Zheng, M.; Davidson, F.; Huang, X. *J. Am. Chem. Soc.* **2003**, *125*, 7790.

(152) Wu, Z.; Chen, J.; Zhang, P.; Jin, R. *Adv. Funct. Mater.* **2011**, *21*, 177.

(153) Ackerson, C. J.; Jadzinskey, P. D.; Kornberg, R. D. *J. Am. Chem. Soc.* **2005**, *127*, 6550.

(154) Rouhana, L. L.; Jaber, J. A.; Schlenoff, J. B. *Langmuir* **2007**, *127*, 12799.

(155) Gentilini, C.; Evangelista, F.; Rudolf, P.; Franchi, P.; Lucarni, M.; Pasquato, L. *J. Am. Chem. Soc.* **2008**, *130*, 15678.

(156) Varnavski, O.; Ramakrishna, G.; Kim, J.; Lee, D.; Goodson, T. *J. Am. Chem. Soc.* **2010**, *132*, 16.

(157) Armer, B.; Schmidbaur, H. *Angew. Chem.* **1970**, *82*, 120.

(158) Burini, A.; Mohamed, A. A.; Fackler, J. P. *Comments Inorg. Chem.* **2003**, *24*, 253.

(159) Haruta, M.; Kobayashi, T.; Sano, H. *Chem. Lett.* **1987**, *16*, 405.

(160) Valden, M.; Lai, X.; Goodman, D. W. *Science* **1998**, *281*, 1647.

(161) Grabow, L. C.; Mavrikakis, M. *Angew. Chem. Int. Ed.* **2008**, *47*, 7390.

(162) Haruta, M. *Nature* **2005**, *437*, 1098.

(163) Herzing, A. A. K., C. J.; Carley, A. F.; Landon, P.; Hutchings, G. J. *Science* **2008**, *321*, 1331.

(164) Liu, Y.; Jia, C.-J.; Yamasaki, J.; Terasaki, O.; Schuth, F. *Angew. Chem. Int. Ed.* **2010**, *49*, 5771.

(165) Jia, C.-J.; Li, Y.; Bongard, H.; Schuth, F. *J. Am. Chem. Soc.* **2010**, *132*, 1520.

(166) Lin, X.; Yang, B.; Benia, H., -M.; Myrach, P.; Yulikov, M.; Aumer, A.; Brown, M. A.; Sterrer, M.; Bondarchuk, O.; Kieseritzky, E.; Rocker, J.; Risse, T.; Gao, H., -J.; Nilius, N.; Freund, H., -J. *J. Am. Chem. Soc.* **2010**, *132*, 7745.

(167) Hashmi, A. S. K.; Hutchings, G. J. *Angew. Chem. Int. Ed.* **2006**, *45*, 7896.

(168) Corma, A.; Garcia, H. *Chem. Soc. Rev* **2008**, *37*, 2096.

(169) Pina, C. D.; Falletta, E.; Prati, L. *Chem. Soc. Rev.* **2008**, *37*, 2077.

(170) Huang, J.; Akita, T.; Faye, J.; Fujitani, T.; Takei, T.; Haruta, M. *Angew. Chem. Int. Ed.* **2009**, *48*, 7862.

(171) Fujitani, T.; Nakamura, I.; Akita, T.; Okumura, M.; Haruta, M. *Angew. Chem. Int. Ed.* **2009**, *48*, 9515.

(172) Mitsudome, T.; Noujima, A.; Mikami, Y.; Mizugaki, T.; Jisukawa, K.; Kaneda, K. *Angew. Chem. Int. Ed.* **2010**, *49*, 5545.

(173) Mitsudome, T.; Noujima, A.; Mikami, Y.; Mizugaki, T.; Jisukawa, K.; Kaneda, K. *Chem.-Eur. J.* **2010**, *16*, 11818.

(174) Noujima, A.; Mitsudome, T.; Mizugaki, T.; Jisukawa, K.; Kaneda, K. *Angew. Chem. Int. Ed.* **2011**, *50*, 2986.

(175) Kyriakou, G.; Beaumont, S. K.; Humphrey, S. M.; Antonetti, C.; Lambert, R. M. *ChemCatChem* **2010**, *2*, 1444.

(176) Lykakis, I. N.; Psyllaki, A.; Stratakis, M. *J. Am. Chem. Soc.* **2011**, *133*, 10426.

(177) Zhu, Y.; Qian, H.; Jin, R. *J. Mater. Chem.* **2011**, *21*, 6793.

(178) Tsunoyama, H.; Sakurai, H.; Negishi, Y.; Tsukuda, T. *J. Am. Chem. Soc.* **2005**, *127*, 9374.

(179) Tsunoyama, H.; Ichikuni, N.; Tsukuda, T. *Langmuir* **2008**, *24*, 11327.

(180) Tsunoyama, H.; Ichikuni, N.; Sakurai, H.; Tsukuda, T. *J. Am. Chem. Soc.* **2009**, *131*, 7086.

(181) Kanaoka, S.; Yagi, N.; Fukuyama, Y.; Aoshima, S.; Tsunoyama, H.; Tsukuda, T.; Sakurai, H. *J. Am. Chem. Soc.* **2007**, *129*, 12060.

(182) Chaki, N. K.; Tsunoyama, H.; Nagishi, Y.; Sakurai, H.; Tsukuda, T. *J. Phys. Chem. C* **2007**, *111*, 4885.

(183) Han, J.; Li, Y.; Guo, R. *J. Am. Chem. Soc.* **2009**, *131*, 2060.

(184) Han, J.; Liu, Y.; Li, L.; Guo, R. *Langmuir* **2009**, *25*, 11054.

(185) Turner, M.; Golovko, V. B.; Vaughan, O. P. H.; Abdulkin, P.; Berenguer-Murcia, A.; Tikhov, M. S.; Johnson, B. F. G.; Lambert, R. M. *Nature* **2008**, *454*, 981.

(186) Zhu, Y.; Qian, H.; Drake, B. A.; R., J. *Angew. Chem. Int. Ed.* **2010**, *49*, 1295.

(187) Liu, Y.; Tsunoyama, H.; Akita, T.; Tsukuda, T. *Chem. Commun.* **2010**, *46*, 550.

(188) Zhu, Y.; Qian, H.; Zhu, M.; Jin, R. *Adv. Mater.* **2010**, *22*, 1915.

(189) Liu, Y.; Tsunoyama, H.; Xie, S.; Akita, T.; Tsukuda, T. *ACS Catal.* **2011**, *1*, 2.

(190) Wei, Y.; Han, S.; Kim, J.; Soh, S.; Grzybowski, B. A. *J. Am. Chem. Soc.* **2010**, *132*, 11018.

(191) Stark, W. J. *Angew. Chem. Int. Ed.* **2011**, *50*, 1242.

(192) De, M.; Ghosh, P. S.; Rotello, V. M. *Adv. Mater.* **2008**, *20*, 1.

(193) Jin, R. *Angew. Chem. Int. Ed.* **2008**, *47*, 2.

(194) Sperling, R. A.; Gil, P. R.; Zhang, F.; Zanella, M.; Parak, W. J. *Chem. Soc. Rev.* **2008**, *37*, 1896.

(195) Giljohann, D. A.; Seferos, D. S.; Danniel, W. L.; Massich, M. D.; Patel, P. C.; Mirkin, C. A. *Angew. Chem. Int. Ed.* **2010**, *49*, 3280.

(196) Boisselier, E.; Astruc, D. *Chem. Soc. Rev.* **2009**, *38*, 1759.

(197) Moyano, O. F.; Rotello, V. M. *Langmuir* **2011**, *27*, 10376.

(198) Connor, E. E.; Mwamuka, J.; Gole, A.; Murphy, C. J.; Wyatt, M. D. *Small* **2005**, *1*, 325.

(199) Han, G.; Ghosh, P.; Rotello, V. M. *Nanomed* **2007**, *2*, 113.

(200) Mishra, B.; Patel, B. B.; Tiwari, S. *Nanomedicine: Nanotechnology, Biology and Medicine* **2010**, *6*, 9.

(201) Joshi, H. M.; Bhumkar, D. R.; Joshi, K.; Pokharkar, V.; Sastry, M. *Langmuir* **2006**, *22*, 300.

(202) Hong, R.; Han, G.; Fernandez, J. M.; Kim, B.-j.; Forbes, N. S.; Rotello, V. M. *J. Am. Chem. Soc.* **2006**, *128*, 1078.

(203) Cheng, Y.; Samia, A. C.; Meyers, J. D.; Panagopoulos, I.; Fei, B.; Burda, C. *J. Am. Chem. Soc.* **2008**, *130*, 10643.

(204) Cheng, Y.; Samia, A. C.; Li, J.; Kenney, M. E.; Resnick, A.; Burda, C. *Langmuir* **2010**, *26*, 2248.

(205) Cheng, Y.; Meyers, J. D.; Broome, A.-M.; Kenney, M. E.; Basilion, J. P.; Burda, C. *J. Am. Chem. Soc.* **2011**, *133*, 2583.

(206) Dhar, S.; Daniel, W.; Giljohann, D. A.; Mirkin, C. A.; Lippard, S. J. *J. Am. Chem. Soc.* **2009**, *131*, 14652.

(207) Agasti, S. S.; Chompoosor, A.; You, C.-C.; Ghosh, P.; Kim, C. K.; Rotello, V. M. *J. Am. Chem. Soc.* **2009**, *131*, 5728.

(208) Kim, C. K.; Ghosh, P.; Pagliuca, C.; Zhu, Z.-J.; Menichetti, S.; Rotello, V. M. *J. Am. Chem. Soc.* **2009**, *131*, 1360.

(209) D'Emanuele, A.; Attwood, D. *Adv. Drug Delivery Rev.* **2005**, *57*, 2147.

(210) Ghosh, P.; Yang, X.; Arvizo, R.; Zhu, Z.-J.; Agasti, S. S.; Mo, Z.; Rotello, V. M. *J. Am. Chem. Soc.* **2010**, *132*, 2642.

(211) Kim, B.; Han, G.; Toley, B. J.; Kim, C.-k.; Rotello, V. M.; Forbes, N. S. *Nat. Nanotechnol.* **2010**, *5*, 465.

(212) Dreaden, E. C.; Mwakwari, S. C.; Sodji, Q. H.; Oyelere, A. K.; EI-sayed, M. A. *Langmuir* **2009**, *20*, 2247.

(213) Brown, S. D.; Nativo, P.; Smith, J.-A.; Stirling, D.; Edwards, P. R.; Venugopal, B.; Flint, D. J.; Plumb, J. A.; Graham, D.; Wheate, N. J. *J. Am. Chem. Soc.* **2010**, *132*, 4678.

(214) Wang, H.; Xu, J.; Wang, T.; Chen, T.; Wang, Y.; Tan, Y. W.; Su, H. *Angew. Chem. Int. Ed.* **2010**, *49*, 8426.

(215) Mulder, W. J. M.; Strijkers, G. J.; Van Tilborg, G. A. F.; Cormode, D. P.; Fayad, Z. A.; Nicolay, K. *Acc. Chem. Res.* **2009**, *42*, 904.

(216) Liu, G.; Swierczewska, M.; Lee, S.; Chen, X. *Nano Today* **2010**, *5*, 524.

(217) Debouttière, P.-J.; Roux, S.; Vocanson, F.; Billotey, C.; Beuf, O.; Favre-Réguillon, A.; Lin, Y.; Pellet-Rostaing, S.; Lamartine, R.; Perriat, P.; Tillement, O. *Adv. Funct. Mater.* **2006**, *16*, 2330.

(218) Hainfeld, J. F.; Slatkin, D. N.; Focella, T. M.; Smilowitz, H. M. *Br. J. Radiol.* **2006**, *79*, 248.

(219) Alric, C.; Taleb, J.; Duc, G. L.; Mandon, C.; Bilotey, C.; Meur-Herland, A. L.; Brochard, T.; Vocanson, F.; Janier, M.; Perriat, P.; Roux, S.; Tillement, O. *J. Am. Chem. Soc.* **2008**, *130*, 5908.

(220) Sun, I.-C.; Eun, D.-K.; Koo, H.; Ko, C.-Y.; Kim, H.-S.; Yi, D. K.; Choi, K.; Kwon, I. C.; Kim, K.; Ahn, C.-H. *Angew. Chem. Int. Ed.* **2011**, *50*, 9348.

(221) Wang, Z.; Ma, L. *Coor. Chem. Rev.* **2009**, *253*, 1607.

(222) Liu, J.; Lu, Y. *J. Am. Chem. Soc.* **2003**, *125*, 6642.

(223) Liu, J.; Lu, Y. *Anal. Chem.* **2004**, *76*, 1627.

(224) Wang, Z.; Levy, R.; Fernig, D. G.; Brust, M. *J. Am. Chem. Soc.* **2006**, *128*, 2214.

(225) Lee, J. H.; Wang, Z.; Liu, J.; Lu, Y. *J. Am. Chem. Soc.* **2008**, *130*, 14217.

(226) Ou, L.-J.; Jin, P., -Y.; Chu, X.; Jiang, J.-H.; Yu, R.-Q. *Anal. Chem.* **2010**, *82*, 6015.

(227) Frasconi, M.; Tortolini, C.; Botre, F.; Mazzei, F. *Anal. Chem.* **2010**, *82*, 7335.

(228) Lin, J.-H.; Chang, C.-W.; Wu, Z.-H.; Tseng, W., . -L. *Anal. Chem.* **2010**, *82*, 8775.

(229) Rica, R. d. e.; Velders, A. H. *Small* **2011**, *7*, 66.

(230) Xie, X.; Xu, W.; Li, T.; Liu, X. *Small* **2011**, *7*, 1393.

(231) Hall, W. P.; Ngatia, S. N.; Duyne, R. P. V. *Small* **2011**, *115*, 1410.

(232) He, P.; Shen, L.; Liu, R.; Luo, Z.; Li, Z. *Anal. Chem.* **2011**, *83*, 6988.

(233) Miranda, O. R.; Creran, B.; Rotello, V. M. *Curr. Opin. Chem. Biol.* **2010**, *14*, 1.

(234) Bunz, U. H. F.; Rotello, V. M. *Angew. Chem. Int. Ed.* **2010**, *49*, 2.

(235) Bajaj, A.; Miranda, O. R.; Kim, I.-B.; Phillips, R. L.; Jerry, D. J.; Bunz, U. H. F.; Rotello, V. M. *Proc. Nat. Acad. Sci. USA* **2009**, *106*, 10912.

(236) Bajaj, A.; Rana, S.; Miranda, O. R.; Yawe, J. C.; Jerry, D. J.; Bunz, U. H. F.; Rotello, V. M. *Chem. Sci.* **2010**, *1*, 134.

(237) Miranda, O. R.; Chen, H.-T.; You, C.-C.; Mortenson, D. E.; Yang, X.-C.; Bunz, U. H. F.; Rotello, V. M. *J. Am. Chem. Soc.* **2010**, *132*, 5285.

(238) Miranda, O. R.; Li, X.; Gonzalez-Garcia, L.; Zhu, Z.-J.; Yan, B.; Bunz, U. H. F.; Rotello, V. M. *J. Am. Chem. Soc.* **2011**, *133*, 9650.

(239) Sun, L.; Liu, D.; Wang, Z. *Anal. Chem.* **2007**, *79*, 773.

(240) Scodeller, P.; Flexer, V.; Szamocki, R.; Calvo, E. J.; Tognalli, N.; Troiani, H.; Fainstein, A. *J. Am. Chem. Soc.* **2008**, *130*, 12690.

(241) Guo, J.; Liu, D.; Wang, Z. *Anal. Chem.* **2008**, *80*, 8822.

(242) Xu, H.; Mao, X.; Zeng, Q.; Wang, S.; Kawde, A.-N.; Liu, G. *Anal. Chem.* **2009**, *81*, 669.

(243) Fang, C.; Fan, Y.; Kong, J.; Gao, Z.; Balasubramanian, N. *Anal. Chem.* **2008**, *80*, 9387.

(244) Yang, Y.-H.; Nam, J.-M. *Anal. Chem.* **2009**, *81*, 2564.

(245) Yoo, S. Y.; Kim, D.-K.; Park, T. J.; Kim, E. K.; Tamiya, E.; Lee, S. Y. *Anal. Chem.* **2010**, *82*, 1349.

(246) Ho, J. A.; Chang, H.-C.; Shih, N.-Y.; Wu, L.-C.; Chang, Y.-F.; Chen, C.-C.; Chou, C. *Anal. Chem.* **2010**, *82*, 5944.

(247) He, Y.; Zeng, K.; Gurung, A. S.; Baloda, M.; Xu, H.; Zhang, X.; Liu, G. *Anal. Chem.* **2010**, *82*, 7169.

(248) Gao, J.; Liu, D.; Wang, Z. *Anal. Chem.* **2010**, *82*, 9240.

(249) Nash, M. A.; Yager, P.; Hoffman, A. S.; Stayton, P. S. *Bioconjugate Chem.* **2010**, *21*, 2197.

(250) Zhang, L.; Li, Y.; Li, D.-W.; Jing, C.; Chen, X.; Lv, M.; Huang, Q.; Long, Y.-T.; Willner, I. *Angew. Chem. Int. Ed.* **2011**, *50*, 6789.

(251) Lin, C. J.; Yang, T.-Y.; Lee, C.-H.; Huang, S. H.; Sperling, R. A.; Zanella, M.; Jimmy, K. L.; Shen, H.-H.; Yeh, H.-I.; Parak, W. J.; Chang, W. H. *ACS Nano* **2009**, *3*, 395.

(252) Lu, Y.; Shi, W.; Qin, J.; Lin, B. *Electrophoresis* **2009**, *30*, 579.

(253) Li, F.; Zhao, Q.; Wang, C.; Lu, X.; Li, X.-F.; Le, X. C. *Anal. Chem.* **2010**, *82*, 3399.

(254) Qian, X.; Li, J.; Nie, S. *J. Am. Chem. Soc.* **2009**, *131*, 7540.

(255) Schwartzberg, A. M.; Grant, C. D.; Wolcott, A.; Talley, C. E.; Huser, T. R.; Bogomolni, R.; Zhang, J. Z. *J. Phys. Chem. B* **2004**, *108*, 19191.

(256) Bonham, A. J.; Braun, G.; Pavel, I.; Moskovits, M.; Reich, N. O. *J. Am. Chem. Soc.* **2007**, *129*, 14572.

(257) Dasary, S. S. R.; Singh, A. K.; Senapati, D.; Yu, H.; Ray, P. C. *J. Am. Chem. Soc.* **2011**, *131*, 13806.

(258) Kim, N.-J. *J. Phys. Chem. C* **2010**, *114*, 13979.

(259) Wustholz, K. L.; Henry, A.-I.; McMahon, J. M.; Freeman, R. G.; Valley, N.; Piolti, M. E.; Natan, M. J.; Schatz, G. C.; Duyne, R. P. V. *J. Am. Chem. Soc.* **2010**, *132*, 10903.

(260) Lu, W.; Singh, A. K.; Khan, S. A.; Senapati, D.; Yu, H.; Ray, P. C. *J. Am. Chem. Soc.* **2010**, *132*, 18103.

(261) Li, J. F.; Huang, Y. F.; Ding, Y.; Yang, Z. L.; Li, S. B.; Zhou, X. S.; Fan, F. R.; Zhang, W.; Zhou, Z. Y.; Wu, D. Y.; Ren, B.; Wang, Z. L.; Tian, Z. Q. *Nature* **2010**, *464*, 392.

(262) Zhang, D.; Ansar, S. M. *Anal. Chem.* **2010**, *82*, 5910.

(263) Bai, X.; Li, X.; Zheng, L. *Langmuir* **2010**, *26*, 12209.

(264) Zhang, B.; Harpster, M. H.; Park, H. J.; Johnson, P. A.; Wilson, W. C. *Anal. Chem.* **2011**, *83*, 254.

(265) Senapati, D.; Dasary, S. S. R.; Singh, A. K.; Senapati, T.; Yu, H.; Ray, P. C. *Chem.-Eur. J.* **2011**, *17*, 8445.

(266) Sengupta, S.; Sasisekharan, R. *Br. J. Cancer* **2007**, *96*, 1315.

(267) Kennedy, L. C.; Bickford, L. R.; Lewinski, N. A.; Coughlin, A. J.; Hu, Y.; Day, E. S.; West, J. L.; Drezek, R. A. *Small* **2011**, *2*, 169.

(268) Chithrani, B. D.; Ghazani, A. A.; Chan, W. C. W. *Nano Lett.* **2006**, *6*, 662.

(269) Perrault, S. D.; Walkey, C.; Jennings, T.; Fischer, H. C.; Chan, W. C. W. *Nano Lett.* **2009**, *9*, 1909.

(270) Bowman, M.-C.; Ballard, T. E.; Ackerson, C. J.; Feldheim, D. L.; Margolis, D. M.; Malander, C. *J. Am. Chem. Soc.* **2008**, *130*, 6896.

(271) Kulkarni, A. A.; Fuller, C.; Korman, H.; Weiss, A. A.; Iyer, S. S. *Bioconjugate Chem.* **2010**, *21*, 1486.

(272) Sun, I.-C.; Lee, S.; Koo, H.; Kwon, I. C.; Choi, K.; Ahn, C.-H.; Kim, K. *Bioconjugate Chem.* **2010**, *21*, 1939.

(273) Sirotkino, M. A.; Elagin, V. V.; Shirmanova, M. V.; Burgrova, M.; Snopova, L. B.; Kamensky, V. A.; Nadtochenko, V. A.; Denisov, N. N.; Zagaynova, E. V. *J. Biophoton.* **2010**, *3*, 718.

(274) Shah, N. B.; Dong, J.; Bischof, J. C. *Mol. Pharmaceutics* **2010**, *8*, 176.

(275) Xiao, Y.; Dane, K. Y.; Uzawa, T.; Csordas, A.; Qian, J.; Soh, H. T.; Daugherty, P. S.; Lagally, E. T.; Heegar, A. J.; Plaxco, K. W. *J. Am. Chem. Soc* **2010**, *132*, 15299.

(276) Gabin, A. M.; Watkins, E. M.; Quevedo, E.; Colvin, V. L.; West, J. L. *Small* **2010**, *6*, 745.

(277) Baram-Pinto, D.; Shulka, S.; Gedanken, A.; Sarid, R. *Small* **2010**, *6*, 1044.

(278) Brandenberger, C.; Muhlfeld, C.; Ali, Z.; Lenz, A.-G.; Schmid, O.; Parak, W. J.; Gehr, P.; Rothen-Rutishauser, B. *Small* **2010**, *6*, 1669.

(279) Lin, S.-Y.; Chen, N.-T.; Sun, S.-P.; Chang, J. C.; Wang, Y.-C.; Yang, C.-S.; Lo, L.-W. *J. Am. Chem. Soc.* **2010**, *132*, 8309.

(280) Wang, S.; Chen, K.-J.; Wu, T.-H.; Wang, -. H.; Lin, W.-Y.; Ohashi, M.; Chiou, P.-Y.; Tseng, H.-R. *Angew. Chem.* **2010**, *122*, 3865.

(281) Huschka, R.; Neumann, O.; Barhoumi, A.; Halas, N. J. *Nano Lett.* **2010**, *10*, 4117.

(282) Wang, H.-H.; Lin, C.-A. J.; Lee, C.-H.; Lin, Y.-C.; Tseng, Y.-M.; Hsieh, C.-L.; Shen, J.-L.; Chan, W.-H.; Chang, W. H.; Yeh, H.-I. *ACS Nano* **2010**, *5*, 4337.

(283) Lee, S.-M.; Park, H.; Choi, J.-W.; Park, Y. N.; Yun, C.-O.; Yoo, K.-H. *Angew. Chem. Int. Ed.* **2011**, *50*, 7581.

(284) Peckys, D. B.; Jonge, N.-d. *Nano Lett.* **2011**, *11*, 1733.

(285) Oh, J.-H.; Lee, J.-S. *Anal. Chem.* **2011**, *83*, 7364.

(286) Jiao, P.; Zhou, H.; Otto, M.; Mu, Q.; Li, L.; Su, G.; Zhang, Y.; Butch, E. R.; Snyder, S. E.; Jiang, G.; Yan, B. *J. Am. Chem. Soc* **2011**, *133*, 13918.

(287) Krug, H. F.; Wick, P. *Angew. Chem. Int. Ed.* **2011**, *50*, 1260.

(288) Warheit, D. B. *Nano Lett.* **2010**, *10*, 4777.

(289) Lewinski, N.; Colvin, V.; Drezek, R. *Small* **2008**, *1*, 26.

(290) Khlebtsov, N.; Dykman, L. *Chem. Soc. Rev.* **2010**, *40*, 1647.

(291) Simpson, C. A.; Huffman, B. J.; Gerdon, A. E.; Cliffel, D. E. *Chem. Res. Toxicol.* **2010**, *23*, 1608.

(292) Su, C. L.; Tseng, W. L. *Anal. Chem.* **2007**, *79*, 1626.

(293) McLean, J. A.; Stumpo, K. A.; Russell, D. H. *J. Am. Chem. Soc* **2005**, *127*, 5304.

(294) Spencer, M. T.; Furutani, H.; Oldenburg, S. J.; Darlington, T. K.; Prather, K. A. *J. Phys. Chem. C* **2008**, *112*, 4083.

(295) Eghlidi, H.; Lee, K. G.; Chen, X.-W.; Goetzinger, S.; Sandoghdar, V. *Nano Lett.* **2009**, *9*, 4007.

(296) Carmeli, I.; Lieberman, I.; Kraversky, L.; Fan, Z.; Govorov, A. O.; Markovich, G.; Richter, S. *Nano Lett.* **2010**, *10*, 2069.

(297) Heaven, M. W.; Dass, A.; White, P. S.; Holt, K. M.; Murray, R. W. *J. Am. Chem. Soc.* **2008**, *130*, 3754.

(298) Jiang, D.-e.; Tiago, M. L.; Luo, W.; Dai, S. *J. Am. Chem. Soc.* **2008**, *130*, 2777.

(299) Soo Choi, H.; Liu, W.; Misra, P.; Tanaka, E.; Zimmer, J. P.; Itty Ipe, B.; Bawendi, M. G.; Frangioni, J. V. *Nat Biotech* **2007**, *25*, 1165.

(300) Herzing, A. A.; Kiely, C. J.; Carley, A. F.; Landon, P.; Hutchings, G. J. *Science* **2008**, *321*, 1331.

(301) Zhu, M.; Lanni, E.; Garg, N.; Bier, M. E.; Jin, R. *J. Am. Chem. Soc.* **2008**, *130*, 1138.

(302) Tsunoyama, H.; Ichikuni, N.; Tsukuda, T. *Langmuir* **2008**, *24*, 11327.

(303) Schaaff, T. G.; Whetten, R. L. *J. Phys. Chem. B* **1999**, *103*, 9394.

(304) Negishi, Y.; Nobusada, K.; Tsukuda, T. *J. Am. Chem. Soc.* **2005**, *127*, 5261.

(305) Tsunoyama, H.; Nickut, P.; Negishi, Y.; Al-Shamery, K.; Matsumoto, Y.; Tsukuda, T. *J. Phys. Chem. C* **2007**, *111*, 4153.

(306) Duan, H.; Nie, S. *J. Am. Chem. Soc.* **2007**, *129*, 2412.

(307) Shaw, C. F. *Chem. Rev.* **1999**, *99*, 2589.

(308) Yu, S.-Y.; Zhang, Z.-X.; Cheng, E. C.-C.; Li, Y.-Z.; Yam, V. W.-W.; Huang, H.-P.; Zhang, R. *J. Am. Chem. Soc.* **2005**, *127*, 17994.

(309) Schneider, J.; Lee, Y.-A.; Perez, J.; Brennessel, W. W.; Flaschenriem, C.; Eisenberg, R. *Inorg. Chem.* **2008**, *47*, 957.

(310) Yam, V. W.-W.; Cheng, E. C.-C. *Chem. Soc. Rev.* **2008**, *37*, 1806.

(311) Bau, R. *J. Am. Chem. Soc.* **1998**, *120*, 9380.

(312) Dass, A.; Stevenson, A.; Dubay, G. R.; Tracy, J. B.; Murray, R. W. *J. Am. Chem. Soc.* **2008**, *130*, 5940.
(313) Smith, A. M.; Nie, S. *J. Am. Chem. Soc.* **2008**, *130*, 11278.
(314) Kairdolf, B. A.; Smith, A. M.; Nie, S. *J. Am. Chem. Soc.* **2008**, *130*, 12866.
(315) Srisombat, L.-o.; Park, J.-S.; Zhang, S.; Lee, T. R. *Langmuir* **2008**, *24*, 7750.
(316) Zhang, S.; Leem, G.; Srisombat, L.-o.; Lee, T. R. *J. Am. Chem. Soc.* **2008**, *130*, 113.
(317) Krpetic, Z.; Nativo, P.; Porta, F.; Brust, M. *Bioconjugate Chem.* **2009**, *20*, 619.
(318) Roux, S.; Garcia, B.; Bridot, J. L.; Salome, M.; Marquette, C.; Lemelle, L.; Gillet, P.; Blum, L.; Perriat, P.; Tillement, O. *Langmuir* **2005**, *21*, 2526.
(319) Abad, J. M.; Mertens, S. F. L.; Pita, M.; Fernandez, V. M.; Schiffrin, D. J. *J. Am. Chem. Soc.* **2005**, *127*, 5689.
(320) Negishi, Y.; Tsukuda, T. *J. Am. Chem. Soc.* **2003**, *125*, 4046.
(321) Li, Z.; Jin, R.; Mirkin, C. A.; Letsinger, R. L. *Nucleic Acids Res* **2002**, *30*, 1558.
(322) Dougan, J. A.; Karlsson, C.; Smith, W. E.; Graham, D. *Nucleic Acids Res* **2007**, *35*, 3668.
(323) Chen, S. W.; Ingram, R. S.; Hostetler, M. J.; Pietron, J. J.; Murray, R. W.; Schaaff, T. G.; Khoury, J. T.; Alvarez, M. M.; Whetten, R. L. *Science* **1998**, *280*, 2098.
(324) Negishi, Y.; Tsukuda, T. *J. Am. Chem. Soc* **2003**, *125*, 4046.
(325) Gronbeck, H.; Walter, M.; Hakkinen, H. *J. Am. Chem. Soc.* **2006**, *128*, 10268.
(326) Parker, J. F.; Choi, J. P.; Wang, W.; Murray, R. W. *J. Phys. Chem. C* **2008**, *112*, 13976.
(327) Wuelfing, W. P.; Templeton, A. C.; Hicks, J. F.; Murray, R. W. *Anal. Chem.* **1999**, *71*, 4069.
(328) Barjat, H.; Morris, G. A.; Smart, S.; Swanson, A. G.; Williams, S. C. R. *J. Magn. Reson. B* **1995**, *108*, 170.
(329) Thurecht, K. J.; Howdle, S. M.; Davis, A. L.; Hyde, J. R. *Macromolecules* **2007**, *40*, 976.
(330) Morris, K. F.; Johnson, C. S. *J. Am. Chem. Soc* **2002**, *114*, 3139.
(331) Bau, R. *J. Am. Chem. Soc* **1998**, *120*, 9380.
(332) Schneider, J.; Lee, Y.-A.; Perez, J.; Brennessel, W. W.; Flaschenriem, C.; Eisenberg, R. *Inorg. Chem.* **2008**, *47*, 957.
(333) Abdou, H. E.; Mohamed, A. A.; Fackler, J. P. *Inorg. Chem.* **2007**, *46*, 141.
(334) Bain, C. D.; Biebuyck, H. A.; Whitesides, G. M. *Langmuir* **1989**, *5*, 723.
(335) Kitagawa, H.; Kojma, N.; Nakajima, T. *J. Chem. Soc., Dalton Trans* **1991**, *11*, 723.
(336) Kaden, W. E.; Wu, T.; Kunkel, W. A.; Anderson, S. L. *Science* **2009**, *326*, 826.
(337) Yu, S.-Y.; Zhang, Z.-X.; Cheng, E. C.-C.; Li, Y.-Z.; Yam, V. W.-W.; Huang, H.-P.; Zhang, R. *J. Am. Chem. Soc.* **2005**, *127*, 17994.
(338) Fackler, J. P. *Inorg. Chem.* **2002**, *41*, 6959.
(339) Link, S.; Beeby, A.; Fitzgerald, S.; EI-Sayed, M. A.; Schaaff, T. G.; Whetten, R. L. *J. Phys. Chem. B* **2002**, *106*, 3410.
(340) Cheng, P. P. H.; Silvester, D.; Wang, G. L.; Kalyuzhny, G.; Douglas, A.; Murray, R. W. *J. Phys. Chem. B* **2006**, *110*, 4637.
(341) Huang, T.; Murray, R. W. *J. Phys. Chem. B* **2001**, *105*, 12498.
(342) Negishi, Y.; Tsukuda, T. *Chem. Phys. Lett.* **2004**, *383*, 161.
(343) Tang, Z.; Xu, B.; Wu, B.; Robinson, D. A.; Bokossa, N.; Wang, G. *Langmuir* **2011**, *27*, 2989.
(344) Jerschow, A.; Muller, N. *J. Magn. Reson.* **1997**, *125*, 372.
(345) Templeton, A. C.; Chen, S.; Gross, S. M.; Murray, R. W. *Langmuir* **1999**, *15*, 66.
(346) Cliffel, D. E.; Zamborini, F. P.; Gross, S. M.; Murray, R. W. *Langmuir* **2000**, *16*, 9699.
(347) Schaaff, T. G.; Whetten, R. L. *J. Phys. Chem. B* **2000**, *104*, 2630.
(348) Peterson, R. R.; Cliffel, D. E. *Anal. Chem.* **2005**, *77*, 4348.
(349) Jiang, D.-e.; Chen, W.; Whetten, R. L.; Chen, Z. *J. Phys. Chem. C* **2009**, *113*, 16983.
(350) Tang, Z.; Xu, B.; Wu, B.; Germann, M. W.; Wang, G. *J. Am. Chem. Soc.* **2010**, *132*, 3367.

(351) Shenhar, R.; Rotello, V. M. *Acc. Chem. Res.* **2003**, *36*, 549.
(352) Lo, C. K.; Paau, M. C.; Xiao, D.; Choi, M. M. F. *Electrophoresis* **2008**, *29*, 2330.
(353) Jimenez, V. L.; Leopold, M. C.; Mazzitelli, C.; Jorgenson, J. W.; Murray, R. W. *Anal. Chem.* **2003**, *75*, 199.
(354) Wilcoxon, J. P.; Martin, J. E.; Provencio, P. *J. Chem. Phys.* **2001**, *115*, 998.
(355) You, C. C.; De, M.; Rotello, V. M. *Curr. Opin. Chem. Biol.* **2005**, *9*, 639.
(356) Templeton, A. C.; Cliffel, D. E.; Murray, R. W. *J. Am. Chem. Soc.* **1999**, *121*, 7081.
(357) Templeton, A. C.; Hostetler, M. J.; Warmoth, E. K.; Chen, S. W.; Hartshorn, C. M.; Krishnamurthy, V. M.; Forbes, M. D. E.; Murray, R. W. *J. Am. Chem. Soc.* **1998**, *120*, 4845.
(358) Carney, R. P.; DeVries, G. A.; Dubois, C.; Kim, H.; Kim, J. Y.; Singh, C.; Ghorai, P. K.; Tracy, J. B.; Stiles, R. L.; Murray, R. W.; Glotzer, S. C.; Stellacci, F. *J. Am. Chem. Soc.* **2008**, *130*, 798.
(359) DeVries, G. A.; Brunnbauer, M.; Hu, Y.; Jackson, A. M.; Long, B.; Neltner, B. T.; Uzun, O.; Wunsch, B. H.; Stellacci, F. *Science* **2007**, *315*, 358.
(360) Jackson, A. M.; Myerson, J. W.; Stellacci, F. *Nat. Mater.* **2004**, *3*, 330.
(361) Guo, R.; Song, Y.; Wang, G.; Murray, R. W. *J. Am. Chem. Soc.* **2005**, *127*, 2752.
(362) Song, Y.; Murray, R. W. *J. Am. Chem. Soc.* **2002**, *124*, 7096.
(363) Hostetler, M. J.; Templeton, A. C.; Murray, R. W. *Langmuir* **1999**, *15*, 3782.
(364) Ramachandran, G. K.; Hopson, M. J.; Rawlett, A. M.; Nagahara, L. A.; Primak, A.; Lindsay, S. M. *Science* **2003**, *300*, 1413.
(365) Vericat, C.; Vela, M. E.; Benitez, G.; Carro, P.; Salvarezza, R. C. *Chem. Soc. Rev.* **2010**, *39*, 1805.
(366) Ingram, R. S.; Hostetler, M. J.; Murray, R. W. *J. Am. Chem. Soc.* **1997**, *119*, 9175.
(367) Wang, G.; Murray, R. W. *Nano Lett.* **2004**, *4*, 95.
(368) Wang, G.; Zhang, J.; Murray, R. W. *Anal. Chem.* **2002**, *74*, 4320.
(369) Mcintosh, C. M.; Esposito, E. A.; Boal, A. K.; Simard, J. M.; Martin, C. T.; Rotello, V. M. *J. Am. Chem. Soc.* **2001**, *123*, 7626.
(370) Warner, M. G.; Hutchison, J. E. *Nat. Mater.* **2003**, *2*, 272.
(371) Verma, A.; Uzun, O.; Hu, Y. H.; Hu, Y.; Han, H. S.; Watson, N.; Chen, S. L.; Irvine, D. J.; Stellacci, F. *Nat. Mater.* **2008**, *7*, 588.
(372) Zheng, J.; Nicovich, P. R.; Dickson, R. M. *Annu. Rev. Phys. Chem.* **2007**, *58*, 409.
(373) Zheng, J.; Zhang, C.; Dickson, R. M. *Phys. Rev. Lett.* **2004**, *94*, 077402.
(374) Yam, V. W.-W.; Cheng, E. C.-C. *Chem. Soc. Rev.* **2008**, 1806.
(375) Gautier, C.; Burgi, T. *J. Am. Chem. Soc.* **2008**, *130*, 7077.
(376) Hou, W.; Dasog, M.; Scott, R. W. *Langmuir* **2009**, *25*, 12954.
(377) Zhang, S.; Leem, G.; Srisombat, L.-o.; Lee, T. R. *J. Am. Chem. Soc.* **2008**, *130*, 113.
(378) Srisombat, L.-o.; Park, J.-S.; Zhang, S.; Lee, T. R. *Langmuir* **2008**, *24*, 7750.
(379) Li, Z.; Jin, R.; Mirkin, C. A.; Letsinger, R. L. *Nucleic Acids Res.* **2002**, *30*, 1558.
(380) Huang, T.; Murray, R. W. *J. Phys. Chem. B* **2001**, *105*, 12498.
(381) Tang, Z.; Xu, B.; Wu, B.; Germann, M. W.; Wang, G. *J. Am. Chem. Soc.* **2010**, *132*, 3367.
(382) Link, S.; Beeby, A.; FitzGerald, S.; El-Sayed, M. A.; Schaaff, T. G.; Whetten, R. L. *J. Phys. Chem. B* **2002**, *106*, 3410.
(383) Varnavski, O.; Ramakrishna, G.; Kim, J.; Lee, D.; Goodson, T. *J. Am. Chem. Soc.* **2009**, *132*, 16.
(384) Ramakrishna, G.; Varnavski, O.; Kim, J.; Lee, D.; Goodson, T. *J. Am. Chem. Soc.* **2008**, *130*, 5032.
(385) Wang, G.; Guo, R.; Kalyuzhny, G.; Choi, J. P.; Murray, R. W. *J. Phys. Chem. B* **2006**, *110*, 20282.

(386) Lee, D.; Donkers, R. L.; Wang, G.; Harper, A. S.; Murray, R. W. *J. Am. Chem. Soc.* **2004**, *126*, 6193.

(387) Knoppe, S.; Dharmaratne, A. C.; Schreiner, E.; Dass, A.; Buergi, T. *J. Am. Chem. Soc.* **2010**, *132*, 16783.

(388) Ramakrishna, G.; Varnavski, O.; Kim, J.; Lee, D.; Goodson, T. *J. Am. Chem. Soc.* **2008**, *130*, 5032.

(389) Qian, H.; Echenhoff, W. T.; Zhu, Y.; Pintauer, T.; Jin, R. *J. Am. Chem. Soc.* **2010**, *132*, 8280.

(390) Garg, N.; Lee, T. R. *Langmuir* **1998**, *14*, 3815.

(391) Wu, Z.; Lanni, E.; Chen, W.; Bier, M. E.; Ly, D.; Jin, R. *J. Am. Chem. Soc.* **2009**, *131*, 16672.

(392) Krpetic, Z.; Nativo, P.; Porta, F.; Brust, M. *Bioconjugate Chem.* **2009**, *20*, 619.

(393) Lee, T. R.; Friedman, J. M.; Garg, N. *Langmuir* **2000**, *16*, 4266.

(394) Wu, Z.; Suhan, J.; Jin, R. *J. Mater. Chem.* **2009**, *19*, 622.

(395) Parker, J. F.; Weaver, J. E. F.; McCallum, F.; Fields-Zinna, C. A.; Murray, R. W. *Langmuir* **2010**, *26*, 13650.

(396) Negishi, Y.; Iwai, T.; Ide, M. *J. Chem. Soc., Chem. Comm* **2010**, *46*, 4713.

(397) Templeton, A. C.; Hostetler, M. J.; Kraft, C. T.; Murray, R. W. *J. Am. Chem. Soc.* **1998**, *120*, 1906.

(398) Pregosin, P. S.; Kumar, P. G. A.; Fernandez, I. *Chem. Rev.* **2005**, *105*, 2977.

(399) Laaksonen, T.; Ruiz, V.; Lijeroth, P.; Quinn, B. M. *Chem. Soc. Rev.* **2008**, *37*, 1836.

(400) Gilbert, B. C.; Laue, H. A. H.; Norman, R. O. C.; Sealy, R. C. *J. Chem. Soc., Perkin Trans.* **1975**, *2*, 892.

(401) Mason, P. R.; Chignell, C. F. *Pharmaco. Rev.* **1982**, *33*, 189.

(402) Moses, P. R.; Chambers, J. Q.; Sutherland, J. O.; Williams, D. R. *J. Electrochem. Soc.* **1975**, *122*, 608.

(403) Aarons, L. J.; Adam, F. C. *Can. J. Chem.* **1972**, *50*, 1390.

(404) Garcia-Morales, V.; Mafe, S. *J. Phys. Chem. C* **2007**, *111*, 7242.

(405) Kobayashi, H.; Ogawa, M.; Alford, R.; Choyke, P. L.; Urano, Y. *Chem. Rev.* **2009**, *110*, 2620.

(406) Choi, H. S.; Nasr, K.; Alyabyev, S.; Feith, D.; Lee, J. H.; Kim, S. H.; Ashitate, Y.; Hyun, H.; Patonay, G.; Strekowski, L.; Henary, M.; Frangioni, J. V. *Angew. Chem. Int. Ed.* **2011**, *50*, 6258.

(407) Choi, H. S.; Liu, W.; Misra, P.; Tanaka, E.; Zimmer, J. P.; Ipe, B. I.; Bawendi, M. G.; Frangioni, J. V. *Nat. Biotech.* **2007**, *25*, 1165.

(408) Jupally, V. R.; Kota, R.; Van Dornshuld, E.; Mattern, D. L.; Tschumper, G. S.; Jiang, D.-e.; Dass, A. *J. Am. Chem. Soc.* **2011**, *133*, 20258.

(409) Tang, Z.; Robinson, D. A.; Bokossa, N.; Xu, B.; Wang, S.; Wang, G. *J. Am. Chem. Soc* **2011**, *133*, 16037.

8 PUBLICATIONS AND MANUSCRIPTS IN PREPARATION

1. Synthesis and Structural Determination of Multidentate 2,3-Dithiol-Stabilized Au Clusters,

Zhenghua Tang, Bin Xu, Baohua Wu, Markus W. Germann, and Gangli Wang*

J. Am. Chem. Soc. **2010,** *132,* 3367-3374.

2. Monolayer Reactions of Protected Au Nanoclusters with Monothiol Tiopronin and 2,3-Dithiol Dimer-captopropanesulfonate,

Zhenghua Tang, Bin Xu, Baohua Wu, Donald A. Robinson, Nadia Bokossa, and Gangli Wang*

Langmuir. **2011,** *27,* 2989-2996.

3. Mixed Dithiolate Durene-DT and Monothiolate Phenylethanethiolate Protected Au130 Nanoparticles with Discrete Core and Core-Ligand Energy States,

Zhenghua Tang, Donald A. Robinson, Nadia Bokossa, Bin Xu, Siming Wang and Gangli Wang*

J. Am. Chem. Soc. **2011,** *133,* 16037-16044.

4. Near Infrared Luminescence of Gold Nanoclusters Affected by the Bonding of 1, 4- Dithiolate Durene and Monothiolate Phenylethanethiolate

Zhenghua Tang, Tarushee Ahuja, Siming Wang and Gangli Wang*

Nanoscale. **2012,** Advance Article.

5. Electrochemistry of Monodisperse Au130 Nanoparticles

Zhenghua Tang,[$] Donald A. Robinson,[$] Dengchao Wang, and Gangli Wang*

Anal. Chem. **2012,** Manuscript in preparation.

($: Those authors contributed equally)

6. Intensity and Lifetime Cell Imaging with Luminescent Gold Nanoclusters

Jian Zhang,* Yi Fu, **Zhenghua Tang,** Ge Li, Richard Y. Zhao, Joseph R. Lakowicz, and Gangli Wang*

ACS nano **2012,** Under review.